UNIVERSITY OF CALIFORNIA

Santa Barbara

Stratigraphy and geochronology of the Nacientes del Teno and Rio Damas formations: insights into Middle to Late Jurassic Andean volcanism

A thesis submitted in partial satisfaction of the requirements for the degree of Master of Science in Earth Science

by

William Deforest Junkin

Committee in charge:

Professor Phillip B. Gans, Chair

Professor André R. Wyss

Professor John M. Cottle

March 2018

The thesis of William Deforest Junkin is approved.

_____

John M. Cottle

_____

André R. Wyss

_____

Phillip B. Gans, Committee Chair

March 2018

Stratigraphy and geochronology of the

Nacientes del Teno and Rio Damas

formations: insights into Middle to Late

Jurassic Andean volcanism

ABSTRACT

Stratigraphy and geochronology of the Nacientes del Teno and Rio Damas formations: insights into Middle to Late Jurassic Andean volcanism

by

William Deforest Junkin

The Nacientes del Teno Formation and the lowermost strata of the Rio Damas Formation in Maule, Chile (35.10°S) comprise a sequence of sedimentary and volcanic rocks deposited along the western margin of the Andean backarc basin during the Middle to Late Jurassic (174-145 Ma). Revised stratigraphy and new U-Pb geochronological data from this classic succession provide insights into the location, composition, and timing of coeval arc volcanic systems.

U-Pb geochronological data from detrital and primary volcanic zircons represent the first absolute ages (ca. 172-161 Ma) reported for the Nacientes del Teno Formation. Detrital zircon ages include a tightly clustered population ca. 165 Ma that coincides with a Middle Jurassic trough present in frequency histogram and relative probability plots of published datasets of U-Pb detrital zircon ages, challenging the notion of a lull in volcanic arc activity at this time.

The dominantly marine deposits of the Nacientes del Teno Formation interfinger with subordinate subaerial strata. The latter include channelized conglomerate with sub-rounded

to sub-angular andesitic clasts up to 40 cm in diameter, suggesting a proximal alluvial fan and fan delta depositional environment with alternating continental and marine deposition. The Nacientes del Teno Formation includes a quartz rhyolite ignimbrite that yielded a U-Pb zircon age of ca. 160 Ma, the first Jurassic rhyolite reported for this portion of the Andes in central Chile, and in stark departure from the commonly assumed Miocene and Triassic ages for local rhyolites. Paleocurrent indicators from the W ± ~90° together with a general eastward decrease in grain size, decrease in volcanic content, and increase in carbonate content of marine deposits, suggest a sediment source to the west. The proximal volcaniclastic stratigraphy and tight distribution of U-Pb detrital zircon ages of the Nacientes del Teno Formation suggest nearby andesitic stratovolcanoes in the Middle Jurassic. These hypothesized volcanoes are located much further east than traditional models for the location of the "main magmatic arc" during the Jurassic, challenging the notion that Jurassic arc volcanism at this latitude was restricted to a single, narrow (a few tens of kilometers wide) volcanic chain located in the present day Coastal Cordillera.

Sedimentological features of lowermost Rio Damas Formation strata at 35.10°S are consistent with deposition in an alluvial fan environment. A maximum depositional age of ca. 151 Ma calculated from U-Pb detrital zircon ages agrees with previously published maximum depositional ages for the Rio Damas Formation. Sedimentological and geochronologic evidence suggest that the Late Jurassic regression represented by the formation resulted from tectonic uplift.

Table of Contents

1. Introduction 1

2. Geologic background 3

A. Late Paleozoic to present tectonic framework 3

B. Western belt 4

C. Eastern belt 5

3. Previous work on the Nacientes del Teno Formation 7

4. Methods 9

A. Geologic mapping 9

B. U-Pb geochronology 9

4. Geologic framework of the Nacimiento del Teno region 12

A. Overview 12

B. Lithostratigraphy 14

i. Jnt_A 14

ii. Jnt_B 16

iii. Jnt_C 20

iv. Jnt_D 21

v. Jnt_E 23

vi. Jurassic Rio Damas Formation (Jrd) 23

vii. Post-Jurassic units 25

5. U-Pb geochronology of Jurassic units 25

A. Summary 25

B. Nacientes del Teno Formation magmatic zircons 26

C. Nacientes del Teno Formation and Rio Damas Formation detrital zircons 27

6. Ammonite biostratigraphy 30

7. Discussion 30

A. Revised stratigraphy of the Nacientes del Teno Formation 30

B. Significance of a ca. 160 Ma rhyolite ignimbrite in the Principal Cordillera at 35.10°S 32

C. Depositional environments and sedimentation of the Nacientes del Teno Formation 33

i. Jnt_A (Fig. 11A-B) 34

ii. Jnt_B (Fig. 11B) 34

iii. Jnt_C 35

iv. Jnt_D (Fig. 11C) 36

v. Jnt_E (Fig. 11D) 37

D. Sediment sources and maximum depositional age of the Rio Damas Formation 37

E. Significance of Nacientes del Teno and Rio Damas formation volcanic detritus in the context of Jurassic arc paleogeography 39

F. Age of the Nacientes del Teno Formation in the context of recent detrital zircon studies 40

8. Conclusions 42

9. Supplementary material 43

10. References 43

11. Figures and Tables 51

Appendix A: Summary of LA-ICP-MS analytical results 71

List of Figures and Tables

Figure 1. Simplified geologic map of central Chile and west-central Argentina 51

Figure 2. Geologic map of the Nacientes del Teno Formation and adjacent rocks, Maule (Region VII), Chile 52

Figure 3. Generalized stratigraphic columns 54

Figure 4. Lithostratigraphic sections of Mesozoic units 56

Figure 5. Rock unit photos 57

Figure 6. Photographs of ammonite remains hosted by the Nacientes del Teno Formation ...61

Figure 7. U-Pb ages for Nacientes del Teno and Rio Damas Formation samples 62

Figure 8. Sample concordia plots of U-Pb ages 64

Figure 9. Stratigraphic level versus age 65

Figure 10. Frequency histogram and relative probability plots of Jurassic U-Pb detrital zircon ages 66

Figure 11. Jurassic paleogeographic reconstruction of the Nacimiento del Teno region 67

Table 1. Depositional ages for sampled strata of the Nacientes del Teno and Rio Damas formations calculated by various methods 68

Table 2. Identifications and ages of photographed ammonite specimens from the Nacientes del Teno Formation 69

Table 3. Samples analyzed for U-Pb data and conditions set during each LA-ICP-MS analytical session 70

Supplementary material: Plate 1. Geologic map of the Nacientes del Teno Formation and adjacent rocks, Maule (Region VII), Chile ..... available from Proquest Dissertations and Theses

1. INTRODUCTION

Convergence along the western margin of South America throughout the Jurassic (201-145 Ma) resulted in intense arc magmatism and deposition of thick sequences of volcanic and sedimentary rocks (Hervé et al., 1987; Charrier et al., 2007). Today, rocks of Jurassic age crop out in two orogen-parallel belts that extend for >2500 km through northern and central Chile and west-central Argentina (Fig. 1). The "western belt," exposed along the Coastal Cordillera of Chile, consists of nearly continuous outcrops of Jurassic plutons and thick, generally east-dipping sequences of volcanic and volcaniclastic rocks. This belt has been traditionally interpreted to be the location of the main magmatic arc during the Jurassic (Charrier et al., 2007). To the east 100-150 km, in the High Andes, Frontal Cordillera, and Principal Cordillera, and further east in the Neuquén Region of east-central Argentina, a parallel "eastern belt" of thinner, generally west-dipping sequences of sedimentary and subordinate volcanic rocks is interpreted to reflect the development of an orogen-scale backarc basin (Vicente, 2005). The relationship between the eastern and western belts is obscured by younger (Cretaceous to Recent) units that overlie Jurassic rocks along faulted or unconformable contacts, potentially obscuring major structures and an unknown amount of Jurassic arc and backarc rocks (Hervé et al., 1987; Charrier et al., 2007; Vicente, 2005).

The overall history, architecture, and distribution of the Jurassic arc and backarc in central Chile (30°-39°S) remain poorly constrained. The locations of volcanoes and precise timing of volcanism within the western belt in the Jurassic remains unclear, due to limited mapping and a paucity of age data from Coastal Cordilleran volcanic deposits. The limited exposure of deposits in the eastern belt, difficulties involved in accessing the mountainous terrain of eastern central Chile, and limited radiometric age information has similarly

hindered our understanding of the locations and activity of volcanic systems that may have developed inboard of the western belt during the Jurassic (Vicente, 2005; Rossel et al., 2014). Perhaps the greatest uncertainties stem from the lack of exposure of Jurassic rocks across the broad expanse (~100 km) of the Central Valley and western flank of the Principal Cordillera, where any such deposits are now covered by younger successions of volcanic and volcaniclastic rocks. Are traditional models correct that consider the Jurassic magmatic arc as a narrow linear feature only a few tens of kilometers wide, or was the arc hundreds of kilometers wide, as proposed for Paleozoic arcs of western South America (Herve et al., 1987)? Were the western and eastern belts of central Chile both derived from volcanoes located along the present day Coastal Cordillera (Coira et al., 1982; Herve et al., 1987; Davidson, 1988), or from a volcanic front that migrated longitudinally during the Jurassic? Or were multiple chains of volcanoes simultaneously active across the width of the arc (Vicente, 1976; Charrier et al., 2007)? Was volcanic activity relatively constant throughout the Jurassic or were there periods of significantly reduced activity (Naipauer et al., 2015a)?

With the aim of clarifying the timing and spatial distribution of Jurassic volcanism in central Chile, this study investigates the geology and geochronology of the Nacientes del Teno Formation and overlying deposits of the Rio Damas Formation, a sequence of ca. 172-150 Ma backarc marine and continental sedimentary and volcanic deposits widely cited as representative of the western margin of the Andean backarc basin (e.g. Riccardi, 1983; Legaretta and Uliana, 1996; Charrier et al., 2007). The rock units were investigated within a ~90 km^2 field area containing the drainages of the Nacimiento del Teno and tributaries (Fig. 1). Located in the Principal Cordillera of Chile at 35.10°S, the investigated sequence crops out farther west than other Jurassic backarc units exposed between 31°S and 36°S and thus

represents a unique opportunity to investigate Middle to Late Jurassic volcanism in the region. The isotopic ages presented below are the first for the Nacientes del Teno Formation, and indeed for all Middle Jurassic stratified deposits in central Chile. Field observations provide new insights on Nacientes del Teno Formation internal stratigraphic relationships, and along with geochronology data, provide strong evidence for the existence of a Middle Jurassic (ca. 165 Ma) volcanic system located well to the east of the present day Coastal Cordillera.

2. GEOLOGIC BACKGROUND

A. Late Paleozoic to Present tectonic framework

Continental extension and rifting during the Late Triassic to Early Jurassic is proposed to have resulted from thermo-mechanical collapse of a Late Paleozoic orogenic belt located along the southwestern margin of Gondwana (Mpodozis and Kay, 1990; Kay, 1993). Andean subduction was underway by the Early Jurassic (Jordan et al., 1983, 1997; Coira et al., 1982), producing a magmatic arc likely on rifted continental crust (Jordan et al., 2001; Digregorio et al., 1984). Rifting is thought to have transitioned to thermal subsidence in the Middle to Late Jurassic (174-145 Ma) (Uliana et al., 1989), with numerous semi-isolated basins coalescing into a single orogen-scale backarc basin (Vicente, 2006; Legarretta and Uliana, 1996, 1999). This backarc basin was bounded by the sagging edge of the South American craton to the south and east and at least partially bounded by the Jurassic arc and possibly by uplifted Paleozoic basement to the west (Digregorio et al., 1984; Vicente, 2005). Changes in parameters of the subducting slab led to Late Cretaceous to present shortening and an eastward shift of the magmatic arc, which is presently superposed on uplifted

Mesozoic and Cenozoic backarc basin deposits of the Principal Cordillera (Oncken et al., 2006; Jordan et al., 2001; Horton et al., 2018).

B. Western belt

Extensive investigations in the Coastal Cordillera of northern Chile (18°-30°S) have yielded ages of plutonic rocks that span the entire Jurassic (Coira et al., 1982; Charrier et al., 2007). Plutonic rocks exposed in the Coastal Cordillera of central Chile (30°-39°S) have yielded U-Pb, K-Ar, and Rb-Sr ages that range from 161-156 Ma (Godoy and Loske, 1996; Gana and Tosdal 1996), well within the range of U-Pb ages (ca. 172-150 Ma) presented in this study (see 'U-Pb geochronology results' section).

In northern and central Chile, Jurassic volcanic and volcaniclastic rocks crop out within the Coastal Cordillera in east dipping sequences that exceed 9000 m in thickness (Buchelt and Tellez, 1988). Radiometric ages are not available for western belt volcanic rocks of central Chile, but Ar-Ar ages of western belt volcanic rocks in northernmost Chile (18°-24°S) range from 175-150 Ma (Oliveros et al., 2006). Between 32°-34°S (Vergara, 1995), the western belt deposits are divided into the marine sedimentary and felsic volcanic Ajial Formation (Thomas, 1958); the marine sedimentary Cerro Calera Formation (Piracés, 1976); and the continental, felsic to andesitic volcanic and volcaniclastic Horqueta Formation (Piracés, 1977). A Bajocian-Bathonian? (170-166 Ma) fossil assemblage from the Cerro Calera Formation (Piracés, 1976; Nasi and Thiele, 1982) indicates a transition from a partially submerged, low-relief arc to a subaerial environment sometime during or following the Middle Jurassic (174-164 Ma). Correlative units have been mapped within the Coastal Cordillera at the latitude of the field area (35.10°S) by Morel (1981) as the Hualmapu Formation, described as a >3600 m thick sequence of andesitic lava flows, volcanic breccias,

and minor marine sedimentary intercalations with Toarcian (183-174 Ma) fauna (Corvalán, 1982). Volcanic and volcaniclastic deposits of the Coastal Cordillera thin south of 35°S and disappear around 35.5°S (Charrier et al., 2007) (Fig. 1).

C. Eastern belt

Detritus from the magmatic arc to the west and from Precambrian-Triassic rocks to the south and east accumulated in intermittently flooded basins (Legaretta and Uliana, 1996, 1999) thought to have been linked to the Pacific via connections through the volcanic arc (Vicente, 2005). Rifted Triassic basement rocks and syntectonic rift deposits of the Permo-Triassic Choiyoi Group (Groeber, 1946; Kleiman and Japas, 2009) are thought to underlie Jurassic backarc deposits in Chile and Argentina (Charrier et al., 2007; Legarreta and Uliana, 1996).

Backarc deposits of the Neuquén Basin of Argentina are world-renowned for their nearly complete Jurassic to Early Cretaceous fossil record (Riccardi et al., 1983; Howell et al., 2005). Predominantly marine and marginal-marine deposits record sedimentation in eastern margin and axial settings of the Neuquén Basin (Davidson and Vicente, 1973), i.e., well to the east of Jurassic arc volcanoes. Deposits generally thin towards the east and are dominated by siliciclastic material derived from pre-Jurassic sources to the south and east, with subordinate carbonate and evaporite deposits and sparse volcanic intercalations thought to be arc-derived based on Jurassic U-Pb ages (Legarreta and Uliana, 1996; Kamo and Riccardi, 2009).

Jurassic successions in eastern Chile are typically less well exposed and more structurally complex than correlative units in Argentina. Stratigraphic and geochronologic work on Jurassic successions of the Principal Cordillera in Chile has therefore mainly relied

on biostratigraphic correlations with Argentinian successions. Precise ages of key Jurassic successions (e.g. Nacientes del Teno Formation) have remained poorly constrained, as upper Middle to Late Jurassic (168-145 Ma) stage boundaries are poorly constrained (Kamo and Riccardi, 2009). Jurassic backarc deposits in Chile include the Nacientes del Teno Formation at 35.10°S (Klohn, 1960; Davidson and Vicente, 1973) and between 36°S and 37°S (informal "Estratos del Toro" unit (Cornejo Carreño et al., 1982)), the Valle Grande Formation (Gonzales and Vergara, 1962) at 35.5°S, and the Nacientes del Biobio Formation (De la Cruz and Suarez, 1997) at 38.5°S. These units have been described as predominantly marine volcaniclastic rocks and calcareous sandstones, subordinate carbonates and evaporites, and sparse volcanic intercalations. An exception occurs at 38.5°S, where volcanic deposits consisting of pillow basalts, breccias, and basaltic lavas several hundred meters thick constitute a substantial proportion of the Jurassic sequence (De la Cruz and Suarez, 1997).

The latest Late Jurassic in eastern central Chile is represented by continental volcanic and volcaniclastic deposits of the Rio Damas Formation (Klohn, 1960), and, farther east, by time-equivalent sedimentary deposits of the Tordillo Formation (Klohn, 1960; Arcos, 1987). Rio Damas Formation volcanic detritus has been interpreted as derived from either the main magmatic arc located along the present day Coastal Cordillera (Davidson, 1971; Davidson and Vicente, 1973; Rossel et al., 2014), an "andesitic volcanic arc" located some distance inboard of a "rhyodacitic volcanic arc" located along the present day Coastal Cordillera (Vicente, 1976), or backarc volcanic systems (Charrier et al., 2007). Correlative backarc continental deposits in northern Chile (Lagunillas Formation, 26°-31°S) indicate that the regression represented by Late Jurassic backarc continental deposits was regional in extent, although no consensus has been reached concerning what caused this regression (Charrier et

al. 2007; Vicente, 2005; Hallam, 1991; Rossel et al. 2014; Spalletti et al. 2008; Mpodozis and Cornejo 1988).

3. PREVIOUS WORK ON THE NACIENTES DEL TENO FORMATION

The Nacimiento del Teno field area (Fig. 2) was first investigated by Burckhardt (1900), who focused on marine fossils in the Mesozoic units. The field area contains all the outcrops in Chile originally included within the Nacientes del Teno Formation by Klohn (1960), who was first to map the geology of the region. Klohn (1960) divided the Nacientes del Teno Formation into two lower members of uncertain stratigraphic position, the clastic Quebrada la Zorra and Valle Villagra members, and an upper section consisting of the clastic and carbonate Rinconada member and overlying evaporitic and carbonate Santa Elena member. Klohn (1960) tentatively estimated the Nacientes del Teno Formation thickness at approximately 1600 m while recognizing that snow cover and the presence of undetected structures added considerable uncertainty to his estimates. The age of the Nacientes del Teno Formation was reported as Bajocian to Oxfordian (170-157 Ma) based on ammonite biostratigraphy (Klohn, 1960).

Summary descriptions of the Nacientes del Teno Formation members of Klohn (1960) follow: The Quebrada la Zorra member consists of marine sedimentary rocks with a ~50 m thick interval of quartz-rich tuffite near the member base. Klohn (1960) tentatively assigned a Triassic age to the tuffite and assigned the Quebrada la Zorra member to the base of the formation, in part based on (1) compositional similarities between the tuffite and rhyolite ignimbrites of suspected Triassic age nearby in Argentina, and (2) the position of the member in the core of the Teno anticline, a regionally extensive, ~20 km wavelength fold affecting Mesozoic units (Klohn 1960). The Valle Villagra member consists of purple, dark

gray, dark red, and red sandstone and conglomerate with abundant andesite clasts, as well as green sandstone and conglomerate with andesite clasts, and gray calcareous sandstone and yellowish marls. The Rinconada member yielded Callovian bivalves and ammonites and consists, in ascending order, of sandstone and conglomerate intervals of poorly constrained thickness, approximately 70 m of fossiliferous limestone, and approximately 80 m of very dark gray calcareous shale with abundant microfolds and no fossils. The Santa Elena member concordantly overlies the Rinconada member and consists of gypsum and anhydrite evaporite deposits that yielded Oxfordian fossils.

Early authors described the Rio Damas Formation as concordantly overlying the Santa Elena member (Klohn, 1960; Gonzales and Vergara, 1962; Davidson and Vicente, 1973); elsewhere this contact has been described as locally unconformable (Mescua et al., 2011; Charrier et al., 2007).

Davidson (1971), Davidson and Vicente (1973), and Davidson (1988) conducted stratigraphic investigations and additional reconnaissance mapping to reconstruct Jurassic paleogeography at the latitude of the field area. These authors estimated a thickness of 500-750 m for the Nacientes del Teno Formation and concluded the formation was deposited primarily by debris flows and turbidity currents onto submarine fans that built a prograding volcaniclastic apron. Based on the abundance of andesitic clasts and fragmented pumice, Davidson (1988) proposed that the fans were supplied by volcaniclastic debris derived from erosion of the Jurassic Horqueta and Altos de Hualmapu formations that crop out today within the Coastal Cordillera.

4. METHODS

A. Geologic mapping

Geologic mapping was conducted at a scale of 1:5,000 (Fig. 2) in areas with accessible Jurassic outcrops, and in less detail elsewhere. Representative sections distributed across the field area (Fig. 3-4) were analyzed to identify spatial variations in key sedimentological features, thickness, and composition. Unit contacts and major structures were characterized and precisely mapped in the field using handheld GPS and traditional field methods. Direct field measurement of unit thicknesses was typically precluded by the rugged relief. Accordingly, thickness estimates for each of the representative sections (Fig. 4) were calculated trigonometrically from bedding attitudes, a 30 m resolution digital elevation model (NASA, 2014), and precisely mapped unit contacts. Within subaerial horizons of the Nacientes del Teno Formation (Jnt_{B3}), 14 unidirectional and 16 bidirectional paleocurrent indicators were measured and unrotated to restore bedding to horizontal (Fig. 3B, 5O). The amount of rotation about a vertical axis by Jnt_B beds is not known and adds additional uncertainty to paleocurrent directions.

B. U-Pb geochronology

Sampling sites for zircon geochronology were selected so as to best represent the suite of Jurassic units and subunits characterized during field studies. Samples collected from the Nacientes del Teno Formation (Jnt) include two (Jnt_C-001 and Jnt_C-750) from a primary rhyolite ignimbrite, five (Jnt_{A1}-088, Jnt_{A2}-019, Jnt_{A2}-070, Jnt_{A2}-005, Jnt_{D1}-274) from different intervals of marine sandstone, and one (Jnt_{B1}-279) from a bed of subaerial to transitional fine-grained red sandstone. In addition, two samples were collected from the Rio Damas Formation (Jrd) including one from a bed of fine- to medium-grained fluvial sandstone (Jrd-

001) and one from a 0.5 m-diameter andesite cobble (Jrd-007) from a fluvial conglomerate. For detrital zircon samples, outcrops of well sorted sandstone with high hornblende, biotite, and quartz content and low pyroxene content were selected to maximize zircon yield. Outcrop alteration state was generally ignored in light of the resistance of the mineral zircon to hydrothermal alteration. To assess relative zircon abundances, a similar amount of material (2 ~1-liter bags) was collected for each detrital zircon sample. A single one-liter bag of material was collected for primary volcanic zircon samples from the ignimbrite (Jnt_C-001 and Jnt_C-750).

Samples were crushed and sieved to <350 μm, then processed on a water table to concentrate "heavy" minerals. This concentrate was repeatedly run through a Frantz magnetic separator to acquire a non-magnetic (< 60V) separate. The ρ>3.3 fraction of the non-magnetic separate was sunk in methylene iodide to produce a heavy mineral concentrate. Separates of samples Jrd-007, Jnt_{D1}-274, and Jnt_{A1}-088 each yielded fewer than 22 zircons, all of which were mounted in epoxy, polished to expose grain interiors, and analyzed. Separates of the remaining samples (Jrd-001, Jnt_C-750, Jnt_C-001, Jnt_{B1}-279, Jnt_{A2}-005, Jnt_{A2}-070, Jnt_{A2}-019) each yielded hundreds to thousands of zircon grains. For these samples, repeated splits of bulk grain piles resulted in the random selection of ~300 grains that were then mounted in epoxy and polished to expose grain interiors. Final selection of grains to be analyzed was accomplished by randomly selecting fields of view within a sample mount, then analyzing all visible grains with polished surfaces large enough to accommodate the laser spot size. This process was repeated until the desired number of grains was analyzed.

U-Pb data were collected on the LA-ICP-MS facility at the Department of Earth Sciences of the University of California Santa Barbara (Cottle et al., 2012, 2013).

Instrumentation consisted of a Photon Machines 4-ns-pulse duration, 193-nm-wavelength ArF excimer laser attached to a Nu Plasma HR multicollector (MC) ICP-MS configured to measure U, Th, and Pb isotopic ratios. Samples were analyzed over four sessions. Samples analyzed and analytical conditions set during each session are provided in Table 3. Data reduction, including corrections for baseline, instrumental drift, mass bias, and down-hole fractionation was performed in Igor Pro and the plugin Iolite v. 2.1.3 (Paton et al., 2010). For all analyzes, "91500" (Wiedenbeck et al., 1995) was the primary reference zircon used to monitor and correct for instrumental drift, mass bias, and down-hole interelement fractionation. Secondary reference zircons were analyzed between runs and treated as unknowns to assess accuracy and precision within each analytical session. For all analytical sessions, secondary reference zircons "GJ-1" (Jackson et al., 2004) and "Plešovice" (Sláma et al., 2008) were analyzed. "Peixe" (Dickinson and Gehrels, 2003) was used as an additional secondary reference zircon for sessions 1 and 2 (Table 3).

All uncertainties are quoted at 2σ and include contributions from the reproducibility of reference zircons for $^{207}Pb/^{206}Pb$, $^{206}Pb/^{238}U$, and $^{207}Pb/^{235}U$. A common-$^{207}Pb/^{206}Pb$ value of 0.837 (Stacey and Kramers, 1975) was used to calculate ^{207}Pb-corrected ages. All U-Pb data were originally plotted using the Isoplot Excel plugin version 3.75 (Ludwig, 2012).

For all samples, zircon rims were targeted in an attempt to measure the youngest crystallization age of each grain. 40 grains were analyzed from each primary volcanic sample. For detrital zircon samples that yielded fewer than 120 zircon grains, all grains were separately analyzed. For detrital zircon samples that yielded abundant zircon grains (except Jnt_{A2}-019, which was misidentified during field work as a primary volcanic deposit), a minimum of 117 grains were analyzed to maximize the probability of detecting all major

components of the detrital zircon population (Vermeesch, 2004). Sample coordinates and complete geochronology results are provided in Appendix A.

4. GEOLOGIC FRAMEWORK OF THE NACIENTES DEL TENO REGION

A. Overview

A major focus of this study is the stratigraphy of the Jurassic units of the Nacimiento del Teno field area. Isolated outcrops offer excellent exposures of Jurassic units (Fig. 5A), but correlations between some of the isolated outcrops remain unclear due to widespread cover of Jurassic rocks by younger units, and due to structural complexity. In addition to the ENE-WSW oriented Teno anticline, Jurassic units are affected by abundant folds with wavelengths ranging from centimeters to hundreds of meters. Several populations of faults cut Jurassic units, including the youngest population of oblique right-lateral strike slip faults trending from SSW-NNE to SSE-NNW; north-, south-, and west-dipping normal faults; and a population of subhorizontal thrust faults cut by the previously mentioned faults. Field observations and the great diversity of orientations and senses of slip on faults suggest significant portions of the field area may have been affected by recent slumps and landsliding.

The oldest rocks in the field area all belong to the Nacientes del Teno Formation (Jnt), which crops out within the core of the Teno anticline. Outcrops form an ENE- to WSW-trending swath that runs roughly parallel to the Rio Nacimiento del Teno drainage in the north-central portion of the field area, extends to the southwest within the Rio Vergara drainage and Cajón Villagra, and extends east into Argentina across the Paso de Santa Elena (Fig. 2).

Jnt_A, the lowest exposed unit of the Nacientes del Teno Formation, consists of fine- to coarse-grained greenish gray and brown marine sandstone and mudstone beds that transition upwards into coarsening upward packages of greenish brown marine sandstone and conglomerate deposits. Toward the top of unit Jnt_A, marine strata appear to interdigitate with coarsening-upwards, red sedimentary strata and subordinate mafic to intermediate lava flows of Jnt_B. Jnt_B deposits are conformably overlain by pale green, purple, and gray rhyolitic rocks of unit Jnt_C, including a quartz-bearing rhyolite ignimbrite. Jnt_D marine strata are deposited on Jnt_C rocks and consist of sandstone, siltstone, conglomerate, shale and carbonate. The top of the Nacientes del Teno Formation consists of calcareous gypsum and anhydrite deposits of Jnt_E, which conformably overlie Jnt_D strata. A cumulative thickness of ~1 km is estimated for the Nacientes del Teno Formation, although the depositional base of the formation is not exposed in (Fig. 4).

Volcaniclastic and volcanic strata of the Late Jurassic Rio Damas Formation (Jrd) crop out in both limbs of the Teno anticline and overlie Nacientes del Teno strata along an unexposed and locally discordant contact. Along the western edge of the field area, an angular unconformity separates the Nacientes del Teno Formation from volcanic and volcaniclastic deposits of the Cretaceous-Miocene Abanico Formation (KTab) (Charrier et al., 1996, 2007). In the remainder of the field area, Nacientes del Teno Formation strata are unconformably overlain by Plio-Pleistocene rhyolite ignimbrites and andesite lavas (QT_{uv}) (personal communication, Phil Gans, February 8, 2015) that extend north from the international border and pinch out along the southern flank of the Nacimiento del Teno drainage, and by Recent unconsolidated deposits mapped as younger alluvium (Q_{a2}), older

alluvium (Q_{a1}), landslide deposits (Q_{ls}), and talus (Q_t). Jurassic units are cut by an extensive system of Miocene dacitic dikes and sills (Ti).

B. Lithostratigraphy

i. Jnt_A

The oldest rock unit crops out in the western half of the field area. This unit is dominated by broadly coarsening and shallowing upward sequences of volcaniclastic turbidites and other subaqueous gravity flow deposits with volumetrically subordinate intercalations of laminated mudstone and carbonate.

Deposits weather to dark green, dark brown, dark gray, and in the case of beds with high carbonate content, tan brown to orange (Fig. 5B). Coarser, more resistant intervals form cliffs over 100 m tall that crop out from rubbly slopes of talus and colluvium. Finer, less resistant intervals are best exposed in canyon walls of steeply incised drainages.

Jnt_A reaches a maximum exposed thickness in the center of the field area, where a ~620 m thick section crops out in the streambeds of the Estero de Guanaco and adjacent portions of the Rio Nacimiento del Teno (Fig. 2). This section contains a ~100 m thick lower subunit (Jnt_{A1}) dominated by sandstone and mudstone that transitions to an upper subunit (Jnt_{A2}) dominated by sandstone and conglomerate. At locations to the west the lower Jnt_A strata (Jnt_{A1}) are not exposed, but outcrops up to 300 m thick of upper Jnt_A strata (Jnt_{A2}) are exposed on the slopes of the Rio de Vergara drainage and on the southeast slope of the Cajón Villagra.

The lower ~100 m of Jnt_A strata (Jnt_{A1}) are dominated by cyclic, normally graded sequences of 10-50 cm thick beds of immature sandstone, siltstone, and mudstone interpreted as volcaniclastic turbidites (geochronology sample Jnt_{A1}-088). Intercalated within the

turbidites are sparse ~1 m thick beds of massive, medium- to coarse-grained sandstone interpreted as individual subaqueous sandy debris flow deposits or high concentration turbidites, as well as sparse laminated carbonate and mudstone deposits representing periods of suspension settling between the arrivals of subaqueous mass flows. Jnt_{A1} strata show no signs of soft-sediment deformation. In addition, although Jnt_{A1} strata exhibit sparse, faint impressions of indistinct mollusk remains, no identifiable ammonite remains were observed in this unit.

Jnt_{A2} strata consist of multiple cyclic, broadly coarsening-upwards sequences 100s of m in thickness (Fig. 5B). These consist of predominantly sandstone and conglomerate with subordinate laminated carbonate and mudstone. Each coarsening-upwards package culminates in a capping interval tens of meters in thickness dominated by 1-10 m thick beds of conglomerate.

Conglomerate deposits include orthoconglomerate and paraconglomerate. Some paraconglomerate deposits are interpreted as olistostromes (Fig. 5C). These consist of a mélange of angular, laminated, commonly deformed carbonate and shale olistoliths of a lithology consistent with fine-grained beds distributed throughout unit Jnt_A, as well as sparse subrounded to subangular, pebble- to cobble-sized andesitic clasts in a coarse-grained sandy matrix. Orthoconglomerate deposits are interpreted as subaqueous debris flow deposits and contain a coarse-grained sandy matrix and pebble- to cobble-sized andesitic clasts. Some orthoconglomerate deposits contain well-rounded andesitic cobbles, likely derived from a beach or fluvial environment (Fig. 5D).

As with Jnt_{A1}, finer-grained Jnt_{A2} strata include normally graded volcaniclastic turbidite sequences of sandstone, siltstone, and mudstone (Fig. 5E), as well as massive

sandstone beds and sparse laminated carbonate and mudstone deposits. Jnt_{A2} contains a higher proportion of massive sandstone beds than Jnt_{A1}, several of which contain sparse pumice fragments altered to clay minerals, and quartz (geochronology samples Jnt_{A2}-005, Jnt_{A2}-019, and Jnt_{A2}-070 collected from quartz-bearing Jnt_{A2} sandstone beds). Also in contrast to Jnt_{A1}, laminated carbonate and mudstone beds from Jnt_{A2} commonly show signs of soft sediment deformation (slumping) (Fig. 5F), although no consistent orientation in slump direction was identified in the field. Abundant ammonite remains occur within unit Jnt_{A2}.

In the center of the field area (Fig. 4 columns 8.1-8.2), a lateral facies transition occurs between Jnt_{A2}, Jnt_{B3} and Jnt_C. At this location, Jnt_{A2} carbonate-supported sandstone and conglomerate with abundant fragmented shelly debris transition upwards into a coarse-grained volcaniclastic sandstone composed mainly of tightly packed angular feldspar altered to clay, along with sparse pumice fragments altered to clay, and abundant quartz. These deposits are interpreted as reworked beach and/or nearshore marine facies equivalent to Jnt_{B3} volcaniclastic apron deposits and the overlying Jnt_C ignimbrite, respectively. A similar subaerial to submarine lateral facies transition likely underlies Recent cover in the northwest of the field area (Fig. 4 columns 4-5).

ii. Jnt_B

Jnt_B consists of a coarsening-upwards sequence of finer-grained (Jnt_{B1}) and coarser-grained (Jnt_{B3}) volcaniclastic red beds with intercalated basaltic-andesite lava and/or volcanic breccia deposits (Jnt_{B2}). Clasts are subrounded to subangular, variably altered andesite, with the exception of mudstone rip-up clasts clearly sourced from Jnt_{B3} mudstone laminae.

Jnt_{B1} strata are easily eroded, form very steep slopes covered in colluvium, and are best observed in steeply incised canyon walls. Strata are mostly dark red to brown in color, but pale green to gray intervals occur towards the lowest exposed levels of the unit, giving outcrops a mottled appearance. Jnt_{B2} deposits, exposed mainly within inaccessible cliffs, are very rubbly, hydrothermally altered, and dark brown and purple in color. Jnt_{B3} strata form red, purplish-gray, and reddish-gray ledges that form resistant outcrops and are well-exposed across much of the field area.

Exposed Jnt_B sections range from ~40-340 m thick and generally thin towards the east, west, and south and thicken towards the north and center of the field area. In the western half of the field area (Fig. 2), Jnt_{B1} strata are absent and Jnt_{B3} strata intercalate with and transition downward into green-colored pebbly sandstone, pebble conglomerate, and coarse conglomerate assigned to the uppermost portion of unit Jnt_{A2} (Fig. 4 columns 5-8). Within sections surveyed in the eastern-central part of the field area, the base of Jnt_{B3} either is not exposed (Fig. 4 columns 9-10, and 12-13), or undergoes a gradational transition down section into Jnt_{B1} (Fig. 4 column 11). In the easternmost part of the field area, less than one kilometer east of the international border, Jnt_{B3} strata are absent and Jnt_{B1} strata directly underlie Jnt_C deposits (Fig. 4 column 16). The depositional base of Jnt_{B1} is not exposed in the field area.

Towards the center of the field area, sparse, 2-40 m thick intercalations of basaltic-andesite lava deposits and/or volcanic breccia deposits (Fig. 5G) crop out at various stratigraphic levels within Jnt_B and are grouped into subunit Jnt_{B2}.

Jnt_{B1} consists predominantly of thinly-bedded, broadly coarsening-upwards, rhythmic deposits of micaceous siltstone and fine-grained sandstone. Although most beds are plane-laminated, rare outcrops exhibit ripple cross-lamination, symmetric ripples (indicating

oscillating current), and wavy bedding (Fig. 5H). Based on sedimentary structures, fine grain size, and red color, Jnt_{B1} deposits are interpreted as shallow marine deltaic deposits interfingering with subaerial distal fan deposits.

Jnt_{B3} is composed of a broadly coarsening-upwards sequence of rhythmic, poorly sorted red beds that include pebbly and sandy mudstone, medium- to coarse-grained sandstone, sandy pebble conglomerate, sandy coarse conglomerate, and mudstone laminae. In the thickest exposed Jnt_{B3} section, located in the north of the field area (Fig. 4 column 11), the lowermost ~75 m of strata consist of thin (1-10 cm), tabular beds of poorly sorted sandstone and sandy mudstone interpreted as sheet flood deposits (geochronology sample Jnt_{B3}-279); thin to medium (10-30 cm) lenses of conglomerate and moderately well sorted sandstone with cross beds interpreted as shallow braided stream deposits; and several thick (0.5-3 m) tabular beds of matrix-supported pebbly mudstone interpreted as debris flow deposits.

75 m above the base of the thickest exposed section of Jnt_{B3}, beds transition over the span of a few meters from dominated by mud- and sand- sized clasts to sand- and pebble-sized clasts. The next ~150 m of strata at this location, and all but the uppermost ~30 m of strata at other exposed sections of Jnt_{B3}, are dominated by tabular, well bedded, thin to thick (1-50 cm) beds of poorly sorted coarse-grained sandstone, moderately well sorted sandstone with cross bedding, and pebble conglomerate. These deposits are indicative of highly unsteady and non-uniform flows, and are interpreted as shallow braided stream, sheet flood, and debris flow deposits.

The best-exposed and most accessible Jnt_{B3} outcrops are formed by the uppermost ~30 m of the unit. These outcrops at all locations contain tabular and lenticular deposits of

sandstone and pebble conglomerate (interpreted as debris flow, sheet flood, and shallow braided stream deposits), as well as thick (1-3 m) deposits of coarse orthoconglomerate and paraconglomerate (interpreted as debris flow and possibly debris avalanche deposits). Both tabular (Fig. 5I) and channelized (Fig. 5H, 5K) conglomerate deposits are present, some channels cutting several meters into underlying strata (Fig. 5K). Clasts in coarse conglomerate deposits range from subrounded (Fig. 5J) to angular and reach 50 cm in diameter (Fig. 5L, 5I), although most clasts are 0.5 to 5 cm in diameter. Ortho- and paraconglomerate matrices consist of medium- to coarse-grained, poorly sorted sand composed predominantly of angular altered feldspar grains and clay minerals. Sandstone deposits are the same composition as conglomerate matrix and include tabular, massively bedded, poorly sorted sandstone beds with no sedimentary features and commonly with upper contacts eroded to form cut and fill structures (Fig. 5J, 5I); as well as moderately well sorted, lenticular sandstone deposits exhibiting cross bedding. The uppermost ~30 m of Jnt_{B3} contains volumetrically subordinate laminations of mudstone that exhibit mudcracks (Fig. 5L, 5M), often with curled edges, and raindrop impressions (Fig. 5N), confirming a subaerial terrestrial environment. Sparse mudstone rip-up clasts with curled edges are entrained in some deposits. Also within the upper 30 m of Jnt_{B3}, finer-grained intervals host very sparse paleocurrent indicators, including ripples, obstacle scours (Fig. 5O), flutes and grooves, and parting lineations. A total of 14 unidirectional and 16 bidirectional indicators were measured, unrotated along strike, and plotted on rose diagrams (Fig. 3B). Paleocurrent data are consistent with a west to east transport direction.

iii. Jnt_C

Jnt_C consists of a quartz-bearing rhyolite ignimbrite and associated fall and possibly surge deposits, as well as reworked versions of the same rocks. Jnt_C overlies Jnt_B red beds along a sharp, unambiguously depositional contact (Fig. 5P), except at the northwest end of the field area (Fig. 4 column 4), where Jnt_C deposits overlie green volcaniclastic conglomerate deposits interpreted as shallow marine Jnt_{A2} deposits.

Jnt_C varies in appearance significantly across the field area, reflecting degree of welding and predominant clast type. Welded deposits form thick (0.5-1 m), gray to pale lavender, resistant ledges. Unwelded deposits, including fall/surge deposits and epiclastic pumiceous sandstone, range in color from very pale turquoise-gray (predominantly fine-grained altered ash) to dark gray (lithic-rich) to deep turquoise (altered pumice-rich). Unwelded deposits are typically less resistant than adjacent units and form recessed outcrops.

Jnt_C ranges in thickness from ~20 to ~80 m, with thicker deposits located in the northwest, north, and central portion of the field area (Fig.4 columns 4, 8, 11-13). In the northwest of the field area (Fig. 4 column 4), Jnt_C consists of a thick (80 m), dark gray, poorly sorted, pumice-poor, lithic- and crystal-rich volcaniclastic sandstone (geochronology sample Jnt_C-750). Based on its low proportion of altered pumice and its deposition on green volcaniclastic conglomerate deposits interpreted as marine (Jnt_{A2}), the Jnt_C sandstone is interpreted to represent reworked and redeposited unwelded pyroclastic sediments deposited in a shallow marine environment.

At one location in the northeast of the field area (Fig. 4 column 13), the uppermost ~20 m of Jnt_C consists of massively bedded reworked pyroclastic material sparsely

intercalated with thin (10-20 cm) tabular, normally graded, fine- to medium-grained sandstone beds interpreted as volcaniclastic turbidites.

The most densely welded Jnt_C deposit crops out in the center of the field area (Fig. 4 column 8.1). Here, the base of the unit consists of <10 cm of coarse-grained, well sorted, crystal- and lithic fragment-rich deposits suggestive of a basal surge or fallout origin (Fig. 5P). Overlying the basal deposits is a medium- to coarse-grained (~0.2-5 mm), crystal rich (~15%), welded ignimbrite with 10-12% milky feldspar, abundant quartz (2-4%), <2% biotite, highly flattened pumice lapilli (~1%) that define a subtle compaction foliation, and a matrix of purple-colored clay devitrification products. No cooling breaks or epiclastic deposits were observed within the ignimbrite, indicating the deposit represents a single cooling unit.

iv. Jnt_D

Jnt_D consists of a ~150 m thick sequence of marine sedimentary rocks divided into three subunits: greenish-gray, very well-bedded, volcaniclastic fine-grained sandstone turbidites with intercalations of conglomerate (interpreted as debris flow and possibly rock avalanche deposits) (Jnt_{D1}); fossiliferous intercalated sandy limestone and fine- to coarse-grained sandstone (Jnt_{D2}); and fossil-poor light to dark brown calcareous siltstone and shale (Jnt_{D3}). Unit Jnt_D overlies the Jnt_C rhyolite along a depositional contact.

Jnt_D color variations and resistance to weathering appear to be largely controlled by carbonate content, with more calcareous strata (e.g. Jnt_{D2}) forming tan brown to orange, more recessed, more gently sloping cliff faces and plateaus, and less calcareous strata (e.g. Jnt_{D1}) forming greenish-gray, steep cliffs (Fig. 5A).

Jnt_D is relatively uniform in thickness across the field area but varies in terms of lithology. The majority of Jnt_D consists of volcaniclastic deposits (Jnt_{D1}). These are dominated by well-bedded turbidites in the center of the field area (Fig. 4 column 8) and consist of roughly equal proportions of turbidites and cobble conglomerate in the northwest and east-central parts of the field area (Fig. 4 columns 3, 11-13). Towards the eastern (Fig. 4 columns 14, 16) and southwestern (Fig. 4 column 6) edges of the field area, volcaniclastic strata (Jnt_{D1}) grade upward and laterally into calcareous sandstone and sandy limestone (Jnt_{D2}) (Fig. 5Q). A similar upward and lateral transition likely separates calcareous sandstone and sandy limestone deposits (Jnt_{D2}) from deeper marine calcareous siltstone and shale (Jnt_{D3}) observed in the easternmost portion of the field area (Fig. 4 column 15), although the transition between these two units is not well exposed.

Jnt_{D1} consists of a marine sequence of predominantly fine- to coarse-grained volcaniclastic sandstone and conglomerate, along with siltstone, and subordinate limestone and shale. The lowermost Jnt_{D1} beds are coarse-grained sandstone and pebble conglomerate with minor quartz (<1%) and altered pumice fragments (~5%) derived from reworking of underlying Jnt_C rhyolite deposits. Up section, the unit transitions into cycling, normally graded sequences of very well bedded sandstone, siltstone, shale, and sparse pebble conglomerate (Fig. 5R). These beds, ranging from 10-40 cm in thickness, contain abundant ammonite fossils (Fig. 6b-c) and exhibit asymmetric linear ripple trains and graded beds, suggesting sub wave base deposition by turbidity currents. Most beds also contain variable amounts of biotite and angular lithic fragments suggestive of a volcanic source. Very sparse beds contain coarse quartz grains and fragments of altered pumice. Towards the top of Jnt_{D1}, channelized green and purple conglomerate deposits cut underlying finer-grained strata; the

conglomerate deposits are both clast- and matrix-supported with subrounded to angular, andesitic clasts typically <10 cm in diameter (Fig. 5Q, 5S).

Jnt_{D2} consist of light to dark gray calcareous sandstone, siltstone, and shale. It contains abundant ammonite fossils. Algal laminations and abundant shelly debris crop out within the westernmost exposures of Jnt_{D2}.

Jnt_{D3} consists of dark gray calcareous shale observed at two locations near the northern (Fig. 4 column 11) and eastern (Fig. 4 column 15) edges of the field area. Beds contain no visible fossils and exhibit a tight undulating foliation (10 cm wavelength) roughly equivalent in attitude to underlying Jnt_{D2} bedding.

v. Jnt_E

Silty, calcareous gypsum deposits constitute Jnt_E. Deposits vary significantly in thickness (3- ~100 m) but exhibit similar lithology across the field area. In the northwest, gypsum is scarcer and significantly thinner and more deformed than at other locations, suggestive of partial removal of the unit by faulting or dissolution. White to dark gray bands (<mm-1 cm thick) reflect variations in carbonate content. Bands exhibit intense microfolds (<1 cm wavelength) with inconsistent orientations and geometries. Microfolds and the geometry of outcrops suggest highly variable bedding attitudes.

vi. Jurassic Rio Damas Formation (Jrd)

The lower several hundred meters of the Jurassic Rio Damas Formation are exposed in the field area (Klohn, 1960). This unit is poorly exposed, with scattered recessive outcrops and indistinct bedding. The majority of outcrops are colored purplish-brown and are steep, crumbly, and difficult to access, and it is not always clear whether the rocks are in place. The

best exposed Jrd rocks crop out in the north-central part of the field area at the bottom of the Quebrada La Zorra, and within gullies cut into steep hillslopes.

The bulk of the Rio Damas Formation in the field area consists of volcaniclastic sandstone, paraconglomerate, and orthoconglomerate (Fig. 5T). Conglomerate clasts are well-rounded, exclusively andesitic, and generally 1-10 cm, with some clasts approaching 1 m. Stacked basaltic lava flow deposits overlie Jrd fluvial deposits at the northwest edge of the field area (Fig. 4 column 3). These flows measure at least 200 m in cumulative thickness. The lowermost flow exhibits a heavily vesiculated rubbly base and massive interior, and contains abundant plagioclase phenocrysts and glomerocrysts >1 cm in diameter. The north-central part of the field area (Fig. 4 column 8) hosts an outcrop of abundant cm- to dm-sized angular andesite blocks in an ashy matrix, suggestive of a block and ash flow deposit.

The nature of the contact between the Nacientes del Teno Formation and Rio Damas Formation is not clear and may not be the same in all parts of the field area. In the southwest corner and across the eastern third of the field area (Fig. 2), talus and colluvium obscure the upper and lower contacts of Jnt_E, and bedding planes are difficult to observe in overlying Jrd deposits. A single Jrd bedding plane measured in the eastern third of the field area (Fig. 2, north bank of Estero Tiburcio) is consistent with bedding of underlying Jnt_D strata, perhaps consistent with a depositional contact. In the northwest corner of the field area, Jnt_D strata are in contact with a 0 to ~4 m thick sliver of gypsum discordantly overlain by well exposed, well bedded Jrd strata, indicating a faulted contact or angular unconformity. The contacts between Jnt_D, Jnt_E, and Jrd are conspicuously faulted where exposed in canyons in the north-central part of the field area.

vii. Post-Jurassic units

In the western part of the map area, Jnt_A, Jnt_{D1}, and Jnt_{D2} (?) are discordantly overlain by strata Late Cretaceous to Miocene Abanico Formation (Charrier et al., 1996), a suite of volcanic and volcaniclastic rocks. The remaining units in the field area are undifferentiated Plio-Pleistocene volcanic and volcaniclastic deposits and Quaternary cover. Post-Jurassic units were not investigated as part of this work.

5. U-PB GEOCHRONOLOGY OF JURASSIC UNITS

A. Summary

All analyses of individual grains from each sample are shown in Figure 7. A 10% discordancy filter was applied to single-grain analyses that yielded ages younger than 800 Ma, resulting in the rejection of 37 of 625 (~6%) of analyses. Seven analyses were older than 800 Ma, all of which were within 80% concordant. Four analyses had ages >1400 Ma and for which $^{207}Pb/^{206}Pb$ ages are used in Figure 7 and Appendix A; all other single-grain ages are reported as ^{207}Pb-corrected $^{206}Pb/^{238}U$ ages. Full geochronology results are provided in Appendix A.

Estimated depositional ages were calculated in three different ways, depending on the nature of the sample and zircon systematics. The three different approaches are explained below.

<u>Weighted mean of all concordant ages younger than 200 Ma</u>: Sedimentation caused by stratovolcano erosion is commonly most rapid immediately after large eruptions (Hackett and Houghton, 1989); thus large eruptions register nearly instantly (a few hundred to a few hundreds of thousands of years) in the sedimentary record (Kuenzi et al., 1979; Vessel and Davies, 1981). For each of the four samples from units Jnt_{A2} and Jnt_{B1}, single-grain ages are

clustered tightly together, with ~90% of Jurassic ages overlapping within uncertainty. Based on the tight distribution of single-grain ages, the source rocks for these sedimentary rocks are interpreted as volcanic deposits (tephra, lava flows) erupted immediately prior to the deposition of the sampled sedimentary rocks. For each of these samples, we therefore consider the mean of all the concordant Jurassic zircon ages as very close to the depositional age of the sampled stratum, and interpret this age as dating a pulse in both volcanic activity and sedimentation.

Weighted mean of the youngest 10 concordant ages that overlap within 2σ uncertainty: Samples Jrd-001, Jrd-007, Jnt_{D1}-274, and Jnt_{A1}-088 each yielded either few zircons or a large number of zircons having an age spread well beyond what would be expected from just analytical uncertainties. It is thus unclear how much time elapsed between the crystallization of the youngest zircons and the deposition of the sampled stratum. For these samples, a maximum depositional age was determined by calculating the weighted mean of the cluster of the youngest 10 concordant ages that overlap within 2σ uncertainty (Dickinson and Gehrels, 2009) (Table 1).

Lower intercept age: For primary volcanic deposits in which the crystallization ages of zircons are considered equivalent to their eruptive ages, the lower intercept age was chosen as the preferred age (Fig. 8).

B. Nacientes del Teno Formation magmatic zircons

Sample Jnt_C-001 is a crystal-rich, quartz-rich, pumiceous tuff from the interior of the welded ignimbrite cropping out at the Quebrada la Zorra locality (Fig. 2). The sample yielded abundant zircons, 40 of which were analyzed (Fig. 7). Four grains yielded discordant ages. Of the remaining 36 grains, one yielded an age of ca. 170 Ma, which we interpret as an

inherited/recycled grain. The remaining 35 grains yielded ages ranging from ca. 158-165 Ma, with a lower intercept age of 162 ± 3 Ma and an MSWD of 1.3 (Fig. 8c).

Sample Jnt_C-750 is a coarse rhyolitic sandstone from an unwelded, reworked upper portion of the Jnt_C ignimbrite ~2 m below a gradational contact with Jnt_D. The sample yielded abundant zircons, 44 of which were analyzed. Two grains yielded discordant ages. The remaining 42 grains yielded ages ranging from ca. 156-164 Ma, with a lower intercept age of 158 ± 3 Ma and an MSWD of 0.9.

Distributions of single-grain ages yielded by zircons from samples Jnt_C-001 and Jnt_C-750 (sampled from the same rock unit) are similar in slope and variance, but lower intercept ages calculated for each of the units differ by ~3 Ma. The two lower intercept ages overlap within uncertainty, and field observations confirm the two samples come from the same depositional unit Jnt_C. The difference in ages therefore is attributed to either long term uncertainty in reproducibility of secondary standards (as two the samples were analyzed in separate sessions over 24 months apart) or perhaps incorporation of a slightly younger group of zircons (e.g. post ignimbrite tephra eruption) into sample Jnt_C-750.

C. Nacientes del Teno Formation and Rio Damas Formation detrital zircons

Sample Jnt_{A1}-088 is a medium-grained, well sorted, immature sandstone from a 0.5 m thick bed 1 m above the exposed base of the thickest section of Jnt_A exposed in the field area. Eleven zircons grains were separated and analyzed, one of which yielded a discordant age. The remaining grains yielded ages ranging from ca. 167-175 Ma. The preferred age of 172 ± 3 Ma for sample Jnt_A-088 (Table 1) is the weighted mean age of all 10 concordant analyses.

Sample Jnt_{A2}-019 is a coarse-grained, crystal-rich, quartz-rich, pumiceous, poorly sorted sandstone collected from a 0.8 m thick bed from the uppermost strata of a 250 m thick

section of Jnt_{A2} located in the western part of the field area in the Valle Vergara. Forty zircons were analyzed, one of which was rejected for discordancy. The remaining grains yielded ages ranging from ca. 160-173 Ma. The preferred age of 166 ± 3 Ma for sample Jnt_{A2}-019 (Table 1) is the weighted mean age of all 39 concordant analyses.

Sample Jnt_{A2}-005 is a fine- to coarse-grained, poorly sorted, quartz- and feldspar-rich volcanic sandstone from a 0.5 m thick bed near the top of a 400 m thick section of Jnt_{A2} exposed in the center of the field area. A total of 120 grains were analyzed, 4 of which were rejected for discordancy. The remaining grains yielded single-grain ages that range from ca. 159-176 Ma. The preferred age of 165 ± 3 Ma for sample Jnt_{A2}-005 (Table 1) is the weighted mean age of all 116 concordant analyses.

Sample Jnt_{A2}-070 is a fine- to coarse-grained, poorly sorted, quartz- and feldspar-rich volcanic sandstone from a 1 m thick Jnt_{A2} bed several hundred meters up section from the bed that supplied sample Jnt_{A1}-088. A total of 120 grains were analyzed, of which 9 were rejected for discordancy. The remaining grains yielded single-grain ages that range from ca. 156-172 Ma. The preferred age of 165 ± 3 Ma for sample Jnt_{A2}-070 is the weighted mean age of all 111 concordant analyses (Table 1). The sample yielded several U-Pb ages significantly younger than the majority of analyses from the sample. These anomalously young analyses may reflect radiation damage to the zircon crystal and subsequent Pb loss (due to high U content). Rejecting all analyses with greater than 700 ppm U and recalculating the mean of the cluster of the youngest 10 concordant ages that overlap within 2σ uncertainty, all mean ages agree with the observed stratigraphy except for sample Jnt_{D1}-274 (Table 1). A full explanation for the disagreement between observed stratigraphy and the ages of the very youngest grains in select samples is beyond the scope of this study.

Sample Jnt_{B1}-279 is a fine- to medium-grained oxidized sandstone from a 0.1 m thick bed ~50 m above the base of the thickest section of Jnt_B exposed in the field area. A total of 120 grains were analyzed, five of which yielded discordant analyses. 105 grains yielded single-grain ages that range from ca. 156-193 Ma. The remaining ten grains yielded single-grain ages including five Permo-Triassic ages, one Carboniferous age, one Upper Devonian age, one Middle Ordovician age, and two Proterozoic ages. The preferred age of 165 ± 3 Ma for sample Jnt_{B1}-279 (Table 1) is the weighted mean age of all post 200 Ma concordant ages.

Sample Jnt_{D1}-274 is a medium-grained, moderately well sorted, immature sandstone from a 0.15 m thick bed <50 m below the contact with Jnt_E on the west bank of the Rio Nacimiento del Teno, directly west of the Paso Santa Elena. Of the 24 grains separated and analyzed, two were rejected for discordancy. Of the remaining grains, 17 yielded ages ranging from ca. 151-195 Ma, and five yielded Proterozoic ages (Fig. 8). The preferred age of 161 ± 3 Ma for sample Jnt_{D1}-274 (Table 1) is the weighted mean of the youngest ten concordant ages that overlap within uncertainty.

Sample Jrd-001 is a fine- to medium-grained, moderately well sorted, immature, oxidized sandstone from a sedimentary sequence of the Rio Damas Formation located ~35 m above a discordant contact with Jnt_E. The 135 grains analyzed yielded 128 concordant single-grain ages that range from ca. 148-183 Ma and one concordant age of ca. 283 Ma. The preferred age of 151 ± 3 Ma for sample Jrd-001 (Table 1) is the weighted mean of the youngest ten concordant ages that overlap within uncertainty.

Sample Jrd-007 is an andesite cobble from a conglomerate bed ~500 m from the exposed base of Jrd in the Quebrada la Zorra locality. Of the eight grains separated and analyzed, two yielded discordant ages, five yielded ages that range from ca. 160-165 Ma, and

one yielded an age of ca. 1196 Ma. The five concordant Jurassic zircons yielded a lower intercept age of 162 ± 3 Ma and an MSWD of 1.3. This age is viewed as a provenance age and suggests that some of the andesite detritus in the Rio Damas Formation was recycled from the Nacientes del Teno Formation or rocks of similar age.

6. AMMONITE BIOSTRATIGRAPHY

Photographs of the remains of 16 ammonite specimens (Fig. 6) from Jnt_A and Jnt_D were identified Alberto Riccardi of the Museo de La Plata, Argentina (Table 2) (personal communication, November 24, 2017). Stratigraphic level versus age of each ammonite specimen is plotted in Figure 9 alongside preferred U-Pb zircon ages. Ammonite identifications agree with isotopic ages within uncertainty.

7. DISCUSSION

A. Revised stratigraphy of the Nacientes del Teno Formation

The Middle to Late Jurassic Nacientes del Teno Formation (ca. 172-161 Ma) is dominated by a ~700 m-thick lower section (Jnt_A-Jnt_C) consisting of stacked sequences of progradational volcaniclastic deposits that generally coarsen upwards and westwards. These include marine strata that interfinger with and transition up section into a coarsening-upwards sequence of subaerial strata capped by a 20-80 m thick rhyolite ignimbrite. The lower section is overlain by a thinner, generally finer-grained (~250 m) upper section. The upper section consists of volcaniclastic and carbonate deposits (Jnt_D) that generally exhibit an upwards and eastwards decrease in grain size, decrease in volcanic content, and increase in carbonate content. Volcaniclastic and carbonate deposits from the upper section are overlain by

subordinate evaporite deposits (Jnt_E). Exposed sections of the Nacientes del Teno Formation reach ~1 km in thickness. The base of the formation is not exposed.

The significant addition to our understanding of the Nacientes del Teno Formation stratigraphy is the identification of a ca. 160 Ma rhyolite ignimbrite and associated fall deposits (Jnt_C). Rhyolitic rocks cropping out within the canyon walls of the Quebrada la Zorra (column 8 in Fig. 2-4; Fig. 5P) were tentatively interpreted by Klohn (1960) as "tuffites" representing reworked Permo-Triassic basement material redeposited near the base of the Nacientes del Teno Formation, and reported by Davidson and Vicente (1973) as consisting of Triassic basement with no exposed base. However, these rhyolitic rocks are welded at this and other locations and clearly overlie red beds (Jnt_B) along a depositional contact (Fig. 5P). The rhyolitic rocks are thus neither basement rocks nor reworked "tuffite" deposits (at other locations the unit shows evidence for reworking). In addition, zircons from Jnt_C-001, collected from this same key outcrop, yielded a tight cluster of ages ca. 160 Ma, ruling out the previous Triassic identification. The new stratigraphy for the Nacientes del Teno Formation therefore includes a previously unrecognized significant primary volcanic component (~5% of strata thickness).

The ~1 km maximum thickness estimated here for the Nacientes del Teno Formation differs from previous thickness estimates of ~1600 m by Klohn (1960) and 500-750 m by Davidson and Vicente (1973). We believe our ~1 km maximum thickness is a more accurate assessment based on detailed mapping and better understanding of the correlations between isolated sections.

Another difference between the stratigraphy proposed here and that of previous studies concerns the east-west variation in grain size of the uppermost marine strata of the

Nacientes del Teno Formation (i.e. Jnt_D or Rinconada member) and correlative units to the east. Whereas Davidson and Vicente (1973) reported no east-west variation in grain size across an area including the field area and extending tens of kilometers to the east, within the field area a clear eastward decrease in overall grain size for these units was observed.

B. Significance of a ca. 160 Ma rhyolite ignimbrite in the Principal Cordillera at 35.10°S

The Jurassic age and revised stratigraphic position determined by this study for unit Jnt_C does not rule out a Permo-Triassic rhyolitic basement underlying the Nacientes del Teno Formation strata, though it raises the possibility that these strata were instead deposited on basement composed of Late Paleozoic arc rocks (Rio Damas deposits have been reported to contain hololeucogranite clasts typical of the late Late Paleozoic attesting to the Kimmeridgian arc having been built on Paleozoic arc basement (Mpodozis et al., 1976)). Because Jurassic rhyolitic rocks are now documented in the area, other rhyolitic rocks previously assigned Triassic or Miocene ages based on lithology warrant reexamination. Backarc-derived rhyolitic rocks also represent an additional potential source for rhyolitic clasts observed in Late Jurassic sedimentary strata, clasts previously interpreted as derived from Permo-Triassic Choiyoi Group rocks uplifted during extension (Spalletti et al., 2008; Mescua et al., 2008).

Possible sources for Jurassic rhyolitic rocks exposed in the central Chilean Andes include the active volcanic front to the west (Vergara et al., 1995) and hypothesized volcanic chains located between the Jurassic western and eastern belts (Charrier et al., 2007). The Jurassic Chon Aike igneous province of Patagonia (Pankhurst et al., 1998) is over 500 km from the field area, too far to transport ignimbrites, which typically travel no more than several tens of kilometers from their vents (Cas and Wright, 1987). The nearest Jurassic

western belt rocks are located >100 km west of the field area in the present day Coastal Cordillera (Morel, 1981), although the eastern extent of the late-Middle to early-Late Jurassic arc is unknown, rhyolitic to dacitic ignimbrites are known to erupt from arc volcanoes, and 100 km or less is a plausible distance for an ignimbrite to travel (Cas and Wright, 1987). Alternatively, the ignimbrite could have been derived from nearby backarc volcanoes. Rhyolitic ignimbrites are more commonly associated with volcanism in intra-arc graben, backarc, and continental extensional tectonic settings (Fisher and Schminke, 1994), and the existence of backarc volcanoes at the latitude of the field area is strongly suggested by sedimentological and geochronological results of this study.

C. Depositional environments and sedimentation of the Nacientes del Teno Formation

Sedimentological features of the Nacientes del Teno Formation in the 35.10°S field area are indicative of sedimentation in fan delta, ring plain, and possibly flanking volcaniclastic fan depositional systems (Hackett and Houghton, 1989). Sedimentation is inferred to have been controlled primarily by growth and erosion cycles of andesitic stratovolcanoes ($Jnt_{A\text{-}B}$) followed by a significant reduction in volcanic activity (Jnt_D). In general, the youngest detrital zircons in Nacientes del Teno Formation strata decrease in age up section (Fig. 9), consistent with volcanism accompanying relatively continuous sedimentation (Gehrels, 2014). The linear relationship between U-Pb depositional age and stratigraphic position of sampled strata indicate sedimentation rates from ca. 172-161 Ma remained relatively constant (~50-300 m/Ma) (Fig. 9). The following sections discuss evidence for sediment sources and depositional environments for each stratigraphic unit of the Nacientes del Teno Formation, from oldest to youngest.

i. Jnt_A (Fig. 11A-B)

Unit Jnt_A formed through epiclastic reworking and mass-flow redeposition in aggrading volcaniclastic submarine fans. Volcaniclastic turbidites and shale beds comprising Jnt_{A1} strata likely reflect deposition in a distal marginal setting consistent with subdued and/or distal volcanism. The transition up section into multiple coarsening-upwards cycles of andesitic volcaniclastic sequences likely reflects growth and erosion cycles of stratovolcanoes. Volcanism was vigorous, as abundant olistostrome deposits suggest high rates of sedimentation led to gravitationally unstable slopes. Volcanism was likely at least partially subaerial, as indicated by the abundance of well-rounded andesite cobbles and the presence of pumice fragments.

ii. Jnt_B (Fig. 11B)

Abundant desiccation structures in Jnt_B and the predominance of red-colored beds indicate that arid or seasonally arid conditions characterized the regional climate during the late Middle-early Late Jurassic (although there was enough precipitation to account for very sparse plant remains preserved in marine strata from unit Jnt_D, and Jnt_{B3} and Jrd fluvial deposits). Jnt_B strata are interpreted to be aggrading volcaniclastic apron/fan delta deposits that include increasing proportions of proximal and subaerial deposits up section, culminating in coarse fluvial and debris flow conglomerate deposits that may represent deposition within volcano-flank fans. Based the absence of sedimentary clasts (as well as geochronological evidence presented below), aggradation likely resulted from relief generated by stratovolcano growth rather than by eustasy or tectonic uplift.

The size and angularity of conglomerate clasts in uppermost strata of Jnt_{B3} (Fig. 5L) indicate sediment sources within tens of kilometers from the field area. A sequence of

predominantly fine-grained red beds (assigned to the Lotena Formation (Stipanicic, 1965; Dellapé, et al., 1979)) equivalent to Jnt_{B1}, crops out discontinuously up to 12 km east of the field area. The general eastward decrease in grain size of Jnt_B deposits and equivalent deposits in Argentina, in conjunction with paleocurrent data (Fig. 3B), argue for a sediment source west of the field area.

iii. Jnt_C

Jnt_C deposits represent an outflow sheet and accompanying surge and/or fallout deposits associated with a Plinian eruption. The ignimbrite source was likely located no more than ~100 km away in the case of an extremely far travelled pyroclastic flow (Cas and Wright, 1987); in this instance however, the source was likely much closer given the presence of proximal fluvial deposits (Jnt_{B3}) containing exclusively of andesitic clasts.

Jnt_C crops out discontinuously across ~30 km^2 within the field area. Assuming these deposits were originally laterally continuous and 20-80 m thick, the volume of the deposits was originally at least ~0.6-2.4 km^3. This is a conservative estimate however, as additional Jnt_C outcrops are visible in aerial imagery as far as ~12 km east of the eastern edge of the field area.

The unit varies little in thickness, implying that it was emplaced on a surface of relatively low relief formed by upper Jnt_B volcaniclastic apron/fan delta deposits. Turbidite intercalations within upper portions of Jnt_C, and variations in grainsize and in crystal, lithic, and pumice content across the field area indicate reworking of unwelded material immediately following the eruption.

iv. Jnt_D (Fig. 11C)

The abrupt upward transition from high-energy fluvial deposits (Jnt_{B3}) to low-energy submarine deposits (Jnt_D), with the transition marked by the presence of a welded ignimbrite (Jnt_C), is noteworthy. Emplacement of a resistant welded ignimbrite may have redirected sediment transport to depocenters outside the field area, preventing deposition on top of the ignimbrite prior to the marine transgression that resulted in deposition of Jnt_D strata.

The decrease in volcaniclastic content and in grain size, and increase in carbonate content upwards and laterally within Jnt_D (in eastern and southwestern field area locations) is interpreted to represent a reduction in volcanically generated relief to the west (due to either waning volcanism and/or westward migration of the volcanic front) and/or base level rise and marine incursion from the east. The coarse conglomerate deposits near the top of Jnt_{D1} may represent a pulse in andesitic volcanic activity rather than a fall in base level, as the conglomerate deposits contain no sedimentary clasts.

The abrupt increase in the variance of detrital zircon ages and decrease in zircon abundance between units JntC and JntD (Fig. 7) suggest a reduction in local silicic volcanic activity. Along with continuous carbonate deposition, sedimentation at this time was characterized by redeposition of Early to Late Jurassic primary arc deposits and/or arc-derived sedimentary rocks. The component of Precambrian zircons (~23%) in sample Jnt_{D1}-274 suggests some sediments were being transported from a cratonic source to the east. Zircons of Permo-Triassic age are notably absent from this sample, suggesting proposed structural basement highs (e.g. Tordillo High) to the east were not a major source of sediment.

v. Jnt_E (Fig. 11D)

Unit Jnt_E represents a regression within the backarc basin accompanied by a reduction in siliciclastic sedimentation.

D. Sediment sources and maximum depositional age of The Rio Damas Formation

The Rio Damas Formation represents the culmination of Late Jurassic marine regression. Deposition likely occurred on volcaniclastic alluvial fans adjacent to elevated terrain formed by volcanism and/or tectonic uplift (Fig. 11E).

The maximum depositional ages of Late Jurassic backarc continental deposits (Rio Damas, Tordillo, and Lagunillas formations) and the nature of the contact separating these units from underlying Oxfordian-Kimmeridgian gypsum deposits are significant because the shift in tectonic conditions responsible for the Late Jurassic regional regression remains unclear (Charrier et al. 2007; Vicente, 2005; Hallam, 1991; Rossel et al. 2014; Spalletti et al. 2008; Mpodozis and Cornejo 1988). Results from this study are inconclusive as to whether the locally discordant contact separating Rio Damas Formation strata from Nacientes del Teno Formation strata in the field area represents local faulting or an important erosional surface. The 151 ± 3 Ma maximum depositional age (10-grain cluster weighted mean age) for sample Jrd-001 suggests a Kimmeridgian-Tithonian age for the Rio Damas Formation at this location, and agrees with maximum depositional ages of the Tordillo Formation in central and southern parts of the Neuquén Basin (ca. 144 Ma graphical peak age) (Naipauer et al., 2012, 2015b), the Rio Damas Formation at its type locality at 35°S (146 ± 4 Ma five-grain cluster weighted mean age) (Rossel et al., 2014), and the Lagunillas Formation in the Tarapacá Basin of northern Chile (multiple-grain cluster weighted mean ages between 149 ±

5 and 145 ± 4 Ma) (Oliveros et al., 2006), supporting a temporal correlation between the continental deposits dated at these locations.

The existence of Middle Jurassic backarc volcanoes at the latitude of the field area has implications for the origin of the voluminous volcanic and volcaniclastic deposits of the Late Jurassic Rio Damas Formation exposed in the Principal Cordillera (Fig. 1). These strata have been interpreted as distal components of a magmatic arc located in the present-day Coastal Cordillera (Davidson, 1971; Davidson and Vicente, 1971) or as backarc volcanic products erupted along normal faults (Charrier et al., 2007). Recently, Rossel et al. (2014) found that based solely on elemental and isotopic composition, products of Rio Damas volcanism and main arc magmatism could not be differentiated in terms of magmatic sources and processes. In addition, a main peak of 158 Ma in a population of detrital zircons separated from a volcanic sandstone is consistent with ages reported for plutons and dikes from the Coastal Cordillera of central Chile (Creixel et al., 2006; Gana and Tosdal, 1996; Godoy and Loske, 1988; Hervé et al., 1988; Parada et al., 1999). Although the possibility that the Rio Damas volcanic products originated in the arc of the Coastal Cordillera cannot be excluded, our results suggest that ca. 165 Ma in the vicinity of the field area, andesitic volcanism occurred at least locally and may have persisted into the Late Jurassic, contributing volcanic material to the Rio Damas Formation.

In contrast to the tightly clustered detrital zircon ages of all but the uppermost Nacientes del Teno Formation samples, the diverse zircon ages from Rio Damas Formation sample Jrd-001, which overlap ages from the Nacientes del Teno Formation (Fig. 7), suggest that deposition of Rio Damas Formation strata exposed in the field area was triggered by a drop in baselevel that promoted the erosion of late Early to Late Jurassic material. Strong

evidence for a global drop in sea level corresponding to the Late Jurassic regression is lacking (Vicente, 2006; Legarreta and Uliana, 1996; Haq et al., 1988), and a local baselevel fall could not have resulted solely from volcanic aggradation, as Late Jurassic volcanism alone cannot account for redeposition of late Early to Middle Jurassic zircons. However, arc/backarc magmatism must have proceeded relatively uninterrupted through late Early to latest Late Jurassic times to account for the continuous distribution of ages of zircons from sample Jrd-001 (Fig. 9). We consider it most likely that the Late Jurassic regression in the field area was caused by tectonic uplift of Middle-Late Jurassic volcanic and volcaniclastic deposits. This interpretation is consistent with the tectonic framework proposed by Charrier et al. (2007), in which Late Jurassic backarc volcanism was promoted by magma ascent along active extensional faults.

E. Significance of Nacientes del Teno and Rio Damas Formation volcanic detritus in the context of Jurassic arc paleogeography

Middle to Late Jurassic radiometric ages (ca. 163-149 Ma) were recently reported (Rossel et al., 2013) for bimodal volcanic and volcaniclastic rocks from the Pre-Cordillera and High Andes of northern Chile (26°-31°S), including a ca. 163 Ma $^{40}Ar/^{39}Ar$ age for hornblende from a lithic fragment from a volcanic breccia. The geochemistry and location of the volcanic rocks >100 km inboard of arc batholiths were used to infer the existence of multiple chains of volcanoes active across the width of the arc. A similar interpretation is envisioned here for central Chile, based on the sedimentological and geochronological evidence for proximity of Middle Jurassic active volcanic systems to the 35.10°S field area. Our interpretation is based largely on the subaerial fraction of the Nacientes del Teno Formation and ages of detrital zircons at various stratigraphic levels of the formation. In

particular, the angularity and size of andesitic clasts in fluvial conglomerate and subaerial debris flow deposits (Fig. 5I-M) are difficult to reconcile with a source located >100 km west in the present day Coastal Cordillera. Additional evidence is the tight clustering of ages of detrital zircons from units Jnt_{B1} and Jnt_{A2} (Fig. 7) around a single Middle Jurassic age (ca. 165 Ma). If Nacientes del Teno Formation strata had received significant contributions of sediment from as far west as the present day Coastal Cordillera, detrital zircons from these units would likely reflect a greater diversity in age of source rocks and show greater variance in ages.

Due to a lack of age data from volcanic units of the Coastal Cordillera at this latitude, we cannot determine from this study alone whether volcanic systems were simultaneously active across the width of the arc, or whether volcanism responsible for western belt deposits occurred at a different time than Nacientes del Teno Formation volcanism. However, U-Pb zircon ages of western belt plutonic rocks from central Chile (ca. 161-156 Ma) (Gana and Tosdal, 1996) fall within the range of ages determined for the Nacientes del Teno and Rio Damas formations (ca. 172-150 Ma), indicating arc magmatism was simultaneously active across a ~100 km wide zone of the continental margin.

F. Age of the Nacientes del Teno Formation in the context of recent detrital zircon studies

A number of recent studies have used the detrital zircon record to investigate backarc magmatism and deformation in the Jurassic Andes (Tunik et al., 2010; Oliveros et al., 2012; Di Giulio et al., 2012; Naipauer et al., 2012, 2015a, 2015b; Rossel et al., 2013, 2014; Horton et al., 2016; Fennell et al., 2017; Balgord and Carrapa, 2017). Frequency histogram and relative probability plots of previously reported U-Pb ages of detrital zircons from the Late

Jurassic Rio Damas and Tordillo formations in the Neuquén Basin and the correlative Lagunillas Formation in the Tarapaca Basin to the north show two peaks corresponding to the Early and Late Jurassic, respectively, and a Middle Jurassic trough at ca. 165 Ma (Fig. 10). The Middle Jurassic trough has been attributed to a decrease in magmatic activity and/or a shift to more mafic magmatism (Naipauer et al., 2015a). In contrast, the peaks in ages of detrital zircons documented in this study plot squarely within the Middle Jurassic (Fig. 10 A-B). If overall zircon production was reduced in the Middle Jurassic, then the tightly clustered Middle Jurassic detrital zircon ages reported in this study are strong evidence for the proximity of the Nacientes del Teno Formation deposits to a Middle Jurassic backarc volcanic system. Alternatively, previous detrital zircon datasets may underrepresent Middle Jurassic volcanic activity. Detrital zircon ages reflect magmatic activity but more specifically reflect which rocks were exposed at the time of deposition, the zircon content and relative erosivity of those rocks, and paleodrainage patterns. Perhaps Middle Jurassic volcanism was concentrated within low-lying or submarine backarc basin settings that promoted the preservation of volcanic and volcaniclastic strata such as the Nacientes del Teno Formation. Late Jurassic rocks deposited over Middle Jurassic rocks may have shielded the latter from erosion during Late Jurassic basin inversion. The Early Jurassic peak present in these datasets is consistent with the erosion of Early Jurassic felsic volcanic products known to have erupted in great volume from the main volcanic arc to the west during the initiation of Andean subduction (Vergara et al., 1995). With the exception of this study, previous attempts to investigate the record of Jurassic magmatism with detrital zircon geochronology have focused on Late Jurassic deposits located tens of kilometers east of any potential Middle Jurassic volcanoes. Additional geochronology studies involving more proximal Jurassic

rocks from the region may clarify the extent to which existing datasets reflect variations in production versus recycling of zircons.

8. CONCLUSIONS

New stratigraphic and geochronologic investigations into the Nacientes del Teno and Rio Damas formations of eastern central Chile provide insights into the location, composition, and timing of arc volcanic systems at this latitude in the Middle-Late Jurassic (174-145 Ma). Based on these new data, we draw the following conclusions:

1. Deposition of the Nacientes del Teno Formation occurred from 172-161 Ma, coeval with nearby volcanism, within volcaniclastic alluvial fan, fan delta, and possibly flanking volcaniclastic fan depositional environments. Volcanoes located well east of the present day Coastal Cordillera challenges the notion that Jurassic volcanism was restricted to a narrow chain of volcanoes located just inland of the present day coast. It remains unclear whether multiple chains of volcanoes were simultaneously active across the width of the continental margin, or whether a volcanic front migrated longitudinally during the Jurassic.
2. U-Pb ages of detrital zircons from the Nacientes del Teno Formation form a distinct peak at ca. 165 Ma. The peak coincides the low abundance of Middle Jurassic age detrital zircons from Late Jurassic and younger backarc deposits. Future studies of Middle Jurassic proximal volcaniclastic backarc deposits may reveal whether the trough in existing datasets reflects variations in production versus recycling of Jurassic zircons.
3. The identification of a Jurassic (160 Ma) rhyolite ignimbrite—the first reported for this portion of the Andes—calls into question Triassic and Miocene ages commonly assumed for local rhyolitic rocks.

4. A maximum depositional age of ca. 151 Ma calculated from U-Pb detrital zircon ages agrees with previously published maximum depositional ages for the Rio Damas Formation. Sedimentological and geochronologic evidence suggests tectonic uplift as the cause of the Late Jurassic regression recorded in the Rio Damas Formation.

9. SUPPLEMENTARY MATERIAL

Plate 1: Geologic map of the Nacientes del Teno Formation and adjacent rocks, Maule (Region VII), Chile

Supplementary material available in ProQuest Dissertations & Theses.

10. REFERENCES

Arcos, R., 1987, Geología del cuadrángulo Termas del Flaco, provincia de Colchagua, VI región, Chile: Memoria de Título (inédito), Universidad de Chile, Departamento de Geología y Geofísica.

Balgord, E. A., and Carrapa, B., 2016, Basin evolution of Upper Cretaceous–Lower Cenozoic strata in the Malargüe fold-and-thrust belt: northern Neuquén Basin, Argentina: Basin Research, v. 28, no. 2, p. 183-206.

Buchelt, M., and Cancino, C. T., 1988, The Jurassic La Negra Formation in the area of Antofagasta, northern Chile (lithology, petrography, geochemistry), The Southern Central Andes, Springer, p. 169-182.

Burckhardt, C. E., and Wehrli, L., 1900, Profils géologiques transversaux de la Cordillère argentino-chilienne: stratigraphie et tectonique, Talleres de publicaciones del Museo.

Busby-Spera, C., 1988, Development of fan-deltoid slope aprons in a convergent-margin tectonic setting: Mesozoic, Baja California, Mexico: Fan deltas: Sedimentology and tectonic settings: New York, Blackie, p. 419-429.

Caminos, R., and González, P. D., 1996, Mapa geológico de la República Argentina, Dirección Nacional del Servicio Geológico Buenos Aires.

Cas, R., and Wright, J., 1987, Volcanic Successions, Modern and Ancient: A Geological Approach to Processes, Products and Successions, 528 pp: Allen and Unwin, London. Cashman, KV (1988), Crystallization of Mount St. Helens dacite: A quantitative textural approach. Bull. Volcanol, v. 50, p. 194-209.

Charrier, R., Pinto, L., and Rodríguez, M. P., 2007, Tectonostratigraphic evolution of the Andean Orogen in Chile, The Geology of Chile.

Charrier, R., Wyss, A., Flynn, J. J., Swisher III, C. C., Norell, M. A., Zapatta, F., McKenna, M. C., and Novacek, M. J., 1996, New evidence for late Mesozoic-early Cenozoic evolution of the Chilean Andes in the upper Tinguiririca valley (35 S), central Chile: Journal of South American Earth Sciences, v. 9, no. 5-6, p. 393-422.

Cohen, K., Finney, S., Gibbard, P., and Fan, J.-X., 2013, The ICS international chronostratigraphic chart: Episodes, v. 36, no. 3, p. 199-204.

Coira, B., Davidson, J., Mpodozis, C., and Ramos, V., 1982, Tectonic and magmatic evolution of the Andes of northern Argentina and Chile: Earth-Science Reviews, v. 18, no. 3-4, p. 303-332.
Cornejo-Carreño, C., Muñoz-Bravo, J., and Covacevich-Castex, V., Presencia de Jurásico sedimentario marino en el Cajón Troncoso, alta Cordillera de los Andes, VII Región, Chile: noticia preliminar, in Proceedings Actas 3 Congreso Geolôgico Chileno (Concepcion 1982)1982, Volume 1, p. A84-A110.
Corvalán, J., El límite Triásico-Jurásico en la Cordillera de la costa de las provincias de Curicó y Talca, in Proceedings Congreso Geológico Chileno1982.
Cottle, J. M., Burrows, A. J., Kylander-Clark, A., Freedman, P. A., and Cohen, R. S., 2013, Enhanced sensitivity in laser ablation multi-collector inductively coupled plasma mass spectrometry: Journal of Analytical Atomic Spectrometry, v. 28, no. 11, p. 1700-1706.
Cottle, J. M., Kylander-Clark, A. R., and Vrijmoed, J. C., 2012, U–Th/Pb geochronology of detrital zircon and monazite by single shot laser ablation inductively coupled plasma mass spectrometry (SS-LA-ICPMS): Chemical Geology, v. 332, p. 136-147.
Creixell, C., Parada, M. A., Morata, D., Roperch, P., and Arriagada, C., 2009, The genetic relationship between mafic dike swarms and plutonic reservoirs in the Mesozoic of central Chile (30°–33° 45′ S): Insights from AMS and geochemistry: International Journal of Earth Sciences, v. 98, no. 1, p. 177-201.
Creixell, C., Parada, M. Á., Morata, D., Vásquez, P., Pérez de Arce, C., and Arriagada, C., 2011, Middle-Late Jurassic to Early Cretaceous transtension and transpression during arc building in Central Chile: evidence from mafic dike swarms: Andean geology, v. 38, no. 1, p. 37-63.
Creixell, C., Parada, M. Á., Roperch, P., Morata, D., Arriagada, C., and de Arce, C. P., 2006, Syntectonic emplacement of the Middle Jurassic Concon mafic dike swarm, Coastal Range, central Chile (33° S): Tectonophysics, v. 425, no. 1-4, p. 101-122.
Davidson, J., 1971, Contribución al estudio geológico de los Andes Meridionales Centrales: Geología del área de las Nacientes del Teno, Provincia de Curicó: Memoria de Título (Inédito), Departamento de Geología, Universidad de Chile.
Davidson, J., and Vicente, J.-C., Características paleogeográficas y estructurales del área fronteriza de las nacientes del Teno (Chile) y Santa Elena (Argentina)(Cordillera Principal, 35° a 35° 15′ latitud sur), in Proceedings Congreso Geológico Argentino1973, p. 11-55.
De la Cruz, R., and Suarez, M., 1997, El Jurásico de la Cuenca de Neuquén en Lonquimay, Chile: Formación Nacientes del Biobío (38-39 S): Andean Geology, v. 24, no. 1, p. 3-24.
Dellapé, D., Mombrú, C., Pando, G., Riccardi, A., Uliana, M., and Westermann, G., 1979, Edad y correlación de la Formación Tábanos en Chacay Melehue y otras localidades de Neuquén y Mendoza: Obra del Centenario del Museo de La Plata5, p. 81-105.
Di Giulio, A., Ronchi, A., Sanfilippo, A., Tiepolo, M., Pimentel, M., and Ramos, V., 2012, Detrital zircon provenance from the Neuquén Basin (south-central Andes): Cretaceous geodynamic evolution and sedimentary response in a retroarc-foreland basin: Geology, v. 40, no. 6, p. 559-562.

Dickinson, W. R., and Gehrels, G. E., 2003, U–Pb ages of detrital zircons from Permian and Jurassic eolian sandstones of the Colorado Plateau, USA: paleogeographic implications: Sedimentary Geology, v. 163, no. 1-2, p. 29-66.
Dickinson, W. R., and Gehrels, G. E., 2009, Use of U–Pb ages of detrital zircons to infer maximum depositional ages of strata: a test against a Colorado Plateau Mesozoic database: Earth and Planetary Science Letters, v. 288, no. 1-2, p. 115-125.
Digregorio, R., Gulisano, C., Gutiérrez Pleimling, A., and Minitti, S., Esquema de la evolución geodinámica de la Cuenca Neuquina y sus implicancias paleogeográficas, in Proceedings Actas Noveno Congreso Geológico Argentino, San Carlos de Bariloche1984, Volume 2, p. 147-162.
Fennell, L. M., Folguera, A., Naipauer, M., Gianni, G., Rojas Vera, E. A., Bottesi, G., and Ramos, V. A., 2017, Cretaceous deformation of the southern Central Andes: synorogenic growth strata in the Neuquén Group (35 30′–37 S): Basin Research, v. 29, no. S1, p. 51-72.
Fisher, R., and Schmincke, H., 1994, Volcaniclastic sediment transport and deposition: Sediment Transport and Depositional Processes. Blackwell Scientific, Oxford, p. 351-388.
Fisher, R. V., and Schmincke, H.-U., 2012, Pyroclastic rocks, Springer Science & Business Media.
Franzese, J., Veiga, G., Schwarz, E., and Gómez-Pérez, I., 2006, Tectonostratigraphic evolution of a Mesozoic graben border system: the Chachil depocentre, southern Neuquén Basin, Argentina: Journal of the Geological Society, v. 163, no. 4, p. 707-721.
Franzese, J. R., and Spalletti, L. A., 2001, Late Triassic–early Jurassic continental extension in southwestern Gondwana: tectonic segmentation and pre-break-up rifting: Journal of South American Earth Sciences, v. 14, no. 3, p. 257-270.
Fuentes, P. d. C. G., and Herve, F., 1983, Geología del basamento cristalino en la Cordillera de la Costa entre los ríos Mataquito y Maule, VII Región: Revista geológica de Chile: An international journal on andean geology, no. 19, p. 37-56.
Gana, P., and Tosdal, R. M., 1996, Geocronología U-Pb y K-Ar en intrusivos del Paleozoico y Mesozoico de la Cordillera de la Costa, Región de Valparaíso, Chile: Andean Geology, v. 23, no. 2, p. 151-164.
Gehrels, G., 2014, Detrital zircon U-Pb geochronology applied to tectonics: Annual Review of Earth and Planetary Sciences, v. 42, p. 127-149.
Gerth, E., 1925, Contribuciones a la estratigrafía y paleontología de los Andes Argentinos. I: Estratigrafía y distribución de los sedimentos mesozoicos en los Andes Argentinos: Actas de la Academia Nacional de Ciencias, v. 9, p. 11-55.
Godoy, E., and Loske, W., 1988, Tectonismo sinplutónico de dioritas jurásicas al sur de Valparaíso: datos U-Pb sobre la'Fase Quintay': Andean Geology, v. 15, no. 2, p. 119-127.
Gonzalez-Ferran, O., and Martínez, M. V., 1962, Reconocimiento geológico de la Cordillera de los Andes entre los paralelos 35 y 38 latitud sur.
Groeber, P., 1946, Observaciones geológicas a lo largo del meridiano 70: Servicio Geológico Minero Nacional, Boletín, v. 1, no. 3, p. 177-208.
Hackett, W., and Houghton, B., 1989, A facies model for a Quaternary andesitic composite volcano: Ruapehu, New Zealand: Bulletin of volcanology, v. 51, no. 1, p. 51-68.

Hallam, A., 1991, Relative importance of regional tectonics and eustasy for the Mesozoic of the Andes: Sedimentation, tectonics and eustasy: Sea-level changes at active margins, p. 187-200.
Haq, B. U., Hardenbol, J., and Vail, P. R., 1987, Chronology of fluctuating sea levels since the Triassic: Science, v. 235, no. 4793, p. 1156-1167.
Hervé, F., Godoy, E., Parada, M. A., Ramos, V., Rapela, C., Mpodozis, C., and Davidson, J., 1987, A general view on the Chilean-Argentine Andes, with emphasis on their early history: Circum-Pacific Orogenic Belts and Evolution of the Pacific Ocean Basin, p. 97-113.
Horton, B. K., Fuentes, F., Boll, A., Starck, D., Ramirez, S. G., and Stockli, D. F., 2016, Andean stratigraphic record of the transition from backarc extension to orogenic shortening: A case study from the northern Neuquén Basin, Argentina: Journal of South American Earth Sciences, v. 71, p. 17-40.
Howell, J. A., Schwarz, E., Spalletti, L. A., and Veiga, G. D., 2005, The Neuquén basin: an overview: Geological Society, London, Special Publications, v. 252, no. 1, p. 1-14.
Jackson, S. E., Pearson, N. J., Griffin, W. L., and Belousova, E. A., 2004, The application of laser ablation-inductively coupled plasma-mass spectrometry to in situ U–Pb zircon geochronology: Chemical Geology, v. 211, no. 1-2, p. 47-69.
Jordan, T. E., Burns, W. M., Veiga, R., Pángaro, F., Copeland, P., Kelley, S., and Mpodozis, C., 2001, Extension and basin formation in the southern Andes caused by increased convergence rate: A mid-Cenozoic trigger for the Andes: Tectonics, v. 20, no. 3, p. 308-324.
Jordan, T. E., Isacks, B., Ramos, V. A., and Allmendinger, R. W., 1983, Mountain building in the Central Andes: Episodes, v. 3, no. 3, p. 20-26.
Jordan, T. E., Reynolds, J. H., and Erikson, J. P., 1997, Variability in age of initial shortening and uplift in the central Andes, 16–33 30′ S, Tectonic uplift and climate change, Springer, p. 41-61.
Kamo, S. L., and Riccardi, A. C., 2009, A new U–Pb zircon age for an ash layer at the Bathonian–Callovian boundary, Argentina: Gff, v. 131, no. 1-2, p. 177-182.
Kay, S. M., Mpodozis, C., Ramos, V. A., and Munizaga, F., 1991, Magma source variations for mid-late Tertiary magmatic rocks associated with a shallowing subduction zone and a thickening crust in the central Andes (28 to 33 S): Geological Society of America Special Paper, v. 265, p. 113-137.
Kay, S. M., Ramos, V., and Marquez, M., 1993, Evidence in Cerro Pampa volcanic rocks for slab-melting prior to ridge-trench collision in southern South America: The journal of Geology, v. 101, no. 6, p. 703-714.
Kleiman, L. E., and Japas, M. S., 2009, The Choiyoi volcanic province at 34 S–36 S (San Rafael, Mendoza, Argentina): Implications for the Late Palaeozoic evolution of the southwestern margin of Gondwana: Tectonophysics, v. 473, no. 3-4, p. 283-299.
Klohn, C., 1960, Geología de la Cordillera de Los Andes de Chile Central, provincias de Santiago, O'Higgins, Colchagua y Curicó. llG Chile: Boletín Nº8.
Kramer, W., Siebel, W., Romer, R. L., Haase, G., Zimmer, M., and Ehrlichmann, R., 2005, Geochemical and isotopic characteristics and evolution of the Jurassic volcanic arc between Arica (18 30′ S) and Tocopilla (22 S), North Chilean Coastal Cordillera: Chemie der Erde-Geochemistry, v. 65, no. 1, p. 47-78.

Kuenzi, W. D., Horst, O. H., and McGEHEE, R. V., 1979, Effect of volcanic activity on fluvial-deltaic sedimentation in a modern arc-trench gap, southwestern Guatemala: Geological Society of America Bulletin, v. 90, no. 9, p. 827-838.
Leanza, H. A., 2012, The Vaca Muerta Formation (Late Jurassic—Early Cretaceous): History, Stratigraphic Context and Events of this Emblematic Unit of the Neuquén Basin, Argentina: Museo Argentino de Ciencias Naturales" Bernardino Rivadavia.
Legarreta, L., and Kozlowski, E., Secciones condensadas del Jurásico-Cretácico de los Andes del sur de Mendoza: estratigrafía y significado tectosedimentario, in Proceedings Congreso Geológico Argentino, 9, Actas1984, Volume 1, p. 286-297.
Legarreta, L., and Uliana, M. A., 1996, The Jurassic succession in west-central Argentina: stratal patterns, sequences and paleogeographic evolution: Palaeogeography, Palaeoclimatology, Palaeoecology, v. 120, no. 3-4, p. 303-330.
Legarreta, L., and Uliana, M. A., 1999, El Jurásico y Cretácico de la Cordillera Principal y la Cuenca Neuquina: Geología Argentina (Caminos, R.; editor). Servicio Geológico Minero Argentino, Anales, v. 29, no. 16, p. 399-416.
Lucassen, F., Kramer, W., Bartsch, V., Wilke, H.-G., Franz, G., Romer, R. L., and Dulski, P., 2006, Nd, Pb, and Sr isotope composition of juvenile magmatism in the Mesozoic large magmatic province of northern Chile (18–27 S): indications for a uniform subarc mantle: Contributions to Mineralogy and Petrology, v. 152, no. 5, p. 571.
Ludwig, K., 2012, Isoplot/Ex, v. 3.75: Berkeley Geochronology Center Special Publication, v. 5.
Mescua, J. F., 2011, Evolución estructural de la cordillera principal entre Las Choicas y Santa Elena (35° S), provincia de Mendoza, Argentina: Facultad de Ciencias Exactas y Naturales. Universidad de Buenos Aires.
Mescua, J. F., Giambiagi, L. B., and Bechis, F., 2008, Evidencias de tectónica extensional en el Jurásico tardío (Kimeridgiano) del suroeste de la provincia de Mendoza: Revista de la Asociación Geológica Argentina, v. 63, no. 4, p. 512-519.
Minería, C. S. N. d. G. y., Muñoz, J., and Niemeyer, H., 1984, Hoja Laguna del Maule: regiones del Maule y del BioBio: carta geológica de Chile 1: 250.000, Servicio Nacional de Geología y Minería.
Morel, R., 1981, Geología del sector norte de la hoja Gualleco, entre los 35 00'y los 35 10'latitud sur, provincia de Talca, VII región, Chile: Geología del sector norte de la hoja Gualleco, entre los 35° 00'y los 35° 10'latitud sur, provincia de Talca, VII región, Chile.
Mpodozis, C., and Kay, S. M., 1990, Provincias magmáticas ácidas y evolución tectónica de Gondwana: Andes chilenos (28-31 S): Andean Geology, v. 17, no. 2, p. 153-180.
Mpodozis, C., and Ramos, V., 1989, The Andes of Chile and Argentina: Geology of the Andes and its relation to hydrocarbon and mineral resources (Ericksen, GE, p. 59-90.
Mpodozis, C., Rivano, S., Parada, M., and Vicente, J., 1976, Acerca del plutonismo tardi-hercinico en la Cordillera Frontal entre los 30° y 33° sur (Provincia de Mendoza y San Juan, Argentina; Coquimbo, Chile): Actus V. Congr. Geol. Arg, v. 1, p. 143-171.
Mpodozis, C., and Cornejo, P., 1988, Carta Geológica de Chile, hoja Pisco Elqui, IV Región de Coquimbo a escala 1:250,000: Servicio Nactional de Geología y Minería.
Naipauer, M., Morabito, E. G., Marques, J. C., Tunik, M., Vera, E. A. R., Vujovich, G. I., Pimentel, M. P., and Ramos, V. A., 2012, Intraplate Late Jurassic deformation and

exhumation in western central Argentina: constraints from surface data and U–Pb detrital zircon ages: Tectonophysics, v. 524, p. 59-75.
Naipauer, M., Tapia, F., Mescua, J., Farías, M., Pimentel, M. M., and Ramos, V. A., 2015a, Detrital and volcanic zircon U–Pb ages from southern Mendoza (Argentina): An insight on the source regions in the northern part of the Neuquén Basin: Journal of South American Earth Sciences, v. 64, p. 434-451.
Naipauer, M., Tunik, M., Marques, J. C., Vera, E. A. R., Vujovich, G. I., Pimentel, M. M., and Ramos, V. A., 2015b, U–Pb detrital zircon ages of Upper Jurassic continental successions: implications for the provenance and absolute age of the Jurassic–Cretaceous boundary in the Neuquén Basin: Geological Society, London, Special Publications, v. 399, no. 1, p. 131-154.
Nasi, C., and Thiele, R., 1982, Estratigrafía del Jurásico y Cretácico de la Cordillera de la Costa, al sur del Río Maipo, entre Melipilla y Laguna de Aculeo (Chile Central): Andean Geology, no. 16.
Oliveros, V., Féraud, G., Aguirre, L., Fornari, M., and Morata, D., 2006, The Early Andean Magmatic Province (EAMP): 40Ar/39Ar dating on Mesozoic volcanic and plutonic rocks from the Coastal Cordillera, northern Chile: Journal of Volcanology and Geothermal Research, v. 157, no. 4, p. 311-330.
Oliveros, V., Labbé, M., Rossel, P., Charrier, R., and Encinas, A., 2012, Late Jurassic paleogeographic evolution of the Andean back-arc basin: New constrains from the Lagunillas Formation, northern Chile (27 30′–28 30′S): Journal of South American Earth Sciences, v. 37, p. 25-40.
Oliveros, V., Morata, D., Aguirre, L., Féraud, G., and Fornari, M., 2007, Jurassic to Early Cretaceous subduction-related magmatism in the Coastal Cordillera of northern Chile (18° 30'-24° S): geochemistry and petrogenesis: Andean Geology, v. 34, no. 2.
Oncken, O., Hindle, D., Kley, J., Elger, K., Victor, P., and Schemmann, K., 2006, Deformation of the central Andean upper plate system—Facts, fiction, and constraints for plateau models, The Andes, Springer, p. 3-27.
Pankhurst, R., Leat, P., Sruoga, P., Rapela, C., Márquez, M., Storey, B., and Riley, T., 1998, The Chon Aike province of Patagonia and related rocks in West Antarctica: A silicic large igneous province: Journal of volcanology and geothermal research, v. 81, no. 1-2, p. 113-136.
Parada, M., Nyström, J., and Levi, B., 1999, Multiple sources for the Coastal Batholith of central Chile (31–34 S): geochemical and Sr–Nd isotopic evidence and tectonic implications: Lithos, v. 46, no. 3, p. 505-521.
Parada Morales, R. E., 2008, Análisis Estructural del Borde Oriental de la Cuenca Terciaria de Abanico en el Valle del Río Teno, 7ma Región.
Parfitt, E. A., and Wilson, L., 2008, Fundamentals of Physical Volcanology, Malden, MA, USA, Blackwell Publishing, 230 p.:
Paton, C., Hellstrom, J., Paul, B., Woodhead, J., and Hergt, J., 2011, Iolite: Freeware for the visualisation and processing of mass spectrometric data: Journal of Analytical Atomic Spectrometry, v. 26, no. 12, p. 2508-2518.
Piquer, J., Castelli, J. C., Charrier, R., and Yáñez, G., 2010, El Cenozoico del alto río Teno, Cordillera Principal, Chile central: estratigrafía, plutonismo y su relación con estructuras profundas: Andean geology, v. 37, no. 1, p. 32-53.

Piracés, R., Estratigrafía de la Cordillera de la Costa entre la cuesta El Melón y Limache, Provincia de Valparaíso, Chile, in Proceedings Congreso Geológico Chileno1976, p. A65-A82.
Piracés, R., 1977, Geología de la Cordillera de la Costa entre Catapilco y Limache, Región de Aconcagua: Memoria de Titulo (Inédito). Universidad de Chile, Departamento de Geología.
Ramos, V. A., 1988, The tectonics 0f the Central Andes; 30 to 33 S latitude: Processes in continental lithospheric deformation, v. 218, p. 31.
Riccardi, A., 1983, The Jurassic of Argentina and Chile: The Phanerozoic Geology of the World II. The Mesozoic, B, p. 201-263.
Rossel, P., Oliveros, V., Ducea, M. N., Charrier, R., Scaillet, S., Retamal, L., and Figueroa, O., 2013, The Early Andean subduction system as an analog to island arcs: Evidence from across-arc geochemical variations in northern Chile: Lithos, v. 179, p. 211-230.
Sláma, J., Košler, J., Condon, D. J., Crowley, J. L., Gerdes, A., Hanchar, J. M., Horstwood, M. S., Morris, G. A., Nasdala, L., and Norberg, N., 2008, Plešovice zircon—a new natural reference material for U–Pb and Hf isotopic microanalysis: Chemical Geology, v. 249, no. 1-2, p. 1-35.
Spalletti, L. A., Queralt, I., Matheos, S. D., Colombo, F., and Maggi, J., 2008, Sedimentary petrology and geochemistry of siliciclastic rocks from the upper Jurassic Tordillo Formation (Neuquén Basin, western Argentina): implications for provenance and tectonic setting: Journal of South American Earth Sciences, v. 25, no. 4, p. 440-463.
Stacey, J. t., and Kramers, J., 1975, Approximation of terrestrial lead isotope evolution by a two-stage model: Earth and planetary science letters, v. 26, no. 2, p. 207-221.
Stipanicic, P., 1966, El Jurásico en Vega de la Veranada (Neuquén), el Oxfordense y el diastrofismo divesiano (Agassiz-Yaila) en Argentina: Revista de la Asociación Geológica Argentina, v. 20, no. 4, p. 403-478.
Thomas, H., 1958, Geología de la Cordillera de la Costa entre el valle de La Ligua y la cuesta de Barriga: Instituto de Investigaciones Geológicas Boletín, v. 2, p. 1-80.
Troncoso, A., and Herbst, R., 2000, La Tafoflora Triásica del Cajón Troncoso, Alta Cordillera del Maule, 7ª Región, Chile: Revista del Museo Argentino de Ciencias Naturales nueva serie, v. 2, no. 2, p. 137-144.
Tunik, M., Folguera, A., Naipauer, M., Pimentel, M., and Ramos, V. A., 2010, Early uplift and orogenic deformation in the Neuquén Basin: constraints on the Andean uplift from U–Pb and Hf isotopic data of detrital zircons: Tectonophysics, v. 489, no. 1-4, p. 258-273.
Uliana, M., Biddle, K., and Cerdan, J., 1989, Mesozoic extension and the formation of Argentine sedimentary basins, Extensional tectonics and stratigraphy of the North Atlantic margins, Volume 46, American Association of Petroleum Geologists Tulsa, Memoir, p. 599-614.
Vergara, M., Levi, B., Nyström, J. O., and Cancino, A., 1995, Jurassic and Early Cretaceous island arc volcanism, extension, and subsidence in the Coast Range of central Chile: Geological Society of America Bulletin, v. 107, no. 12, p. 1427-1440.
Vermeesch, P., 2004, How many grains are needed for a provenance study?: Earth and Planetary Science Letters, v. 224, no. 3-4, p. 441-451.
Vessell, R. K., and Davies, D. K., 1981, Nonmarine sedimentation in an active fore arc basin: Special Publications of SEPM, v. 31, p. 31-45.

Vicente, J., 1976, Exemple devolcanisme initial euliminaire': les complexes albitophyriques neo-triasiques et mésojurassiques du secteur côtier des Andes Méridionales centrales (32 à 33 L. Sud)(González-Ferrán, O.; editor): IAVCEI, In Proceedings, p. 267-329.
Vicente, J. C., 2005, Dynamic paleogeography of the Jurassic Andean Basin: pattern of transgression and localisation of main straits through the magmatic arc: Revista de la Asociación Geológica Argentina, v. 60, no. 1, p. 221-250.
Wiedenbeck, M., Alle, P., Corfu, F., Griffin, W., Meier, M., Oberli, F. v., Quadt, A. v., Roddick, J., and Spiegel, W., 1995, Three natural zircon standards for U-Th-Pb, Lu-Hf, trace element and REE analyses: Geostandards and Geoanalytical Research, v. 19, no. 1, p. 1-23.

11. FIGURES AND TABLES

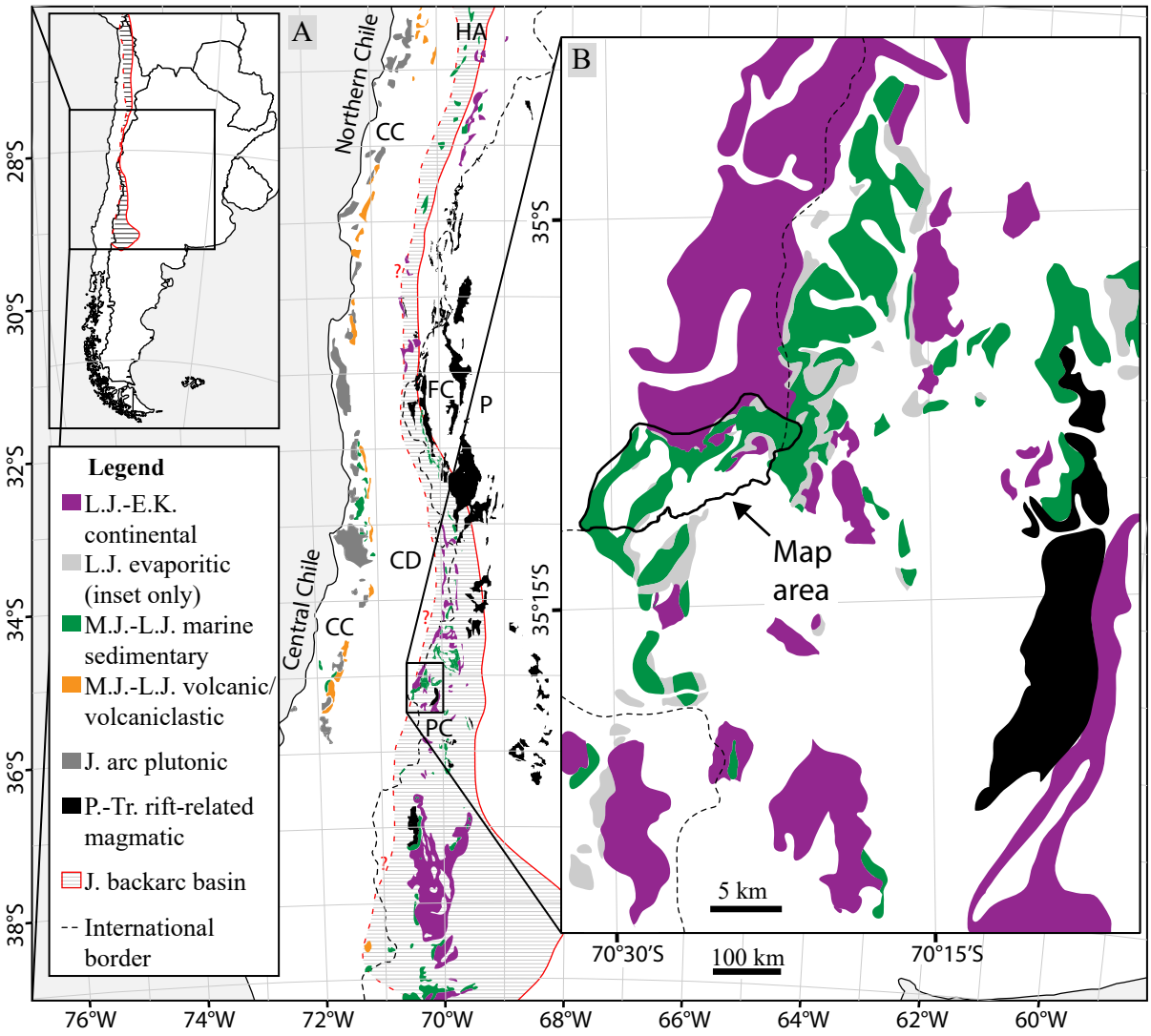

Figure 1. Simplified geologic map of central Chile and west-central Argentina. Permo-Triassic (280-201 Ma) rift-related magmatic and all Early Jurassic to Early Cretaceous (201-140 Ma) units in **(A)** northern and central Chile (Charrier et al., 2007) and western Argentina (Caminos and Gonzales, 1996) (backarc basin after Vicente, 2005, 2006; Permo-Triassic units after Kleiman and Japas, 2009) and **(B)** in the Principal Cordillera between 35°S and 35°30'S (Klohn, 1960; Caminos and Gonzales, 1996; Naipauer et al., 2015). CC: Coastal Cordillera; PC: Principal Cordillera; CD: Central Depression; P: Precordillera; FC: Frontal Cordillera; HA: High Andes.

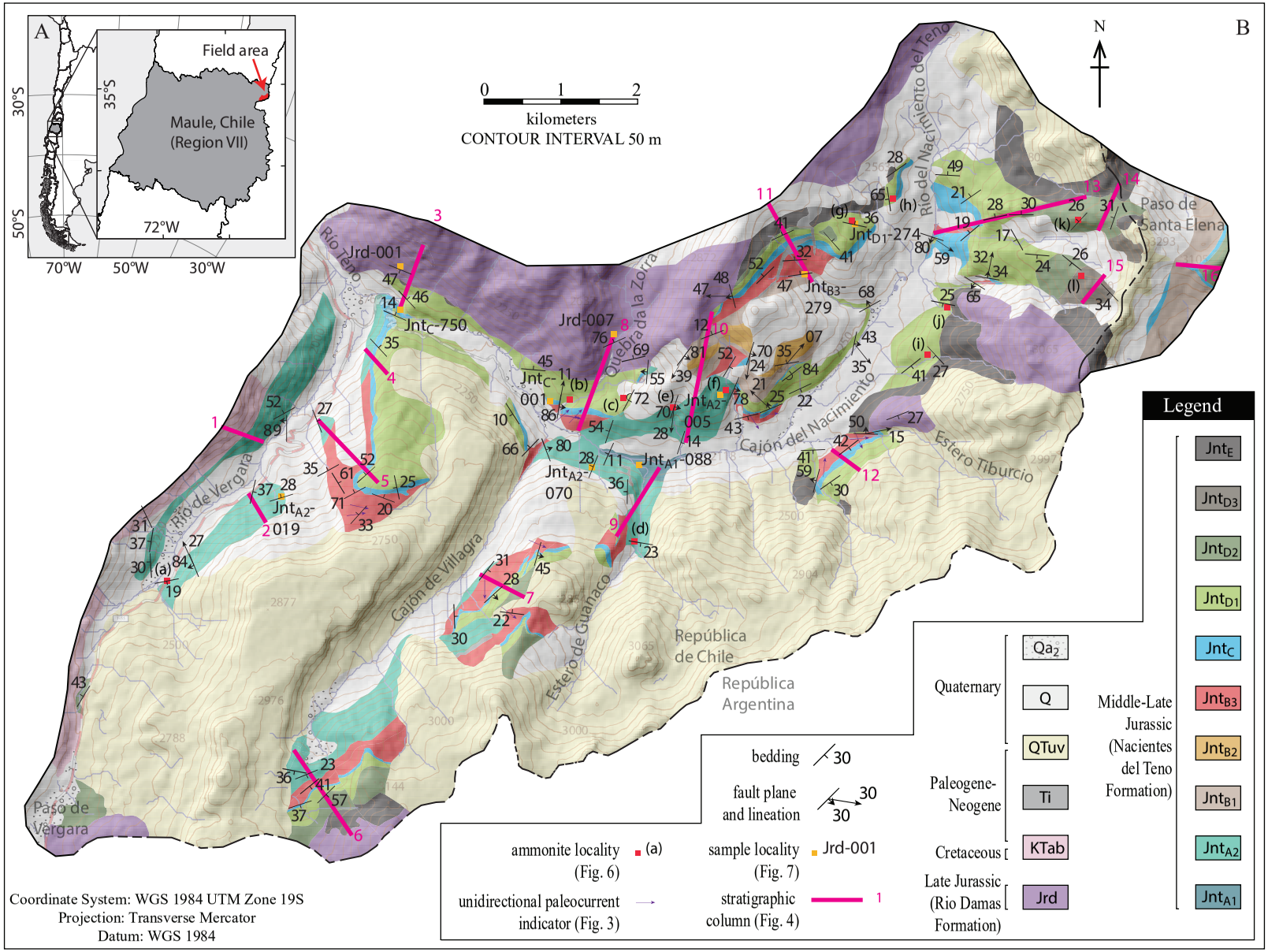
A
Field area
Maule, Chile
(Region VII)
30°S
35°S
50°S
70°W
50°W
30°W
72°W
B
N
0 1 2
kilometers
CONTOUR INTERVAL 50 m
Río Teno
Río del Nacimiento del Teno
Quebrada la Zorra
Cajón del Nacimiento
Cajón de Villagra
Estero de Guanaco
Estero Tiburcio
Río de Vergara
Paso de Santa Elena
Paso de Vergara
República de Chile
República Argentina
Jrd-001
Jrd-007
Jnt$_{C}$-750
Jnt$_{C}$-001
Jnt$_{A2}$-005
Jnt$_{A1}$-088
Jnt$_{A2}$-070
Jnt$_{A2}$-019
Jnt$_{B3}$-279
Jnt$_{D1}$-274
Legend
Quaternary
Qa$_2$
Q
QTuv
Paleogene-Neogene
Ti
Cretaceous
KTab
Late Jurassic (Rio Damas Formation)
Jrd
Middle-Late Jurassic (Nacientes del Teno Formation)
Jnt$_{E}$
Jnt$_{D3}$
Jnt$_{D2}$
Jnt$_{D1}$
Jnt$_{C}$
Jnt$_{B3}$
Jnt$_{B2}$
Jnt$_{B1}$
Jnt$_{A2}$
Jnt$_{A1}$
bedding 30
fault plane and lineation 30 30
ammonite locality (Fig. 6) (a)
sample locality (Fig. 7) Jrd-001
unidirectional paleocurrent indicator (Fig. 3)
stratigraphic column (Fig. 4) 1
Coordinate System: WGS 1984 UTM Zone 19S
Projection: Transverse Mercator
Datum: WGS 1984

Figure 2. (A) Location and **(B)** geologic map of the Nacientes del Teno Formation and adjacent rocks, Maule (Region VII), Chile.

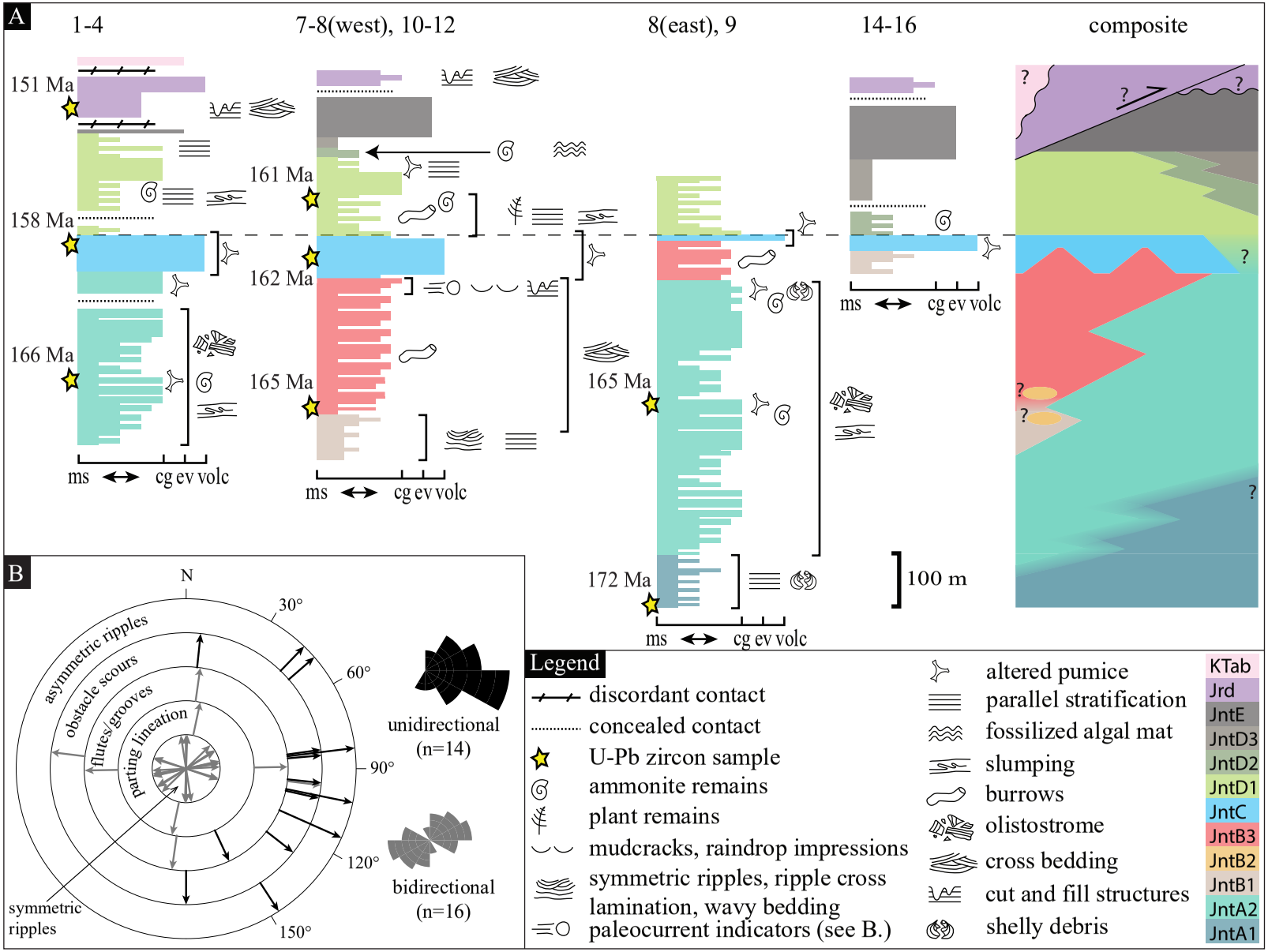
A
1-4
7-8(west), 10-12
8(east), 9
14-16
composite
151 Ma
158 Ma
166 Ma
161 Ma
162 Ma
165 Ma
165 Ma
172 Ma
ms
cg ev volc
100 m
B
N
30°
60°
90°
120°
150°
asymmetric ripples
obstacle scours
flutes/grooves
parting lineation
symmetric ripples
unidirectional (n=14)
bidirectional (n=16)
Legend
discordant contact
concealed contact
U-Pb zircon sample
ammonite remains
plant remains
mudcracks, raindrop impressions
symmetric ripples, ripple cross lamination, wavy bedding
paleocurrent indicators (see B.)
altered pumice
parallel stratification
fossilized algal mat
slumping
burrows
olistostrome
cross bedding
cut and fill structures
shelly debris
KTab
Jrd
JntE
JntD3
JntD2
JntD1
JntC
JntB3
JntB2
JntB1
JntA2
JntA1

Figure 3. Generalized stratigraphic columns. **(A)** Stratigraphy and key sedimentological features of the Nacientes del Teno Formation and the lowermost strata of the Rio Damas Formation. See Figure 2 for column locations. Bedding thicknesses are not drawn to scale but depict generalized variations in grain size throughout units. Unit thicknesses and columns heights are drawn to scale. Unit colors and abbreviations same as Figure 2. **(B)** Rose diagrams of unidirectional (black) and bidirectional (gray) paleocurrent indicators (bin size 30°).

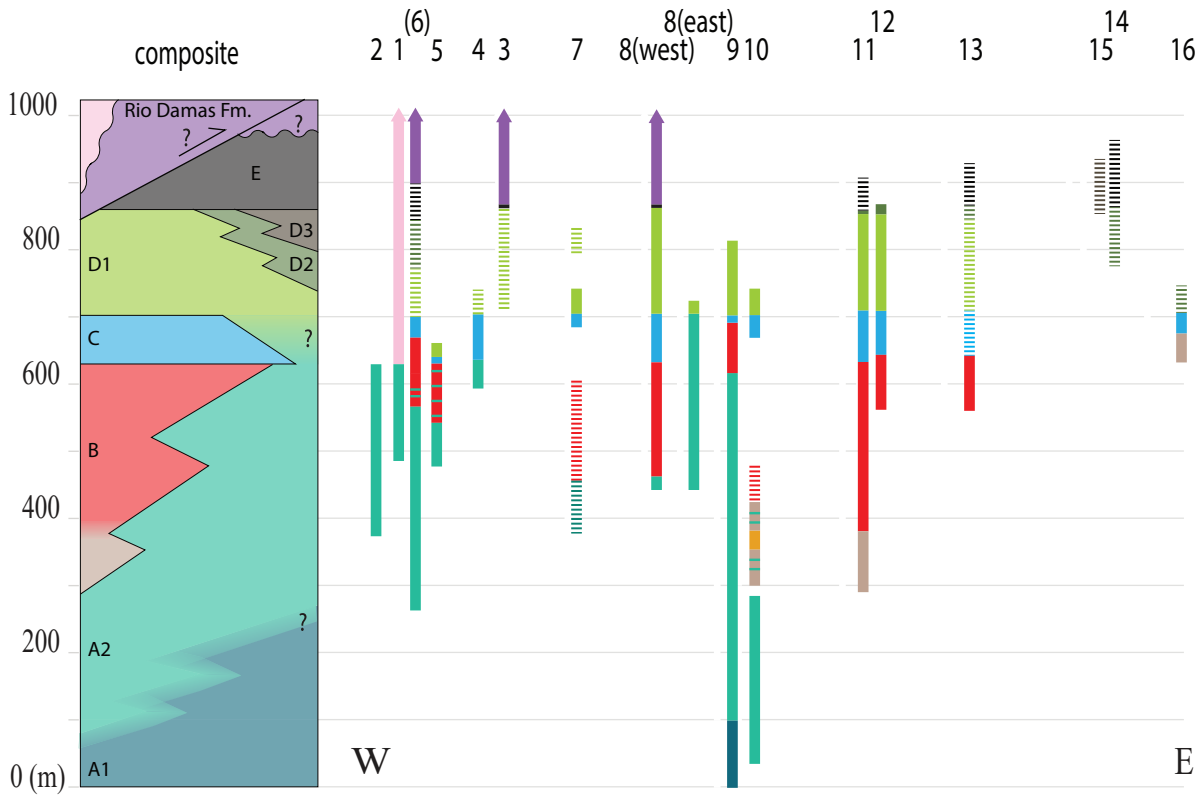

Figure 4. Lithostratigraphic sections (see Fig. 2 for locations and color key) of Mesozoic units projected onto a ~W-E-oriented profile showing thicknesses and relationships between units. Thicknesses are dashed where speculative. Vertical position of sections estimated from field observations.

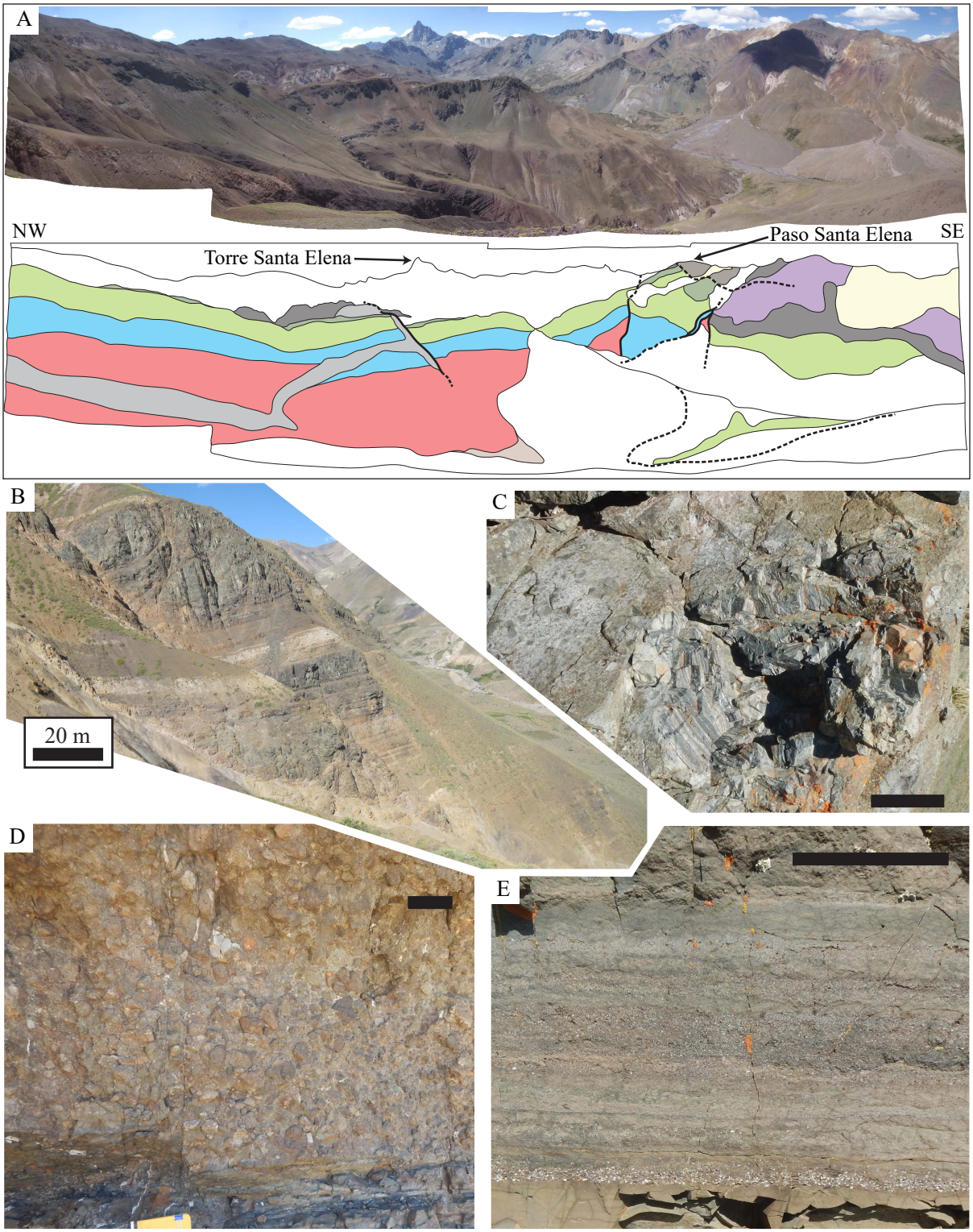
A
NW
Torre Santa Elena
Paso Santa Elena
SE
B
20 m
C
D
E

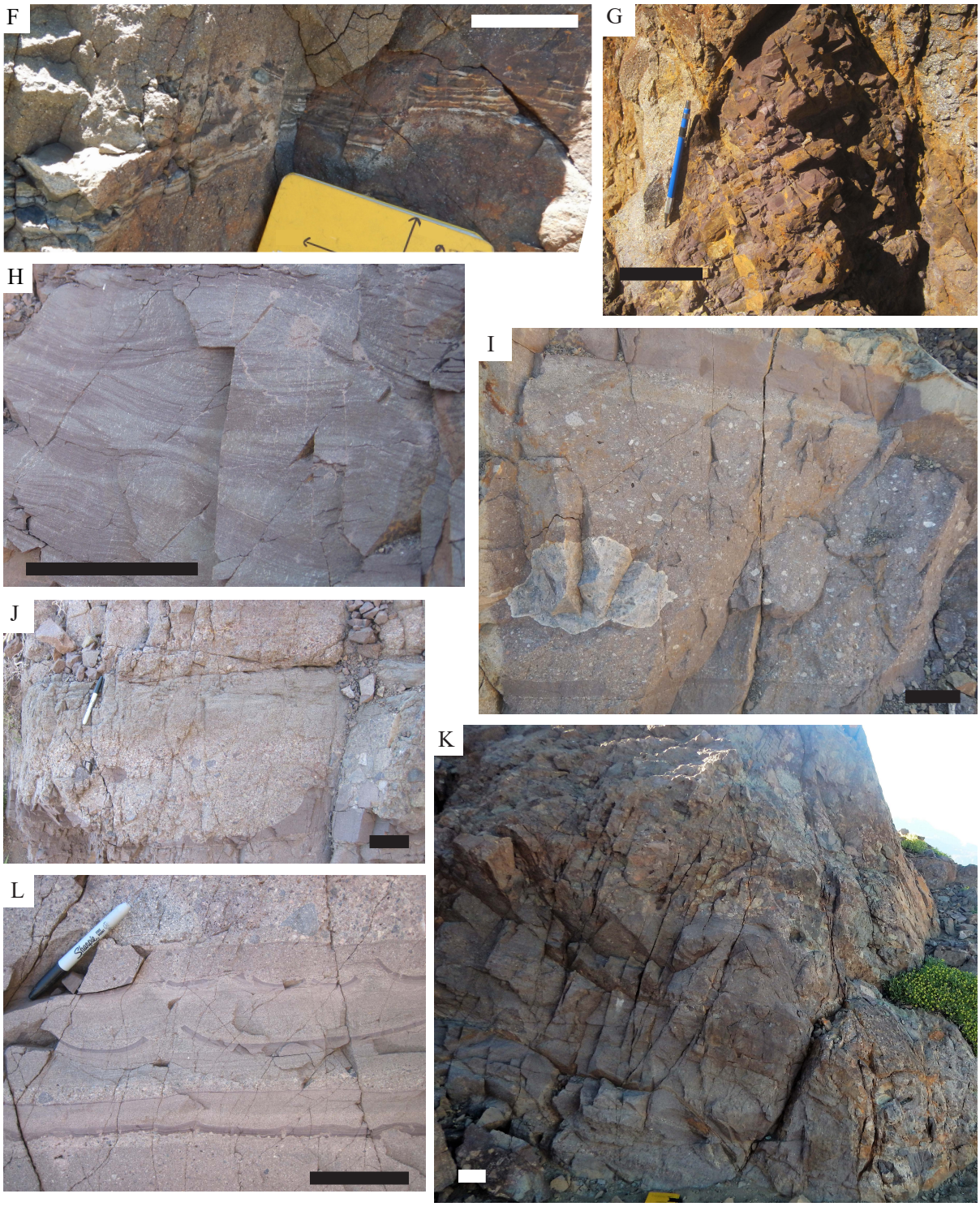
F
G
H
I
J
K
L

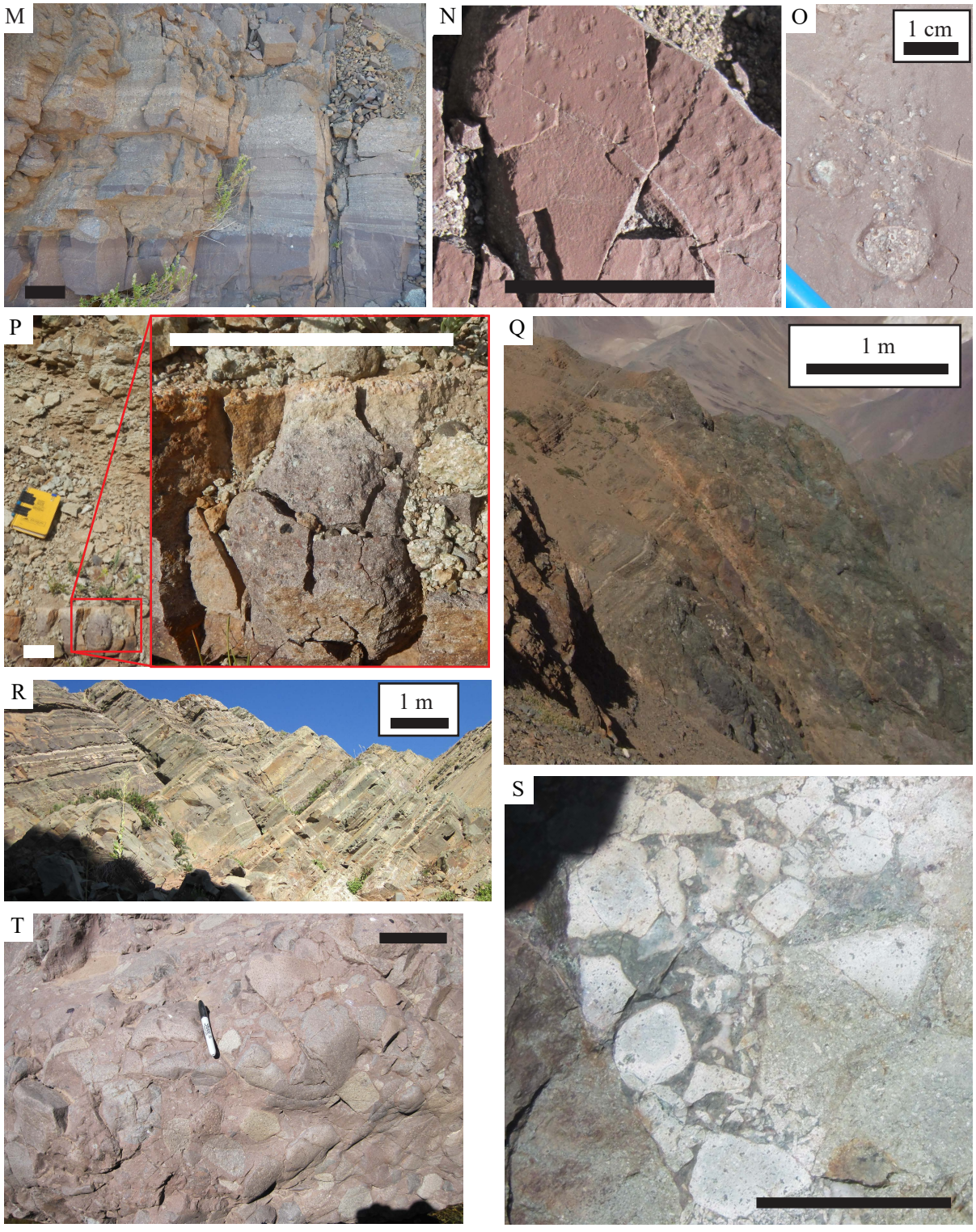
M
N
O
1 cm
P
Q
1 m
R
1 m
S
T

Figure 5. Rock unit photos (unlabeled scale bars 10 cm). **(A)** Annotated panoramic photomosaic of eastern part of field area (bold lines are faults; unit colors same as Fig. 2). **(B)** Cliff with well exposed sequence of three cyclic, coarsening upwards packages of volcaniclastic strata (JntA2). **(C)** Laminated carbonaceous shale olistolith in olistostrome (JntA2). **(D)** A typical orthoconglomerate overlying finer-grained strata along an erosive contact, with the morphology of the underlying strata consistent with soft sediment deformation (slumping). **(E)** Volcaniclastic turbidites: ungraded, massive mudstone overlain by normally graded, fine- to coarse-grained volcaniclastic sandstone with abundant blocky feldspar grains. **(F)** Soft sediment deformation (slumping) structures in laminated carbonaceous shale bed bound above and below by poorly sorted, unstratified sandstone debris flow deposits. **(G)** Basaltic andesite lava deposit or volcanic breccia (JntB2) with an entrained clast of well bedded sandstone likely derived from JntB3 strata. **(H)** Ripple cross lamination, wavy bedding, and symmetric ripples in red fine-grained sandstone (JntB1). **(I)** Tabular, well-bedded, poorly sorted debris flow and flood deposits (JntB3). **(J)** Channelized orthoconglomerate infilling an incised pebbly sandstone debris flow deposit (JntB3). **(K)** Coarse channelized debris flow conglomerate (JntB3). **(L)** Alternating beds of unsorted and unstratified pebble conglomerate, poorly sorted sandstone with plane laminations and low-angle cross bedding, and desiccated mudstone with some mudcracks partially entrained as rip-up clasts in overlying sandstone (JntB3). **(M)** Tabular, well-bedded, poorly sorted sandstone and pebble conglomerate deposits (JntB3). **(N)** Raindrop impressions in mudstone (JntB3). **(O)** Obstacle scour in mudstone (flow direction towards top of page) (JntB3). **(P)** Depositional contact separating poorly sorted pebble conglomerate (JntB3) from overlying well sorted rhyolitic sandstone (JntC) interpreted as a basal surge or basal fallout deposit. **(Q)** Debris flow conglomerate or rock avalanche deposit (JntD1) overlain along sharp contact by fining upwards sequence of fine-grained sandstone (JntD1), and carbonaceous sandstone, siltstone, and shale (JntD2). **(R)** Well-bedded, volcaniclastic turbidites (JntD1). **(S)** Rock avalanche deposit containing angular, exclusively andesitic clasts (JntD1). **(T)** Well-rounded clasts and sandy matrix in fluvial cobble orthoconglomerate.

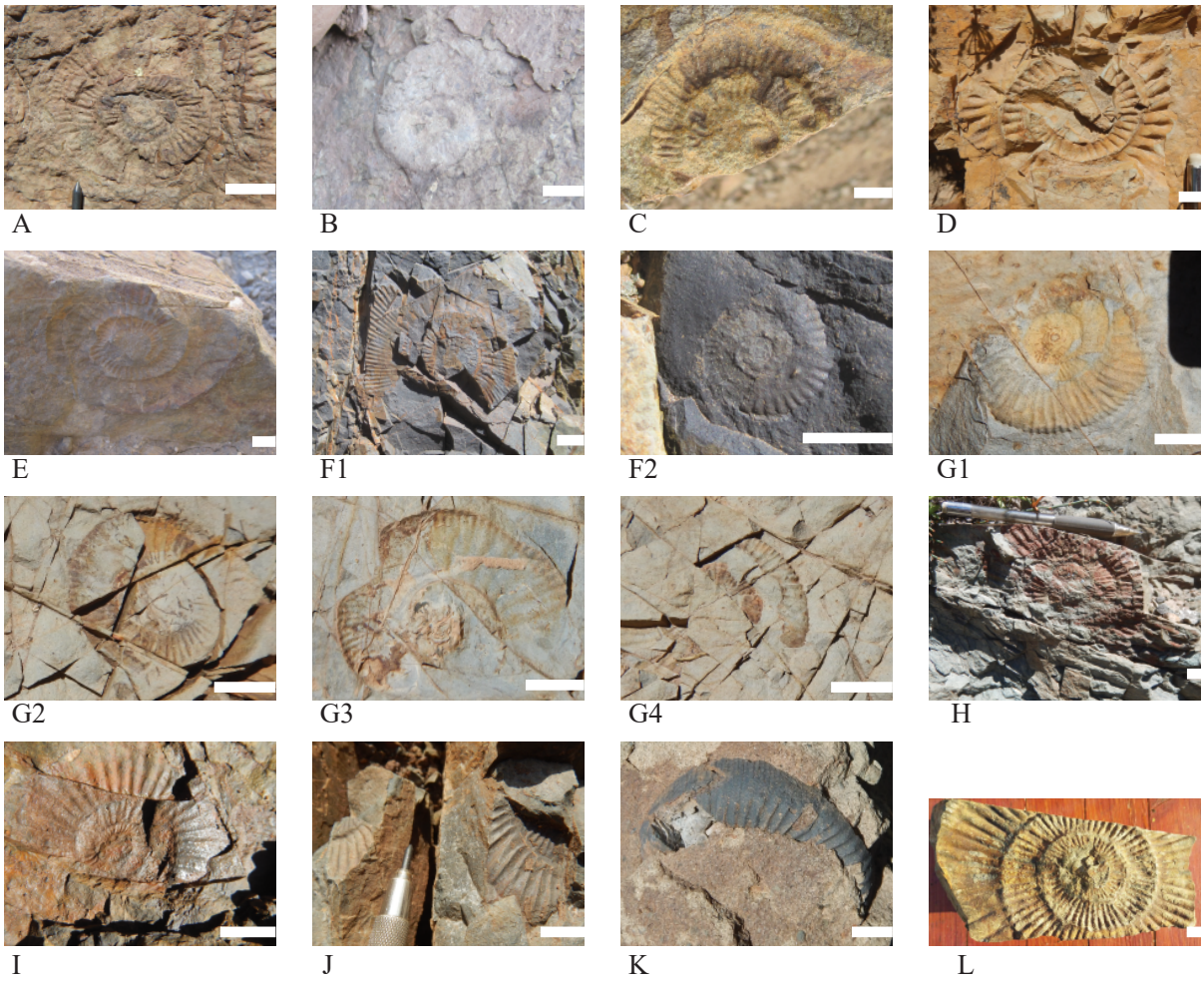

Figure 6. Photographs of ammonite remains hosted by Nacientes del Teno Formation units JntA and JntD (see Fig. 2 for ammonite locations; see Table 3 for ammonite identifications). Scale bars are 1 cm.

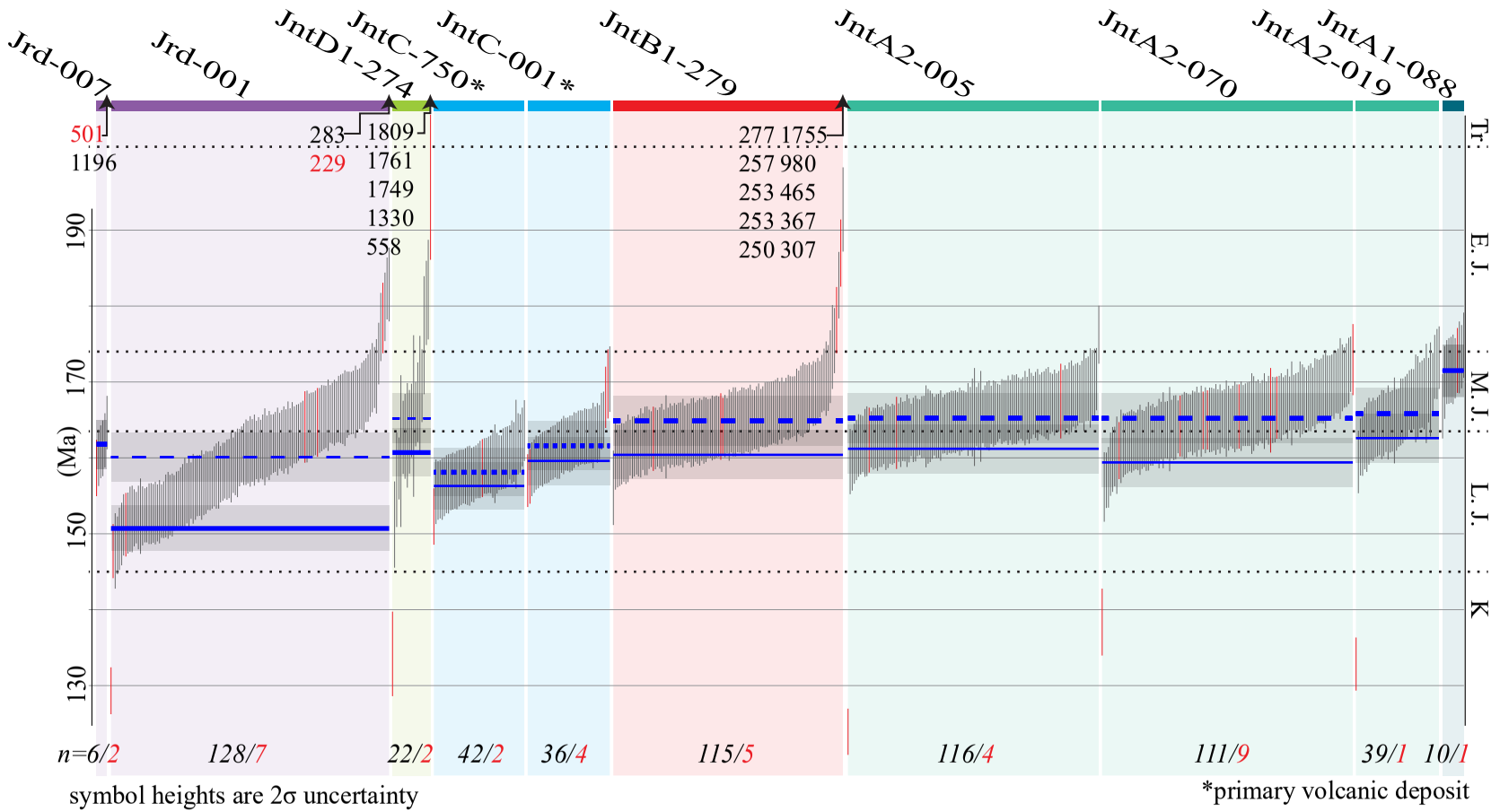

symbol heights are 2σ uncertainty

*primary volcanic deposit

single-grain ages

concordant analysis

discordant analysis

^{207}Pb-corrected $^{238}U/^{206}Pb$ age for analyses younger than 1400 Ma

$^{207}Pb/^{206}Pb$ age for analyses older than 1400 Ma

sample depositional ages

lower intercept age

weighted mean of <200 Ma concordant ages

weighted mean of youngest 10 concordant ages that overlap within 2σ uncertainty

bold lines preferred depositional age

Figure 7. U-Pb ages (vertical lines) for Nacientes del Teno and Rio Damas Formation samples. Sample depositional ages calculated by various methods are plotted as horizontal blue lines. See text for discussion.

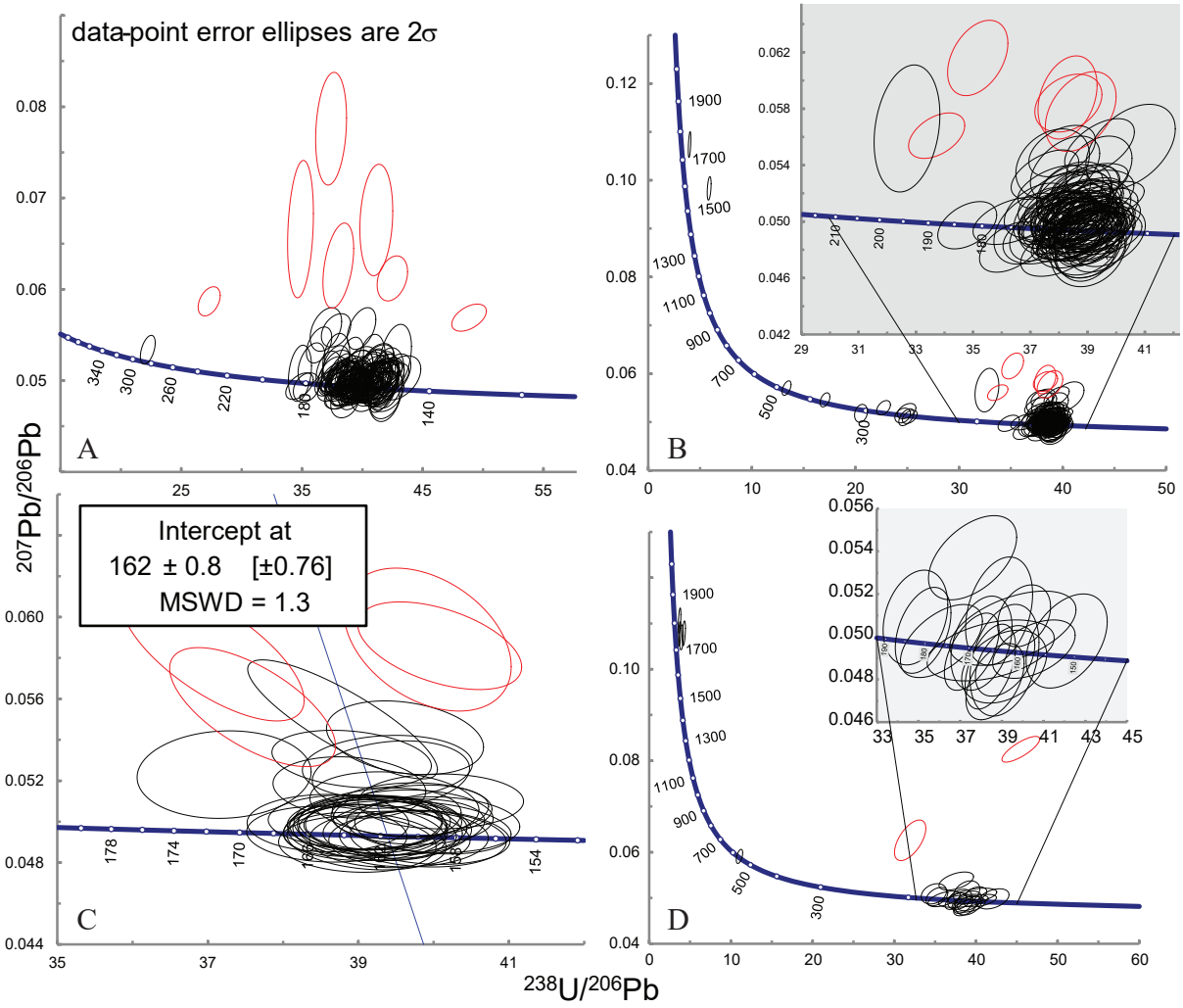

Figure 8. Sample concordia plots of U-Pb ages yielded by zircons from samples **(A)** Jrd-001, **(B)** JntB1-279, **(C)** JntC-001, and **(D)** JntD1-274

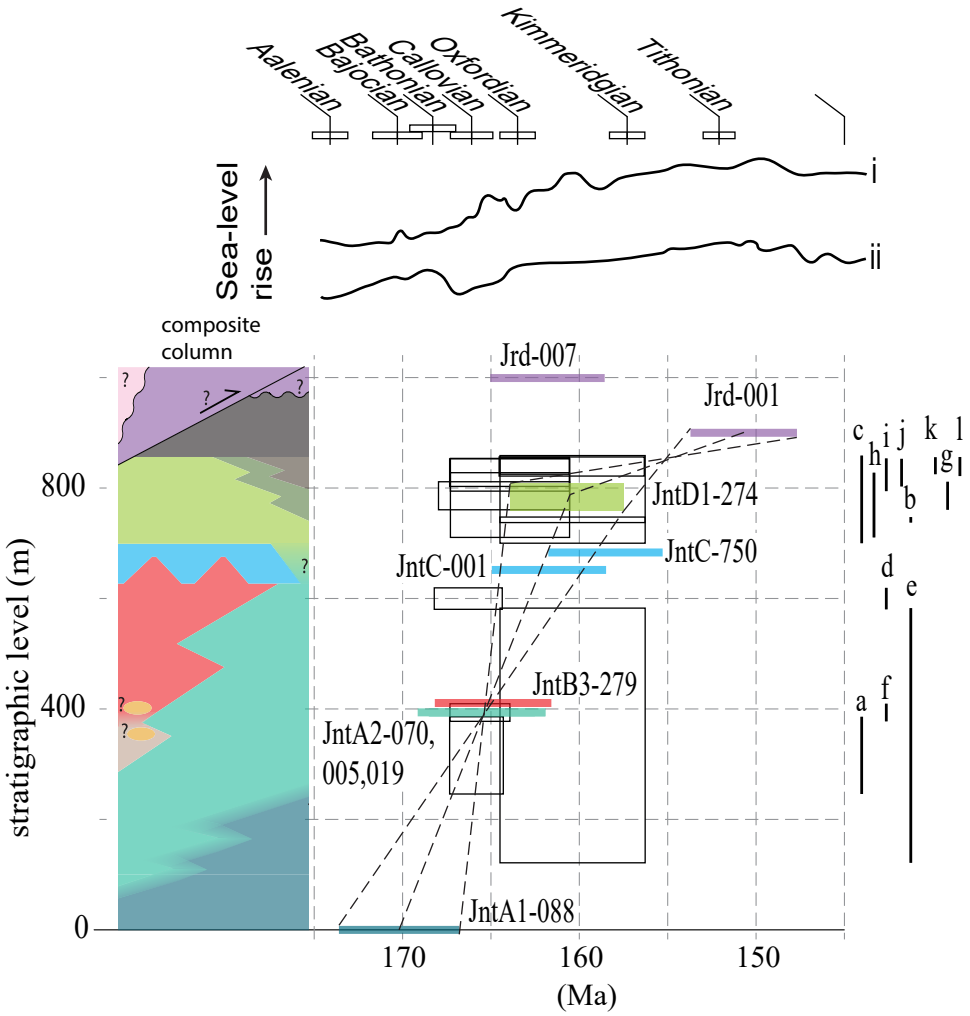

Figure 9. Stratigraphic level versus age. Preferred depositional ages of geochronology samples (labeled on chart) (Table 1) are plotted as colored boxes (colors same as previous figures; bar widths represent 2 sigma uncertainty in age; bar heights represent approximate uncertainty in stratigraphic position relative to JntC-001). Ammonite specimens (Fig. 6; labelled on right vertical axis) are plotted as hollow black boxes (box heights correspond to approximate uncertainty in stratigraphic position relative to JntC-001; ages and box widths are based on age ranges provided by Alberto Riccardi (Table 2) and are plotted with respect to numerical boundaries and uncertainties of Jurassic stages according to the International Commission on Stratigraphy (Cohen et al., 2013)). Sea level curves adapted from (i) Hallam (1988) and (ii) Haq et al., (1987).

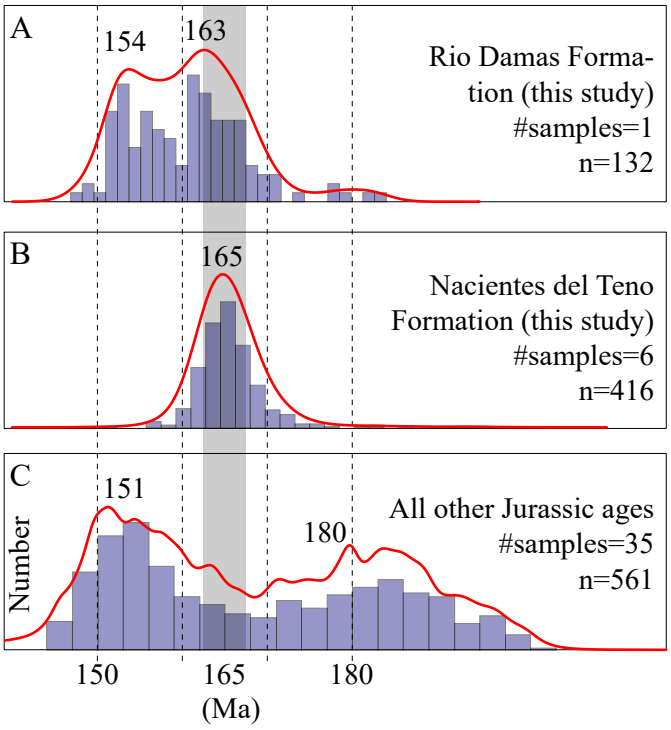

Figure 10. Frequency histogram and relative probability plots of Jurassic U-Pb detrital zircon ages from **(A)** the Rio Damas Formation (sample Jrd-001), **(B)** the Nacientes del Teno Formation (samples JntA1-088, JntA2-019, JntA2-070, JntA2-005, JntB3-279, JntD1-274), and **(C)** all 35 samples from backarc basin deposits in Chile and Argentina for which published data is available (all samples from Late Jurassic and younger deposits) (Tunik et al., 2010; Oliveros et al., 2012; Di Giulio et al., 2012; Naipauer et al., 2012, 2015a, 2015b; Rossel et al., 2013, 2014; Horton et al., 2016; Fennell et al., 2017; Balgord and Carrapa, 2017).

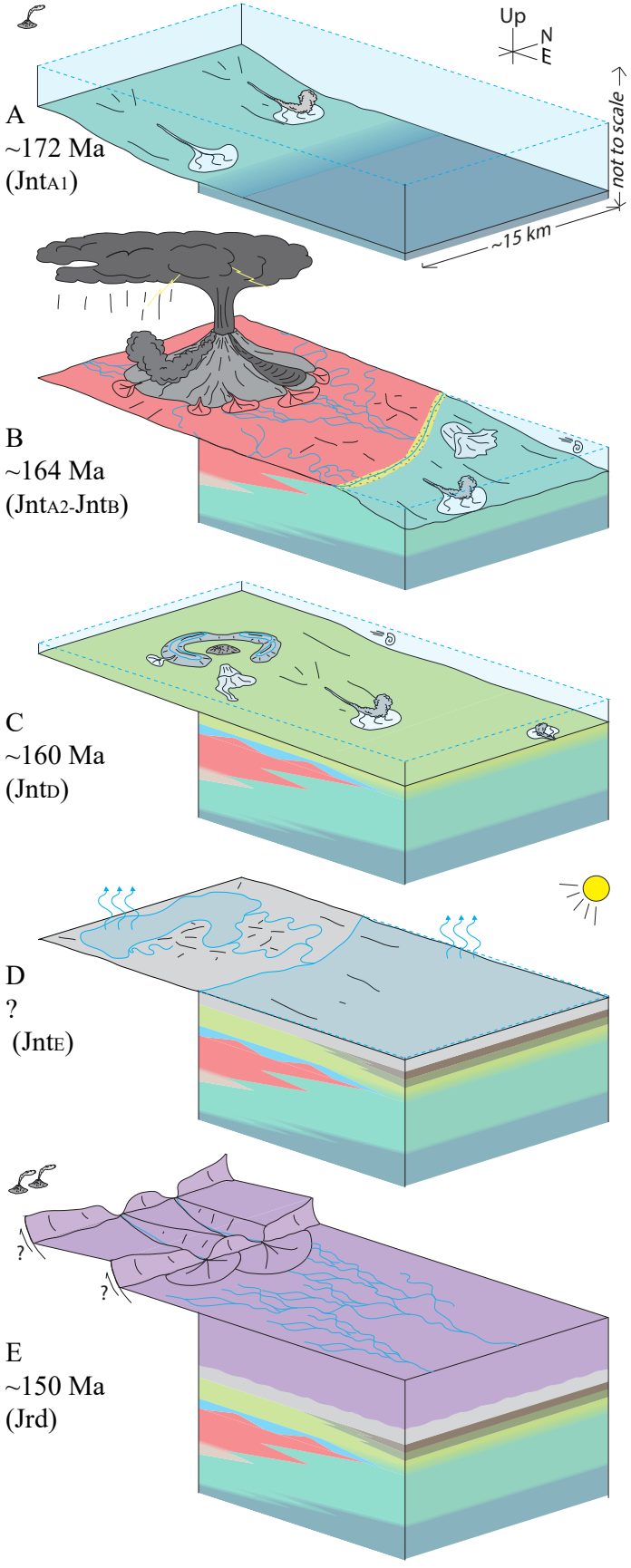

Figure 11. Jurassic paleogeographic reconstruction of Nacimiento del Teno region at time of deposition of **(A)** JntA, **(B)** JntA2 and JntB, **(C)** JntD, **(D)** JntE, and **(E)** Jrd

weighted mean of all concordant ages (Ma)	± (Ma)	weighted mean of youngest 10 concordant ages* with U (ppm) <700 (Ma)	± (Ma)	weighted mean of youngest 10 concordant ages* (Ma)	± (Ma)	weighted mean of all concordant ages <200 (Ma)	± (Ma)	preferred ages (Ma)	± (Ma)
Jnt-750 159	3	Jrd-001 151	3	Jrd-001 151	3	Jnt-750 159	3	Jrd-007 162	3
Jrd-001 161	3	Jnt-750 157	3	Jnt-750 156	3	Jrd-001 160	3	Jrd-001 151	3
Jnt-001 162	3	Jnt-001 160	3	Jnt-070 159	3	Jnt-001 162	3	Jnt-274 161	3
Jrd-007 164	52	Jnt-279 161	3	Jnt-001 160	3	Jrd-007 162	3	Jnt-750 158†	3
Jnt-070 165	3	Jnt-070 162	3	Jnt-279 160	3	Jnt-279 165	3	Jnt-001 162†	3
Jnt-005 165	3	Jnt-005 162	3	Jnt-274 161	3	Jnt-274 165	4	Jnt-279 165	3
Jnt-019 166	3	Jnt-019 163	3	Jnt-005 161	3	Jnt-070 165	3	Jnt-070 165	3
Jnt-279 168	6	Jnt-274 164	3	Jnt-019 163	3	Jnt-005 165	3	Jnt-005 165	3
Jnt-088 172	3	Jrd-007 162	3	Jrd-007 162	3	Jnt-019 166	3	Jnt-019 166	3
Jnt-274 175	50	Jnt-088 172	4	Jnt-088 172	3	Jnt-088 172	3	Jnt-088 172	3

*that overlap within 2σ uncertainty

†lower intercept age

all uncertainties reported at the 2σ confidence level

Table 1. Depositional ages for sampled strata of the Nacientes del Teno and Rio Damas formations calculated by various methods

Ammonite specimen (Fig. 6)	Identification	Age
A	?Rehmannia sp.	Early Callovian
B	?Discosphinctes sp.	Oxfordian
C	?Perisphinctid	Oxfordian
D	Neuqueniceras cf. biscissum (Stehn)	Late Bathonian-Early Callovian
E	?Perisphinctid	Oxfordian
F1	?Rehmannia sp.	Late Early to early Middle Callovian
F2	?Reineckeia sp.	Early Callovian
G1	?Rehmannia sp. Or ?Tenuisphinctes sp.	Early Callovian or Early Oxfordian
G2	?Rehmannia sp. Or ?Tenuisphinctes sp.	Early Callovian or Early Oxfordian
G3	?Rehmannia sp. Or ?Tenuisphinctes sp.	Early Callovian or Early Oxfordian
G4	?Neuqueniceras sp.	Late Bathonian to Early Callovian
H	?Rehmannia sp. Or ?Tenuisphinctes sp.	Early Callovian or Early Oxfordian
I	?Rehmannia sp. Or ?Tenuisphinctes sp.	Early Callovian or Early Oxfordian
J	?Rehmannia sp. Or ?Tenuisphinctes sp.	Early Callovian or Early Oxfordian
K	?Caracoliceras cf. dunkeri (Stein.)	Early to Middle? Oxfordian
L	Perisphinctes (?Antilloceras) sp.	Oxfordian

Table 2. Identifications and ages of photographed ammonite specimens (Fig. 6) from the Nacientes del Teno Formation

Session	**1**	**2**	**3**	**4**
Date	09.17.15	04.18.16	05.09.17	05.13.17
Samples analyzed	Jnt_C-001, Jrd-007	Jnt_C-750	Jnt_{D1}-274, Jnt_{B1}-279, Jnt_{A2}-070, Jnt_{A2}-019, Jnt_{A2}-005, Jnt_{A1}-088	Jrd-001
spot size (μm)	40	25	20	15
laser energy (mJ)	2.5	3.0	3.0	3.0
firing frequency (Hz)	4	4	4	4
average duration (z)	14	13	8	10
shots per analysis	56	52	32	40

Table 3. Samples analyzed for U-Pb data and conditions set during each LA-ICP-MS analytical session

APPENDIX A. Summary of LA-ICP-MS analytical results

Sample Jrd-007 (35° 8' 39.732"" S - 70° 26' 15.530"" W)

spot #	U [ppm]	Th/U	$^{238}U/^{206}Pb$	±2σ [%]	$^{207}Pb/^{235}U$	±2σ [%]	$^{207}Pb/^{206}Pb$	±2σ [%]	rho	$^{206}Pb/^{238}U$ age [Ma]	±2σ [Ma]	$^{207}Pb/^{235}U$ age [Ma]	±2σ [Ma]	Preferred age [Ma]	±2σ [Ma]	concordance
2	504	0.641	38.5208	0.8616	0.2900	0.0199	0.0808	0.0051	-0.611	165.2	1.3	258.6	1.9	158.6	3.7	0.639
4	433	0.688	39.5570	0.9199	0.1890	0.0068	0.0540	0.0016	-0.327	160.9	1.6	175.8	15.0	160.0	3.7	0.916
5	544	0.649	39.6668	0.8594	0.1671	0.0039	0.0479	0.0011	0.244	160.5	1.7	156.9	2.7	160.8	3.5	1.023
3	457	0.711	39.5101	0.9030	0.1695	0.0046	0.0488	0.0011	-0.361	161.1	1.9	159.0	4.8	161.2	3.7	1.013
6	444	0.619	39.2465	0.8612	0.1704	0.0040	0.0490	0.0011	-0.146	162.2	1.3	159.8	1.8	162.3	3.5	1.015
1	536	0.640	38.6250	0.8281	0.1796	0.0043	0.0501	0.0011	-0.173	164.8	1.5	167.7	1.8	164.6	3.5	0.982
7	877	0.043	11.4811	0.4803	1.3780	0.0379	0.1122	0.0031	0.841	538.4	19.0	879.6	11.0	501.5	20.8	0.612
9	693	0.750	4.6211	0.1412	3.6640	0.0855	0.1232	0.0037	0.832	1262.8	27.0	1563.6	9.5	1196.4	36.3	0.808

Sample Jrd-001 (35° 8' 9.589"" S - 70° 28' 4.942"" W)

spot #	U [ppm]	Th/U	$^{238}U/^{206}Pb$	±2σ [%]	$^{207}Pb/^{235}U$	±2σ [%]	$^{207}Pb/^{206}Pb$	±2σ [%]	rho	$^{206}Pb/^{238}U$ age [Ma]	±2σ [Ma]	$^{207}Pb/^{235}U$ age [Ma]	±2σ [Ma]	Preferred age [Ma]	±2σ [Ma]	concordance
7	2814	1.304	48.8281	1.1696	0.1593	0.0041	0.0569	0.0012	0.484	130.7	1.7	150.1	2.3	129.3	3.1	0.871
119	213	0.690	42.4809	1.0273	0.1975	0.0074	0.0612	0.0020	0.294	150.0	2.0	183.0	5.3	147.7	3.6	0.820
136	149	0.593	43.0663	1.4516	0.1604	0.0069	0.0503	0.0020	0.397	148.0	4.0	151.1	5.3	147.7	5.0	0.980
135	104	0.737	42.7350	1.0895	0.1710	0.0099	0.0525	0.0030	0.337	149.1	2.4	160.3	8.1	148.5	3.8	0.930
31	290	0.530	42.5894	1.1673	0.1659	0.0068	0.0506	0.0019	0.465	149.6	2.7	155.9	5.2	149.3	4.1	0.960
18	240	0.532	42.4268	1.1731	0.1627	0.0051	0.0503	0.0013	0.490	150.2	2.8	153.1	3.4	149.9	4.1	0.981
61	109	0.536	42.0875	1.1234	0.1619	0.0093	0.0503	0.0027	0.272	151.4	2.5	152.4	7.6	151.1	4.0	0.994
90	158	0.680	41.1523	1.1102	0.2260	0.0186	0.0676	0.0050	0.163	154.8	2.7	206.9	15.0	151.2	4.2	0.748
21	438	0.798	41.9815	1.1193	0.1678	0.0050	0.0511	0.0012	0.435	151.8	2.6	157.5	3.2	151.4	4.0	0.963
133	857	0.709	41.8585	1.1867	0.1669	0.0053	0.0507	0.0012	0.434	152.2	3.0	156.7	3.6	151.9	4.3	0.971
130	216	0.611	41.9463	1.2156	0.1614	0.0060	0.0488	0.0018	0.271	151.9	3.1	151.9	4.5	151.9	4.4	1.000
26	296	0.857	41.8060	1.0360	0.1684	0.0074	0.0507	0.0018	0.300	152.4	2.2	158.0	5.7	152.1	3.8	0.964
94	260	0.455	41.8060	0.9354	0.1677	0.0054	0.0506	0.0014	0.332	152.4	1.5	157.4	3.7	152.1	3.4	0.968
53	76	0.624	41.8936	1.1514	0.1602	0.0087	0.0488	0.0027	0.242	152.1	2.8	150.9	7.1	152.1	4.2	1.008
113	128	0.469	41.7886	1.3678	0.1665	0.0062	0.0499	0.0019	0.569	152.4	3.9	156.4	4.5	152.3	5.0	0.975
44	316	0.645	41.7711	1.0666	0.1667	0.0051	0.0500	0.0016	0.435	152.5	2.4	156.6	3.4	152.3	3.9	0.974
72	317	1.133	41.8761	0.9798	0.1566	0.0045	0.0477	0.0015	0.306	152.1	1.8	147.7	2.9	152.4	3.6	1.030
39	383	0.713	41.7711	1.0048	0.1635	0.0056	0.0492	0.0016	0.470	152.5	2.0	153.8	4.0	152.5	3.7	0.992
89	795	0.306	41.6493	1.0953	0.1682	0.0061	0.0508	0.0013	0.433	152.9	2.6	157.9	4.4	152.6	4.0	0.969
99	258	0.658	41.7014	1.0973	0.1646	0.0053	0.0497	0.0019	0.377	152.8	2.6	154.7	3.6	152.6	4.0	0.987
87	144	0.536	41.6840	1.0528	0.1668	0.0078	0.0500	0.0026	0.278	152.8	2.3	156.6	6.1	152.7	3.9	0.976
95	108	0.525	41.6667	1.1305	0.1638	0.0058	0.0501	0.0017	0.458	152.9	2.8	154.0	4.2	152.7	4.1	0.993
47	106	0.550	41.6840	1.0218	0.1652	0.0087	0.0497	0.0026	0.507	152.8	2.1	155.2	7.0	152.7	3.7	0.984
104	586	0.714	41.5973	1.1395	0.1658	0.0047	0.0504	0.0013	0.384	153.1	2.9	155.8	2.9	152.9	4.2	0.983
42	220	0.741	41.5628	0.9617	0.1695	0.0042	0.0507	0.0014	0.396	153.3	1.7	159.0	2.1	152.9	3.5	0.964
136	187	0.493	41.5973	1.0189	0.1641	0.0063	0.0491	0.0016	0.349	153.1	2.1	154.3	4.7	153.1	3.7	0.993
82	607	0.701	41.4422	1.1216	0.1631	0.0061	0.0496	0.0014	0.362	153.7	2.7	153.4	4.5	153.6	4.1	1.002
13	355	0.625	41.4422	1.1935	0.1641	0.0058	0.0492	0.0014	0.391	153.7	3.2	154.3	4.2	153.7	4.4	0.996
67	241	0.567	41.2712	1.0703	0.1716	0.0052	0.0522	0.0015	0.421	154.3	2.5	160.8	3.4	153.7	4.0	0.960
132	179	0.343	41.2882	1.1156	0.1702	0.0069	0.0518	0.0017	0.386	154.3	2.8	159.6	5.2	153.8	4.1	0.967
116	627	0.821	41.2882	0.9804	0.1706	0.0056	0.0504	0.0013	0.421	154.3	2.0	159.9	3.9	154.0	3.6	0.965
118	1018	0.750	41.2712	0.9986	0.1628	0.0040	0.0486	0.0011	0.433	154.3	2.0	153.2	2.1	154.4	3.7	1.008
74	273	0.709	41.1862	0.9682	0.1656	0.0059	0.0494	0.0016	0.278	154.6	1.9	155.6	4.2	154.6	3.6	0.994
22	156	0.542	41.0846	1.0321	0.1695	0.0090	0.0503	0.0026	0.231	155.0	2.4	159.0	7.2	154.8	3.9	0.975
134	217	0.484	41.0678	1.1183	0.1675	0.0072	0.0500	0.0018	0.312	155.1	2.8	157.2	5.6	154.9	4.2	0.986
15	230	0.504	41.0004	1.2612	0.1675	0.0066	0.0499	0.0018	0.489	155.3	3.6	157.2	5.0	155.2	4.7	0.988
115	1840	1.072	40.9836	1.0493	0.1666	0.0041	0.0497	0.0011	0.452	155.4	2.5	156.5	2.1	155.3	4.0	0.993
8	185	0.599	40.8831	1.2179	0.1680	0.0066	0.0505	0.0018	0.425	155.8	3.4	157.7	4.9	155.5	4.6	0.988
76	255	0.537	40.9165	0.9781	0.1639	0.0053	0.0492	0.0014	0.364	155.7	2.0	154.1	3.6	155.6	3.7	1.010

120	124	0.552	40.7830	1.2010	0.1694	0.0065	0.0505	0.0023	0.338	156.2	3.3	158.9	4.8	155.9	4.6	0.983
88	896	1.057	40.7997	1.0965	0.1677	0.0052	0.0499	0.0013	0.440	156.1	2.8	157.4	3.4	156.0	4.2	0.992
58	65	0.495	40.6339	1.0369	0.1793	0.0099	0.0513	0.0031	0.338	156.7	2.5	167.5	7.9	156.3	4.0	0.936
46	291	0.681	40.7000	1.0496	0.1684	0.0057	0.0499	0.0016	0.445	156.5	2.5	158.0	4.0	156.3	4.0	0.990
6	1117	1.032	40.6504	1.1950	0.1700	0.0048	0.0507	0.0011	0.537	156.7	3.3	159.4	2.9	156.4	4.6	0.983
114	178	0.799	40.6174	1.0466	0.1717	0.0065	0.0510	0.0017	0.347	156.8	2.5	160.9	4.8	156.4	4.0	0.974
50	571	0.979	40.6504	1.0798	0.1669	0.0056	0.0488	0.0013	0.397	156.7	2.7	156.7	4.0	156.7	4.1	1.000
25	1954	1.202	40.5515	0.9945	0.1702	0.0047	0.0497	0.0011	0.443	157.0	2.2	159.6	2.8	156.9	3.8	0.984
28	379	1.028	40.5022	1.0122	0.1716	0.0048	0.0504	0.0013	0.510	157.2	2.3	160.8	3.0	157.0	3.9	0.978
40	268	0.636	40.5186	0.9840	0.1721	0.0071	0.0496	0.0017	0.337	157.2	2.1	161.2	5.4	157.1	3.8	0.975
34	1005	1.571	40.4204	1.0193	0.1693	0.0046	0.0493	0.0012	0.494	157.5	2.4	158.8	2.7	157.5	3.9	0.992
70	341	0.893	40.4531	1.1051	0.1643	0.0064	0.0485	0.0015	0.422	157.4	2.9	154.5	4.8	157.6	4.3	1.019
101	487	0.875	40.2901	1.1323	0.1753	0.0066	0.0510	0.0016	0.421	158.0	3.1	164.0	4.8	157.7	4.4	0.964
30	725	1.130	40.3551	0.9520	0.1695	0.0050	0.0491	0.0013	0.391	157.8	1.9	159.0	3.2	157.8	3.7	0.993
86	236	0.693	39.9361	0.9654	0.1892	0.0078	0.0557	0.0019	0.434	159.4	2.2	175.9	5.8	158.1	3.8	0.906
135	1107	1.550	40.1929	0.9387	0.1719	0.0041	0.0499	0.0011	0.451	158.4	1.9	161.1	2.0	158.3	3.7	0.984
78	444	0.883	40.1768	1.0109	0.1680	0.0057	0.0496	0.0016	0.291	158.5	2.4	157.7	4.0	158.4	4.0	1.005
64	166	0.495	40.1284	0.9900	0.1697	0.0062	0.0499	0.0016	0.350	158.7	2.3	159.2	4.5	158.5	3.9	0.997
134	675	1.084	40.0962	1.1937	0.1716	0.0054	0.0494	0.0012	0.437	158.8	3.5	160.8	3.6	158.8	4.7	0.988
32	2407	1.272	40.0160	0.9253	0.1742	0.0043	0.0499	0.0011	0.469	159.1	1.8	163.1	2.2	159.0	3.7	0.976
83	1604	1.326	39.9840	1.0546	0.1686	0.0048	0.0493	0.0012	0.425	159.2	2.7	158.2	2.9	159.2	4.2	1.007
133	123	0.827	39.8565	1.1366	0.1797	0.0067	0.0515	0.0018	0.377	159.7	3.2	167.8	4.9	159.3	4.5	0.952
69	205	0.765	39.7931	0.9435	0.1728	0.0066	0.0494	0.0016	0.410	160.0	2.0	161.8	4.8	160.0	3.8	0.989
1	247	0.639	39.6511	0.9147	0.1751	0.0067	0.0500	0.0018	0.363	160.6	1.8	163.8	4.9	160.4	3.7	0.980
19	1118	1.369	39.6197	1.0110	0.1763	0.0050	0.0505	0.0011	0.468	160.7	2.5	164.9	3.0	160.4	4.1	0.975
117	711	0.959	39.6354	1.0727	0.1713	0.0053	0.0489	0.0013	0.455	160.6	2.9	160.5	3.6	160.7	4.3	1.000
56	1015	1.306	39.6197	1.0208	0.1716	0.0048	0.0491	0.0012	0.514	160.7	2.6	160.8	3.0	160.7	4.1	0.999
43	227	0.758	39.4945	1.1434	0.1791	0.0063	0.0511	0.0018	0.407	161.2	3.3	167.3	4.5	160.8	4.6	0.964
105	743	1.264	39.5570	1.0186	0.1723	0.0048	0.0494	0.0012	0.382	160.9	2.6	161.4	2.9	160.9	4.1	0.997
110	282	0.791	39.4477	1.1526	0.1806	0.0070	0.0512	0.0017	0.423	161.4	3.4	168.6	5.2	161.0	4.7	0.957
35	1348	0.356	39.5570	0.9534	0.1709	0.0042	0.0490	0.0011	0.407	160.9	2.1	160.2	2.2	161.0	3.9	1.005
131	326	0.814	39.4633	1.0555	0.1776	0.0054	0.0507	0.0016	0.389	161.3	2.9	166.0	3.5	161.0	4.3	0.972
100	661	0.848	39.4945	0.9514	0.1729	0.0049	0.0498	0.0013	0.494	161.2	2.1	161.9	3.0	161.1	3.9	0.995
59	1027	0.455	39.4633	1.0555	0.1694	0.0047	0.0489	0.0011	0.581	161.3	2.9	158.9	2.8	161.4	4.3	1.015
93	963	1.147	39.4322	1.2455	0.1731	0.0062	0.0495	0.0012	0.458	161.4	3.9	162.1	4.4	161.4	5.1	0.996
41	578	0.795	39.4166	0.9943	0.1753	0.0053	0.0494	0.0012	0.478	161.5	2.5	164.0	3.5	161.5	4.0	0.985
129	421	0.732	39.4011	1.1171	0.1727	0.0055	0.0493	0.0014	0.346	161.6	3.2	161.8	3.7	161.6	4.6	0.999
107	1679	1.041	39.3701	0.9741	0.1736	0.0049	0.0493	0.0012	0.411	161.7	2.3	162.5	3.0	161.7	4.0	0.995
4	743	0.976	39.2619	0.9441	0.1775	0.0046	0.0508	0.0012	0.473	162.1	2.1	165.9	2.5	161.8	3.9	0.977
33	1094	0.509	39.2465	0.9610	0.1760	0.0047	0.0499	0.0011	0.376	162.2	2.2	164.6	2.7	162.1	3.9	0.985
79	618	1.150	39.2465	1.0889	0.1756	0.0056	0.0498	0.0013	0.268	162.2	3.1	164.3	3.8	162.1	4.5	0.987
57	874	1.030	39.2773	0.8891	0.1707	0.0043	0.0486	0.0011	0.438	162.1	1.7	160.0	2.3	162.2	3.6	1.013
68	797	0.815	39.2157	0.9781	0.1706	0.0048	0.0497	0.0013	0.392	162.3	2.4	159.9	2.9	162.3	4.0	1.015
60	1420	0.985	39.2311	1.0777	0.1731	0.0051	0.0491	0.0011	0.506	162.3	3.0	162.1	3.2	162.3	4.4	1.001
49	393	1.021	39.2003	0.9421	0.1734	0.0070	0.0489	0.0017	0.431	162.4	2.2	162.4	5.3	162.5	3.9	1.000
112	486	0.761	39.1236	1.1606	0.1743	0.0069	0.0499	0.0013	0.450	162.7	3.5	163.1	5.2	162.6	4.8	0.997
77	162	1.074	38.9864	0.9110	0.1802	0.0071	0.0521	0.0022	0.423	163.3	1.9	168.2	5.3	162.7	3.8	0.970
65	299	0.611	39.0625	1.0401	0.1729	0.0066	0.0493	0.0016	0.331	163.0	2.8	161.9	4.9	163.0	4.3	1.006
75	520	0.961	39.0320	0.9046	0.1739	0.0045	0.0498	0.0012	0.425	163.1	1.9	162.8	2.5	163.0	3.8	1.002
20	330	0.670	39.0016	0.9276	0.1761	0.0054	0.0498	0.0014	0.272	163.2	2.1	164.7	3.6	163.1	3.9	0.991
16	1084	0.624	38.9560	0.8948	0.1755	0.0046	0.0498	0.0013	0.443	163.4	1.8	164.2	2.6	163.3	3.7	0.995
54	1890	1.004	38.8803	0.8713	0.1765	0.0043	0.0499	0.0011	0.443	163.7	1.6	165.0	2.2	163.6	3.6	0.992
29	566	0.757	38.8350	0.8989	0.1790	0.0052	0.0503	0.0015	0.315	163.9	1.9	167.2	3.3	163.7	3.8	0.980
71	482	1.112	37.4112	1.0438	0.2830	0.0198	0.0776	0.0050	0.192	170.0	3.2	253.0	15.0	164.0	4.7	0.672
132	454	0.601	38.7297	1.1208	0.1820	0.0071	0.0506	0.0017	0.412	164.3	3.4	169.8	5.3	164.1	4.7	0.968
73	1458	0.674	38.7447	0.9803	0.1737	0.0046	0.0493	0.0011	0.481	164.3	2.5	162.6	2.6	164.3	4.1	1.010
111	572	0.829	38.6847	1.0063	0.1809	0.0059	0.0504	0.0012	0.424	164.5	2.7	168.8	4.1	164.3	4.2	0.974
23	455	0.649	38.6548	0.9957	0.1801	0.0052	0.0506	0.0015	0.358	164.6	2.6	168.1	3.2	164.4	4.2	0.979
81	243	1.132	38.6847	1.0063	0.1743	0.0059	0.0492	0.0016	0.544	164.5	2.7	163.1	4.2	164.6	4.3	1.008
131	189	0.506	38.0084	1.0387	0.2280	0.0157	0.0626	0.0038	0.403	167.4	3.1	208.5	12.0	164.6	4.5	0.803
2	347	0.741	38.5654	1.0020	0.1779	0.0067	0.0501	0.0016	0.512	165.0	2.7	166.3	4.9	164.9	4.3	0.993
5	321	1.271	38.4912	1.0184	0.1772	0.0060	0.0502	0.0016	0.401	165.3	2.8	165.6	4.8	165.2	4.3	0.998
45	745	0.545	38.5357	0.9822	0.1755	0.0048	0.0487	0.0013	0.424	165.2	2.5	164.2	2.9	165.3	4.2	1.006

36	188	0.707	38.5654	0.9651	0.1709	0.0064	0.0478	0.0015	0.253	165.0	2.5	160.2	4.7	165.4	4.1	1.030
97	121	0.958	38.4025	1.0958	0.1778	0.0078	0.0501	0.0023	0.318	165.7	3.3	166.2	6.0	165.6	4.7	0.997
92	495	0.584	38.3436	0.8847	0.1816	0.0050	0.0504	0.0012	0.275	166.0	1.9	169.4	2.9	165.8	3.8	0.980
55	582	0.788	38.3436	0.9318	0.1810	0.0050	0.0500	0.0013	0.331	166.0	2.3	168.9	3.0	165.8	4.0	0.983
128	604	0.778	38.2995	1.0016	0.1834	0.0051	0.0507	0.0014	0.307	166.2	2.8	171.0	3.1	165.9	4.3	0.972
96	307	0.942	38.2848	0.9383	0.1792	0.0064	0.0504	0.0016	0.409	166.2	2.3	167.4	4.6	166.0	4.0	0.993
63	1874	0.410	38.2263	1.0084	0.1798	0.0052	0.0498	0.0011	0.471	166.5	2.8	167.9	3.2	166.4	4.4	0.992
109	526	0.815	38.1971	1.0364	0.1788	0.0054	0.0503	0.0015	0.425	166.6	3.0	167.0	3.5	166.4	4.5	0.997
127	683	0.714	38.2117	1.0670	0.1823	0.0054	0.0500	0.0014	0.381	166.5	3.2	170.0	3.4	166.4	4.6	0.979
51	660	0.859	38.2702	1.1544	0.1735	0.0058	0.0484	0.0012	0.425	166.3	3.7	162.5	4.1	166.5	5.0	1.024
48	603	0.668	37.8215	0.9933	0.2019	0.0058	0.0555	0.0015	0.357	168.2	2.8	186.7	3.5	166.9	4.4	0.901
108	1458	1.003	38.0662	0.9569	0.1797	0.0055	0.0496	0.0011	0.371	167.2	2.5	167.8	3.6	167.1	4.2	0.996
38	605	0.866	38.1243	0.9415	0.1737	0.0046	0.0483	0.0011	0.433	166.9	2.4	162.6	2.6	167.1	4.1	1.026
52	662	0.924	38.0518	0.9564	0.1800	0.0057	0.0492	0.0012	0.430	167.2	2.5	168.1	3.8	167.3	4.2	0.995
84	127	0.736	37.9507	1.0867	0.1867	0.0068	0.0510	0.0019	0.296	167.7	3.4	173.8	4.9	167.3	4.8	0.965
17	279	0.698	37.8358	0.9076	0.1918	0.0097	0.0524	0.0023	0.270	168.2	2.2	178.2	7.6	167.5	4.0	0.944
11	142	0.732	37.8215	0.8993	0.1865	0.0075	0.0517	0.0017	0.350	168.2	2.2	173.6	5.5	167.7	4.0	0.969
85	657	0.820	37.8358	1.0031	0.1807	0.0057	0.0500	0.0012	0.459	168.2	2.9	168.7	3.8	168.1	4.4	0.997
10	568	0.697	37.8215	1.0710	0.1820	0.0048	0.0502	0.0012	0.510	168.2	3.3	169.8	2.8	168.1	4.7	0.991
102	327	0.639	37.6364	0.9421	0.1845	0.0061	0.0502	0.0014	0.478	169.0	2.5	171.9	4.1	168.9	4.2	0.983
106	418	0.718	37.5516	0.9924	0.1828	0.0063	0.0507	0.0016	0.428	169.4	2.9	170.5	4.7	169.2	4.4	0.994
62	704	0.879	37.4813	0.9806	0.1816	0.0048	0.0493	0.0012	0.433	169.7	2.8	169.4	2.7	169.8	4.4	1.002
12	763	1.161	37.2995	1.0012	0.1850	0.0052	0.0498	0.0012	0.450	170.6	3.0	172.4	3.1	170.5	4.5	0.990
91	160	0.405	37.2440	0.8816	0.1881	0.0067	0.0508	0.0020	0.248	170.8	2.1	175.0	4.8	170.5	4.0	0.976
14	448	0.946	36.9823	1.0647	0.2055	0.0076	0.0556	0.0019	0.371	172.0	3.5	189.8	5.4	170.7	4.9	0.906
9	711	1.255	36.4166	0.8566	0.2045	0.0065	0.0539	0.0016	0.431	174.6	2.1	188.9	4.3	173.7	4.1	0.924
27	164	0.468	35.7910	0.9111	0.2013	0.0079	0.0518	0.0019	0.397	177.6	2.7	186.2	5.8	177.2	4.5	0.954
24	250	0.699	34.8797	0.8720	0.2650	0.0256	0.0666	0.0061	0.227	182.2	2.7	238.7	20.0	178.3	4.6	0.763
37	473	0.803	35.3732	0.8888	0.1915	0.0058	0.0492	0.0013	0.273	179.7	2.7	177.9	3.6	179.8	4.5	1.010
98	118	0.683	34.8311	0.7804	0.2040	0.0093	0.0508	0.0025	0.261	182.5	1.8	188.5	7.1	182.2	4.1	0.968
66	551	0.860	34.7947	0.9303	0.1946	0.0054	0.0494	0.0012	0.498	182.7	3.2	180.5	3.2	182.7	4.8	1.012
103	502	0.594	27.3224	0.7459	0.2954	0.0087	0.0587	0.0013	0.398	231.7	4.2	262.8	5.0	229.4	6.2	0.882
3	698	0.433	22.2272	0.5015	0.3313	0.0084	0.0534	0.0013	0.475	283.7	2.9	290.6	4.0	283.2	6.3	0.976

Sample JntD1-274 (35° 7' 54.219"" S - 70° 24' 10.724"" W)

spot #	U [ppm]	Th/U	$^{238}U/^{206}Pb$	±2σ [%]	$^{207}Pb/^{235}U$	±2σ [%]	$^{207}Pb/^{206}Pb$	±2σ [%]	rho	$^{206}Pb/^{238}U$ age [Ma]	±2σ [Ma]	$^{207}Pb/^{235}U$ age [Ma]	±2σ [Ma]	Preferred age [Ma]	±2σ [Ma]	concordance
17	6740	1.334	45.4959	1.8894	0.2515	0.0064	0.0825	0.0023	0.789	140.2	0.0	227.8	0.0	134.2	5.6	0.615
23	358	1.123	42.1053	1.5889	0.1656	0.0075	0.0498	0.0018	0.413	151.3	5.0	155.6	3.2	151.2	5.7	0.972
25	1284	1.046	40.5351	1.6149	0.1735	0.0063	0.0494	0.0011	0.478	157.1	4.8	162.5	5.8	157.1	6.2	0.967
1	989	1.358	40.0641	1.0369	0.1780	0.0041	0.0510	0.0012	0.293	158.9	5.3	166.3	4.5	158.6	4.1	0.955
15	313	0.551	39.5257	2.4732	0.1764	0.0089	0.0504	0.0014	0.498	161.1	2.6	165.0	1.8	160.8	10.0	0.976
18	517	0.737	39.1543	1.1620	0.1750	0.0071	0.0489	0.0013	0.449	162.6	9.2	163.7	7.1	162.7	4.8	0.993
19	103	1.054	39.1236	1.3516	0.1730	0.0075	0.0489	0.0021	0.318	162.7	3.5	162.0	5.4	162.8	5.6	1.004
9	208	1.202	39.1083	1.6636	0.1753	0.0093	0.0486	0.0014	0.338	162.8	4.5	164.0	5.7	162.9	6.9	0.992
6	111	0.750	38.8651	1.3123	0.1814	0.0083	0.0512	0.0021	0.315	163.8	6.1	169.3	7.4	163.4	5.5	0.968
14	341	0.522	38.6698	1.1399	0.1711	0.0068	0.0479	0.0015	0.476	164.6	4.4	160.4	6.5	164.9	4.8	1.026
20	856	1.589	38.4615	2.4887	0.1793	0.0100	0.0494	0.0012	0.405	165.5	3.5	167.5	5.1	165.5	10.6	0.988
3	466	1.058	38.4468	0.9883	0.1755	0.0070	0.0486	0.0016	0.478	165.5	9.7	164.2	8.0	165.7	4.2	1.008
24	267	1.080	38.0228	1.1977	0.1829	0.0072	0.0497	0.0018	0.341	167.3	2.7	170.6	5.3	167.3	5.2	0.981
12	846	1.007	37.5940	1.7269	0.1977	0.0100	0.0537	0.0016	0.490	169.2	4.0	183.2	5.3	168.3	7.7	0.924
22	645	0.522	37.5516	1.0695	0.1836	0.0076	0.0493	0.0015	0.547	169.4	6.8	171.2	8.5	169.5	4.8	0.990
8	476	0.901	36.1011	1.6052	0.1913	0.0084	0.0498	0.0014	0.542	176.1	3.4	177.7	5.7	176.1	7.8	0.991
21	174	1.027	35.2237	1.0896	0.2004	0.0084	0.0503	0.0016	0.404	180.5	7.0	185.5	6.4	180.3	5.5	0.973
7	144	1.058	34.8554	1.2661	0.2017	0.0104	0.0509	0.0018	0.273	182.3	4.2	186.6	6.3	182.1	6.6	0.977
13	308	0.873	31.9489	1.5654	0.2680	0.0169	0.0626	0.0036	0.593	198.7	5.4	241.1	8.1	195.5	9.5	0.824
4	832	0.603	11.0497	0.3204	0.7420	0.0218	0.0591	0.0013	0.508	558.5	8.4	563.6	13.0	558.3	15.8	0.991
26	1887	0.959	4.2355	0.1636	3.5300	0.1307	0.1078	0.0022	0.420	1366.4	11.0	1534.0	9.0	1329.8	50.2	0.891
10	1293	0.936	3.9216	0.2005	3.8300	0.1956	0.1070	0.0022	0.108	1464.2	41.0	1599.1	27.0	1748.6	38.4	0.916
16	1322	1.323	3.7216	0.1179	4.0800	0.1291	0.1077	0.0022	0.451	1534.2	63.0	1650.3	38.0	1761.2	37.0	0.930
11	2118	0.387	3.7120	0.1329	4.1800	0.1462	0.1106	0.0023	0.491	1537.8	33.0	1670.1	21.0	1809.1	37.6	0.921

Sample JntC-750 (35° 8' 28.449"" S - 70° 28' 4.435"" W)

spot #	U [ppm]	Th/U	$^{238}U/^{206}Pb$	±2σ [%]	$^{207}Pb/^{235}U$	±2σ [%]	$^{207}Pb/^{206}Pb$	±2σ [%]	rho	$^{206}Pb/^{238}U$ age [Ma]	±2σ [Ma]	$^{207}Pb/^{235}U$ age [Ma]	±2σ [Ma]	Preferred age [Ma]	±2σ [Ma]	concordance
31	277	0.588	41.5110	1.0161	0.1843	0.0046	0.0554	0.0012	0.545	153.5	4.1	171.8	4.9	152.2	3.7	0.893
21	1302	1.324	40.9836	1.1264	0.1650	0.0051	0.0487	0.0012	0.671	155.4	2.2	155.1	2.2	155.5	4.2	1.002
26	784	0.968	40.9333	1.0169	0.1644	0.0051	0.0487	0.0013	0.371	155.6	1.5	154.5	2.5	155.7	3.8	1.007
40	1176	0.450	40.8497	1.0141	0.1687	0.0050	0.0497	0.0011	0.657	155.9	2.1	158.3	2.3	155.8	3.8	0.985
18	413	0.702	40.8497	1.0656	0.1678	0.0044	0.0495	0.0013	0.533	155.9	2.4	157.5	3.0	155.8	4.0	0.990
32	547	0.667	40.5844	1.0052	0.1811	0.0056	0.0531	0.0014	0.557	156.9	2.0	169.0	2.2	156.1	3.8	0.928
2	488	0.660	40.6835	0.9988	0.1674	0.0042	0.0494	0.0011	0.434	156.5	1.6	157.2	2.4	156.5	3.8	0.996
17	381	0.724	40.7166	1.0195	0.1654	0.0044	0.0485	0.0011	0.618	156.4	2.5	155.4	3.5	156.5	3.9	1.006
38	382	0.584	40.4695	0.9643	0.1773	0.0050	0.0521	0.0012	0.629	157.4	2.3	165.7	2.7	156.8	3.7	0.949
4	460	0.594	40.5186	0.9748	0.1715	0.0043	0.0506	0.0011	0.577	157.2	1.7	160.7	2.4	156.9	3.8	0.978
43	776	0.660	40.5844	0.9418	0.1680	0.0039	0.0492	0.0011	0.576	156.9	2.0	157.7	2.0	156.9	3.6	0.995
24	650	0.737	40.5844	0.9956	0.1650	0.0042	0.0486	0.0011	0.693	156.9	1.8	155.1	4.5	157.0	3.8	1.012
11	414	0.568	40.4695	0.9643	0.1685	0.0041	0.0495	0.0011	0.582	157.4	1.9	158.1	2.7	157.3	3.7	0.995
37	1078	1.197	40.4040	0.9365	0.1708	0.0056	0.0502	0.0014	0.640	157.6	1.9	160.1	2.3	157.4	3.6	0.984
19	539	0.818	40.3226	0.9105	0.1751	0.0046	0.0512	0.0012	0.490	157.9	4.9	163.8	5.2	157.5	3.5	0.964
14	641	0.738	40.4040	0.9449	0.1684	0.0043	0.0495	0.0011	0.661	157.6	1.9	158.0	2.6	157.5	3.7	0.997
25	447	0.646	40.4040	0.9992	0.1690	0.0049	0.0492	0.0011	0.580	157.6	2.3	158.6	2.5	157.6	3.9	0.994
5	288	0.549	40.3714	1.0176	0.1702	0.0049	0.0498	0.0012	0.540	157.7	2.6	159.6	2.5	157.6	3.9	0.988
30	554	0.691	40.2739	0.9092	0.1750	0.0048	0.0511	0.0013	0.603	158.1	1.7	163.7	2.6	157.7	3.5	0.966
16	583	0.666	40.3389	0.9430	0.1710	0.0045	0.0498	0.0011	0.546	157.9	1.5	160.3	2.3	157.7	3.7	0.985
20	252	0.594	40.2577	0.8942	0.1687	0.0043	0.0496	0.0011	0.558	158.2	2.9	158.3	3.4	158.1	3.5	0.999
23	432	0.687	40.2577	0.9242	0.1681	0.0041	0.0488	0.0011	0.655	158.2	2.6	157.8	3.2	158.3	3.6	1.003
44	871	0.774	40.1606	0.9636	0.1713	0.0046	0.0499	0.0011	0.621	158.5	1.7	160.5	2.1	158.4	3.8	0.988
33	399	0.669	39.5257	0.9524	0.2121	0.0069	0.0613	0.0017	0.523	161.1	2.2	195.3	2.2	158.6	3.8	0.825
12	378	0.718	39.8248	0.9119	0.1883	0.0065	0.0540	0.0018	0.651	159.9	2.3	175.2	3.1	158.9	3.6	0.913
13	273	0.555	40.0641	0.9348	0.1693	0.0046	0.0493	0.0011	0.591	158.9	2.3	158.8	3.4	158.9	3.7	1.001
6	445	0.589	40.0000	0.9413	0.1725	0.0043	0.0498	0.0012	0.527	159.2	2.4	161.6	2.5	159.1	3.7	0.985
28	1262	1.105	39.9840	0.9580	0.1738	0.0045	0.0500	0.0012	0.708	159.2	2.1	162.7	2.4	159.1	3.8	0.979
42	480	0.558	40.0000	1.1201	0.1714	0.0061	0.0495	0.0013	0.484	159.2	2.1	160.6	2.4	159.1	4.4	0.991
1	919	0.802	39.6983	1.2960	0.1899	0.0068	0.0551	0.0015	0.712	160.4	1.6	176.5	2.8	159.2	5.2	0.908
36	966	1.066	39.8089	0.9983	0.1825	0.0051	0.0526	0.0013	0.614	159.9	2.1	170.2	2.4	159.3	4.0	0.940
10	560	0.691	40.0000	0.9092	0.1676	0.0044	0.0485	0.0012	0.646	159.2	2.3	157.3	3.7	159.3	3.6	1.012
7	806	0.902	39.9521	0.9004	0.1691	0.0044	0.0494	0.0012	0.623	159.4	2.1	158.6	4.5	159.3	3.6	1.005
27	158	1.057	39.8565	0.9999	0.1675	0.0044	0.0488	0.0012	0.645	159.7	2.1	157.2	2.4	159.8	4.0	1.016
8	180	1.171	39.7931	1.0171	0.1711	0.0053	0.0494	0.0012	0.460	160.0	2.3	160.4	3.0	160.0	4.1	0.998
39	759	0.746	39.6825	0.9486	0.1731	0.0045	0.0499	0.0012	0.676	160.4	2.4	162.1	3.0	160.3	3.8	0.990
3	284	0.634	39.4011	0.8784	0.1870	0.0047	0.0536	0.0013	0.601	161.6	1.9	174.1	3.9	160.7	3.6	0.928
22	655	0.695	39.5883	1.0296	0.1718	0.0051	0.0497	0.0012	0.633	160.8	2.0	161.0	3.0	160.7	4.2	0.999
41	740	0.980	39.6040	0.9727	0.1727	0.0056	0.0494	0.0011	0.650	160.8	2.1	161.8	2.5	160.7	3.9	0.994
15	985	1.263	39.3391	1.4279	0.1744	0.0069	0.0496	0.0011	0.539	161.8	2.3	163.2	3.2	161.8	5.8	0.991
35	577	0.884	39.3391	0.9823	0.1730	0.0049	0.0494	0.0014	0.749	161.8	2.2	162.0	3.8	161.8	4.0	0.999
34	252	0.677	39.2003	0.9337	0.1831	0.0047	0.0519	0.0014	0.524	162.4	3.1	170.7	4.3	161.9	3.8	0.951
29	799	0.783	39.1083	0.9309	0.1777	0.0045	0.0496	0.0011	0.632	162.8	1.8	166.1	1.7	162.7	3.8	0.980
9	730	0.748	38.9105	0.9589	0.1737	0.0047	0.0495	0.0011	0.589	163.6	2.1	162.6	2.7	163.5	4.0	1.006

Sample JntC-001 (35° 9' 7.606"" S - 70° 26' 48.782"" W)

spot #	U [ppm]	Th/U	$^{238}U/^{206}Pb$	±2σ [%]	$^{207}Pb/^{235}U$	±2σ [%]	$^{207}Pb/^{206}Pb$	±2σ [%]	rho	$^{206}Pb/^{238}U$ age [Ma]	±2σ [Ma]	$^{207}Pb/^{235}U$ age [Ma]	±2σ [Ma]	Preferred age [Ma]	±2σ [Ma]	concordance
9	823	0.348	40.0802	0.8895	0.2010	0.0071	0.0586	0.0018	-0.484	158.9	1.7	186.0	8.3	157.0	3.5	0.854
38	1484	0.755	39.9202	0.9070	0.2050	0.0106	0.0589	0.0029	-0.377	159.5	1.5	189.3	4.9	157.5	3.6	0.842
7	281	0.601	40.0962	0.8970	0.1747	0.0041	0.0510	0.0011	0.005	158.8	3.0	163.5	11.0	158.4	3.5	0.971
35	667	0.753	40.0481	0.8957	0.1721	0.0042	0.0499	0.0011	-0.070	159.0	2.2	161.2	8.4	158.9	3.5	0.986
34	450	0.600	39.9361	0.8927	0.1724	0.0042	0.0497	0.0010	-0.247	159.4	2.8	161.5	17.0	159.3	3.5	0.987
40	512	0.737	39.9521	0.8665	0.1699	0.0042	0.0492	0.0011	-0.136	159.4	1.3	159.3	3.2	159.4	3.4	1.000
19	640	0.836	39.6197	0.8523	0.1869	0.0053	0.0541	0.0015	-0.254	160.7	1.6	174.0	2.3	159.7	3.4	0.924
37	329	0.698	39.8565	0.9052	0.1706	0.0044	0.0492	0.0011	-0.118	159.7	1.9	159.9	2.8	159.8	3.6	0.999
3	933	1.386	39.7141	0.8668	0.1756	0.0041	0.0506	0.0011	0.025	160.3	1.3	164.3	2.6	160.0	3.5	0.976
2	93	0.369	39.7141	0.8799	0.1736	0.0041	0.0502	0.0011	-0.053	160.3	2.6	162.5	4.5	160.1	3.5	0.986

8	577	0.567	39.6983	0.8431	0.1747	0.0039	0.0505	0.0011	0.211	160.4	1.2	163.5	2.7	160.1	3.4	0.981
31	549	0.645	39.6668	0.8656	0.1717	0.0043	0.0492	0.0011	0.035	160.5	1.9	160.9	3.1	160.5	3.5	0.998
13	1336	0.334	39.6040	0.8770	0.1744	0.0042	0.0497	0.0011	0.212	160.8	1.5	163.2	1.8	160.7	3.5	0.985
10	1133	0.560	39.4322	0.8536	0.1829	0.0047	0.0523	0.0013	0.184	161.4	1.4	170.6	1.9	160.8	3.5	0.947
26	763	0.727	39.4789	0.9176	0.1788	0.0051	0.0509	0.0013	-0.184	161.3	1.1	167.0	1.4	160.9	3.7	0.965
24	511	0.733	39.3856	0.9229	0.1845	0.0050	0.0527	0.0013	0.103	161.6	1.5	171.9	2.0	160.9	3.7	0.940
20	569	0.574	39.4166	0.8721	0.1729	0.0045	0.0491	0.0011	-0.034	161.5	1.4	161.9	1.6	161.5	3.6	0.997
1	624	0.705	39.3546	0.9385	0.1730	0.0046	0.0498	0.0012	-0.140	161.8	1.6	162.0	2.1	161.7	3.8	0.998
23	899	0.396	39.3391	0.8513	0.1740	0.0045	0.0496	0.0012	-0.155	161.8	1.5	162.9	1.8	161.7	3.5	0.993
29	907	0.736	39.3236	0.8569	0.1755	0.0039	0.0499	0.0010	0.049	161.9	1.6	164.2	2.0	161.8	3.5	0.986
33	470	0.719	39.3236	0.9131	0.1731	0.0042	0.0497	0.0011	0.015	161.9	1.8	162.1	2.2	161.8	3.7	0.999
15	669	0.711	39.2773	0.8891	0.1749	0.0044	0.0501	0.0012	0.192	162.1	1.7	163.7	2.0	161.9	3.6	0.990
36	643	0.670	39.2157	0.8874	0.1745	0.0045	0.0495	0.0011	-0.159	162.3	1.1	163.3	2.0	162.3	3.6	0.994
16	589	0.689	39.1543	0.8253	0.1755	0.0042	0.0499	0.0012	-0.071	162.6	1.7	164.2	2.3	162.5	3.4	0.990
4	603	0.669	39.1389	0.8853	0.1757	0.0042	0.0499	0.0011	0.065	162.6	2.2	164.4	2.4	162.5	3.7	0.990
28	566	0.673	39.1236	0.8644	0.1752	0.0042	0.0497	0.0012	0.027	162.7	1.7	163.9	2.2	162.6	3.6	0.993
25	234	0.487	39.1236	0.8459	0.1747	0.0044	0.0495	0.0011	-0.239	162.7	1.5	163.5	2.6	162.7	3.5	0.995
32	487	0.592	39.0930	0.8913	0.1757	0.0044	0.0495	0.0011	0.025	162.8	1.5	164.4	2.0	162.8	3.7	0.991
14	465	0.579	38.9105	0.8654	0.1880	0.0046	0.0531	0.0011	-0.237	163.6	1.3	174.9	2.5	162.8	3.6	0.935
30	356	0.604	39.1083	0.8640	0.1754	0.0046	0.0491	0.0011	-0.218	162.8	1.7	164.1	2.4	162.8	3.6	0.992
11	305	0.524	39.0625	0.8628	0.1752	0.0044	0.0498	0.0012	0.230	163.0	1.5	163.9	2.3	162.9	3.6	0.994
21	353	0.542	38.7898	1.0297	0.1960	0.0214	0.0550	0.0024	-0.844	164.1	1.3	181.7	2.3	162.9	4.3	0.903
22	392	0.569	38.8803	0.8290	0.1842	0.0049	0.0517	0.0012	-0.132	163.7	1.5	171.7	2.6	163.2	3.5	0.954
5	559	0.611	38.9560	0.9429	0.1764	0.0045	0.0500	0.0011	-0.075	163.4	1.4	165.0	2.1	163.3	3.9	0.991
27	486	0.481	38.9864	0.8545	0.1742	0.0041	0.0489	0.0011	-0.078	163.3	2.1	163.1	2.6	163.4	3.6	1.001
12	470	0.571	38.5951	0.8774	0.1784	0.0044	0.0499	0.0011	-0.011	164.9	1.9	166.7	2.1	164.8	3.7	0.989
6	725	0.788	38.5803	0.8700	0.1763	0.0043	0.0494	0.0011	-0.089	165.0	1.7	164.9	2.3	165.0	3.7	1.001
18	810	0.706	37.5940	0.9000	0.2040	0.0108	0.0556	0.0024	-0.652	169.2	1.3	188.5	2.0	167.9	4.0	0.898
17	506	0.656	37.0645	0.9921	0.2180	0.0137	0.0583	0.0028	-0.703	171.6	1.7	200.2	2.2	169.7	4.5	0.857
39	440	0.463	37.2162	0.9447	0.1931	0.0066	0.0523	0.0017	0.063	170.9	1.5	179.3	1.9	170.3	4.3	0.953

Sample JntB3-279 (35° 8' 15.659"" S - 70° 24' 37.250"" W)

spot #	U [ppm]	Th/U	$^{238}U/^{206}Pb$	±2σ [%]	$^{207}Pb/^{235}U$	±2σ [%]	$^{207}Pb/^{206}Pb$	±2σ [%]	rho	$^{206}Pb/^{238}U$ age [Ma]	±2σ [Ma]	$^{207}Pb/^{235}U$ age [Ma]	±2σ [Ma]	Preferred age [Ma]	±2σ [Ma]	concordance
12	700	1.514	40.5022	1.2747	0.1866	0.0085	0.0553	0.0025	0.422	157.2	3.8	173.7	6.5	156.0	4.9	0.905
74	834	2.082	39.6511	1.0839	0.1791	0.0048	0.0514	0.0012	0.517	160.6	2.9	167.3	2.7	160.1	4.3	0.960
77	262	0.926	39.7614	1.0259	0.1696	0.0058	0.0489	0.0017	0.398	160.1	2.6	159.1	4.1	160.2	4.1	1.007
99	436	1.151	39.4166	0.9943	0.1901	0.0057	0.0553	0.0016	0.531	161.5	2.5	176.7	3.5	160.3	4.0	0.914
69	434	0.893	39.6197	1.0013	0.1748	0.0049	0.0502	0.0012	0.376	160.7	2.5	163.6	2.9	160.5	4.0	0.982
33	279	0.749	39.4011	0.9399	0.1898	0.0074	0.0538	0.0018	0.303	161.6	2.1	176.5	5.5	160.6	3.8	0.916
89	508	1.389	39.6354	1.0314	0.1673	0.0048	0.0491	0.0012	0.362	160.6	2.6	157.1	3.0	160.7	4.2	1.023
112	323	1.114	39.4166	1.0959	0.1760	0.0053	0.0507	0.0014	0.470	161.5	3.1	164.6	3.4	161.2	4.5	0.981
34	553	1.258	39.4477	0.9013	0.1752	0.0057	0.0496	0.0014	0.340	161.4	1.8	163.9	3.9	161.3	3.7	0.984
10	771	0.886	39.4322	1.0044	0.1727	0.0054	0.0499	0.0012	0.497	161.4	2.5	161.8	3.5	161.3	4.1	0.998
66	223	0.671	39.4322	0.9762	0.1716	0.0065	0.0491	0.0016	0.431	161.4	2.3	160.8	4.8	161.5	4.0	1.004
50	387	0.938	39.4477	0.9247	0.1697	0.0072	0.0486	0.0018	0.337	161.4	1.9	159.2	5.5	161.5	3.8	1.014
113	568	1.276	39.3856	0.9932	0.1725	0.0051	0.0497	0.0016	0.396	161.6	2.4	161.6	3.3	161.5	4.1	1.000
90	408	0.862	39.3082	1.1131	0.1715	0.0069	0.0494	0.0013	0.290	161.9	3.2	160.7	5.2	161.9	4.6	1.008
30	361	0.920	39.2773	0.9117	0.1754	0.0056	0.0492	0.0016	0.348	162.1	1.9	164.1	3.8	162.1	3.7	0.988
56	540	1.087	39.0778	1.0926	0.1869	0.0047	0.0527	0.0011	0.485	162.9	3.1	174.0	2.5	162.2	4.5	0.936
108	252	0.706	39.1696	1.0964	0.1759	0.0074	0.0508	0.0017	0.396	162.5	3.1	164.5	5.6	162.2	4.5	0.988
47	1361	1.451	39.0778	0.9468	0.1821	0.0044	0.0517	0.0011	0.476	162.9	2.2	169.9	2.1	162.4	3.9	0.959
17	212	0.617	39.0473	0.8828	0.1852	0.0052	0.0522	0.0014	0.432	163.0	1.7	172.5	3.2	162.4	3.7	0.945
117	136	0.756	38.7597	1.0091	0.2071	0.0076	0.0578	0.0023	0.376	164.2	2.7	191.1	5.4	162.5	4.2	0.859
59	665	1.217	39.1696	0.9858	0.1745	0.0050	0.0494	0.0011	0.463	162.5	2.5	163.3	3.1	162.5	4.1	0.995
24	152	0.743	39.1543	0.9005	0.1762	0.0072	0.0496	0.0021	0.313	162.6	1.8	164.8	5.4	162.5	3.7	0.987
44	756	1.179	39.0625	0.9729	0.1800	0.0059	0.0512	0.0014	0.470	163.0	2.4	168.1	4.0	162.6	4.0	0.970
101	297	0.726	39.1389	1.0845	0.1713	0.0061	0.0496	0.0014	0.260	162.6	3.1	160.5	4.4	162.6	4.5	1.013
38	451	0.947	39.1236	0.8996	0.1738	0.0049	0.0499	0.0013	0.428	162.7	1.8	162.7	2.9	162.6	3.7	1.000
120	319	0.820	39.0016	1.3199	0.1810	0.0073	0.0517	0.0016	0.441	163.2	4.4	168.9	5.4	162.7	5.5	0.966
28	683	0.776	39.0778	0.8983	0.1768	0.0042	0.0496	0.0012	0.452	162.9	1.8	165.3	1.9	162.8	3.7	0.985
114	334	0.576	39.0930	1.0214	0.1722	0.0051	0.0491	0.0014	0.459	162.8	2.7	161.3	3.2	162.9	4.2	1.009

52	619	1.270	38.9864	0.9354	0.1789	0.0054	0.0509	0.0013	0.448	163.3	2.1	167.1	3.5	162.9	3.9	0.977
15	619	0.803	39.0168	1.0088	0.1768	0.0057	0.0502	0.0013	0.463	163.1	2.7	165.3	3.9	163.0	4.2	0.987
29	311	0.994	38.9257	0.9506	0.1848	0.0057	0.0520	0.0017	0.413	163.5	2.3	172.2	3.7	163.0	4.0	0.950
82	330	0.491	39.0625	1.0009	0.1718	0.0056	0.0489	0.0016	0.309	163.0	2.6	161.0	3.8	163.0	4.2	1.012
67	325	0.550	39.0930	0.9925	0.1700	0.0057	0.0478	0.0015	0.347	162.8	2.5	159.4	4.0	163.1	4.1	1.021
109	407	0.778	38.9712	1.0882	0.1760	0.0069	0.0500	0.0015	0.241	163.3	3.1	164.6	5.1	163.2	4.5	0.992
27	528	0.913	38.9864	0.8742	0.1757	0.0052	0.0497	0.0013	0.347	163.3	1.6	164.4	3.3	163.2	3.6	0.993
62	248	0.607	39.0168	0.9364	0.1708	0.0057	0.0490	0.0018	0.418	163.1	2.1	160.1	4.0	163.2	3.9	1.019
25	423	0.535	38.9560	0.9262	0.1780	0.0049	0.0501	0.0013	0.566	163.4	2.1	166.3	2.9	163.2	3.9	0.982
88	599	1.439	38.9864	1.0888	0.1741	0.0057	0.0494	0.0011	0.379	163.3	3.2	163.0	3.9	163.2	4.5	1.002
63	141	0.704	39.0320	1.0801	0.1707	0.0086	0.0481	0.0022	0.208	163.1	3.1	160.0	6.8	163.3	4.5	1.019
31	198	0.677	39.0016	0.9359	0.1726	0.0084	0.0486	0.0023	0.223	163.2	2.2	161.7	6.7	163.4	3.9	1.009
60	203	0.671	39.0016	0.9987	0.1670	0.0056	0.0485	0.0020	0.235	163.2	2.6	156.8	3.9	163.4	4.2	1.041
85	333	1.190	38.8803	1.0636	0.1774	0.0060	0.0509	0.0015	0.523	163.7	3.0	165.8	4.1	163.4	4.4	0.987
36	382	0.958	38.8651	0.9574	0.1786	0.0055	0.0503	0.0012	0.412	163.8	2.4	166.9	3.6	163.6	4.0	0.981
95	484	1.012	38.9105	1.0545	0.1703	0.0046	0.0493	0.0012	0.406	163.6	2.9	159.7	2.7	163.6	4.4	1.024
61	250	0.692	38.8651	1.0130	0.1750	0.0058	0.0499	0.0017	0.420	163.8	2.7	163.7	4.0	163.7	4.2	1.000
100	413	1.345	38.7297	0.9192	0.1803	0.0056	0.0518	0.0014	0.286	164.3	2.1	168.3	3.7	163.8	3.9	0.976
51	594	0.852	38.8048	0.9215	0.1763	0.0048	0.0502	0.0013	0.466	164.0	2.1	164.9	2.8	163.8	3.9	0.995
107	282	0.858	38.7747	1.0096	0.1780	0.0079	0.0506	0.0020	0.283	164.1	2.7	166.3	6.0	163.9	4.3	0.987
65	455	0.615	38.8500	0.9840	0.1745	0.0065	0.0490	0.0015	0.422	163.8	2.5	163.3	4.8	163.9	4.1	1.003
46	332	1.202	38.7147	0.9702	0.1784	0.0058	0.0510	0.0016	0.421	164.4	2.4	166.7	4.4	164.1	4.1	0.986
55	818	1.533	38.7297	0.9442	0.1793	0.0045	0.0507	0.0012	0.518	164.3	2.3	167.5	2.4	164.1	4.0	0.981
75	304	0.871	38.8350	1.0414	0.1743	0.0069	0.0485	0.0019	0.191	163.9	2.9	163.1	5.1	164.1	4.4	1.005
45	334	0.707	38.7898	0.8901	0.1738	0.0042	0.0493	0.0012	0.510	164.1	1.8	162.7	2.1	164.1	3.7	1.008
118	446	1.179	38.3289	0.9570	0.2094	0.0073	0.0584	0.0017	0.299	166.0	2.5	193.0	5.1	164.1	4.1	0.860
7	139	0.896	38.2995	0.8430	0.2108	0.0092	0.0588	0.0024	0.297	166.2	1.5	194.2	6.9	164.2	3.6	0.855
98	485	0.609	38.7597	1.1113	0.1711	0.0060	0.0492	0.0013	0.462	164.2	3.3	160.4	4.2	164.2	4.7	1.024
42	480	0.809	38.5951	0.9399	0.1812	0.0055	0.0507	0.0016	0.308	164.9	2.3	169.1	3.6	164.6	4.0	0.975
71	269	0.797	38.5357	1.0702	0.1866	0.0071	0.0517	0.0016	0.313	165.2	3.1	173.7	5.2	164.7	4.5	0.951
116	276	1.353	38.5208	1.0696	0.1870	0.0059	0.0520	0.0018	0.297	165.2	3.1	174.1	3.9	164.7	4.6	0.949
43	323	0.650	38.5951	0.9399	0.1759	0.0059	0.0504	0.0014	0.432	164.9	2.3	164.5	4.1	164.7	4.0	1.002
96	1645	1.922	38.6100	0.9666	0.1754	0.0044	0.0499	0.0011	0.510	164.8	2.4	164.1	2.2	164.7	4.1	1.005
57	746	0.922	38.5208	1.0392	0.1831	0.0055	0.0514	0.0013	0.517	165.2	3.0	170.7	3.5	164.8	4.4	0.968
16	312	1.196	38.5654	1.0212	0.1781	0.0060	0.0502	0.0016	0.409	165.0	2.8	166.4	4.2	164.9	4.3	0.992
48	313	1.040	38.5803	0.9656	0.1751	0.0055	0.0497	0.0013	0.514	165.0	2.4	163.8	3.6	164.9	4.1	1.007
73	589	1.234	38.6100	0.9941	0.1748	0.0061	0.0490	0.0015	0.350	164.8	2.7	163.6	4.3	164.9	4.2	1.008
111	365	0.940	38.6100	1.0942	0.1752	0.0052	0.0490	0.0014	0.482	164.8	3.3	163.9	3.3	164.9	4.6	1.006
81	2024	1.611	38.5654	0.9475	0.1773	0.0043	0.0499	0.0011	0.442	165.0	2.3	165.7	2.4	164.9	4.0	0.996
32	478	0.980	38.4320	0.9023	0.1886	0.0054	0.0523	0.0014	0.318	165.6	2.0	175.4	3.2	165.0	3.9	0.944
78	238	0.796	38.5208	0.9725	0.1757	0.0061	0.0494	0.0018	0.402	165.2	2.5	164.4	4.3	165.2	4.2	1.005
86	436	0.916	38.5505	1.0605	0.1739	0.0059	0.0486	0.0015	0.415	165.1	3.1	162.8	4.2	165.2	4.5	1.014
70	339	1.113	38.5060	0.8820	0.1764	0.0074	0.0495	0.0016	0.092	165.3	1.8	165.0	5.7	165.2	3.8	1.002
105	756	1.339	38.3877	0.9332	0.1812	0.0050	0.0513	0.0012	0.417	165.8	2.3	169.1	2.9	165.4	4.0	0.980
19	873	1.449	38.2117	0.9891	0.1933	0.0066	0.0538	0.0018	0.457	166.5	2.7	179.4	4.6	165.6	4.3	0.928
37	397	0.700	38.4025	0.9960	0.1776	0.0057	0.0498	0.0014	0.414	165.7	2.7	166.0	3.9	165.6	4.3	0.998
3	230	0.878	38.1098	0.9496	0.1988	0.0066	0.0550	0.0015	0.417	167.0	2.5	184.1	4.9	165.8	4.1	0.907
68	420	1.023	38.4025	0.9684	0.1750	0.0044	0.0487	0.0011	0.523	165.7	2.5	163.7	2.3	165.9	4.2	1.012
102	5090	1.505	38.2848	0.9468	0.1784	0.0045	0.0505	0.0010	0.430	166.2	2.4	166.7	2.3	166.0	4.1	0.997
1	242	1.136	38.3142	0.9744	0.1773	0.0060	0.0497	0.0016	0.411	166.1	2.6	165.7	4.1	166.0	4.2	1.002
84	287	1.192	38.2848	1.0202	0.1830	0.0057	0.0501	0.0016	0.264	166.2	2.9	170.6	3.8	166.1	4.4	0.974
6	366	0.882	38.2702	0.8826	0.1788	0.0057	0.0500	0.0014	0.456	166.3	1.9	167.0	3.9	166.2	3.8	0.996
80	580	1.250	38.3289	1.0123	0.1773	0.0053	0.0487	0.0012	0.414	166.0	2.8	165.7	3.3	166.2	4.4	1.002
54	397	1.087	38.2117	0.8469	0.1819	0.0047	0.0506	0.0012	0.492	166.5	1.6	169.7	2.6	166.3	3.7	0.981
39	418	0.695	38.2117	0.9359	0.1811	0.0061	0.0499	0.0015	0.331	166.5	2.4	169.0	4.2	166.4	4.1	0.985
94	753	1.428	38.2409	0.9901	0.1710	0.0046	0.0485	0.0011	0.486	166.4	2.7	160.3	2.7	166.6	4.3	1.038
26	321	0.788	38.2263	0.9449	0.1777	0.0049	0.0488	0.0012	0.308	166.5	2.4	166.1	2.9	166.6	4.1	1.002
11	1026	1.243	38.1243	0.9166	0.1809	0.0058	0.0505	0.0014	0.331	166.9	2.2	168.8	3.8	166.7	4.0	0.989
4	426	0.933	38.1098	0.9004	0.1811	0.0055	0.0503	0.0015	0.375	167.0	2.1	169.0	3.5	166.8	3.9	0.988
79	631	1.081	38.1098	1.1041	0.1805	0.0066	0.0499	0.0012	0.464	167.0	3.4	168.5	4.7	166.9	4.8	0.991
41	408	0.712	37.9651	0.9534	0.1863	0.0055	0.0510	0.0013	0.401	167.6	2.5	173.5	3.5	167.3	4.2	0.966
103	447	1.118	37.7786	1.0491	0.1952	0.0073	0.0541	0.0020	0.266	168.4	3.2	181.1	5.2	167.4	4.6	0.930
5	294	0.759	38.0373	1.1220	0.1723	0.0076	0.0480	0.0015	0.485	167.3	3.6	161.4	5.9	167.6	4.9	1.036

40	315	0.987	37.8358	1.0318	0.1882	0.0063	0.0516	0.0016	0.553	168.2	3.0	175.1	4.3	167.7	4.5	0.960
8	3046	1.747	37.7786	0.9917	0.1897	0.0056	0.0525	0.0013	0.524	168.4	2.8	176.4	3.5	167.8	4.4	0.955
53	590	0.488	37.8645	1.0330	0.1803	0.0070	0.0499	0.0018	0.375	168.0	3.1	168.3	5.2	167.9	4.6	0.998
35	272	0.956	37.7644	0.8611	0.1797	0.0058	0.0499	0.0015	0.408	168.5	1.8	167.8	3.9	168.4	3.8	1.004
2	411	0.939	37.7359	0.9630	0.1829	0.0054	0.0504	0.0015	0.556	168.6	2.7	170.6	3.4	168.4	4.3	0.989
13	478	0.598	37.7359	0.9370	0.1820	0.0053	0.0504	0.0014	0.465	168.6	2.5	169.8	3.3	168.4	4.2	0.993
18	358	0.619	37.5094	0.9637	0.1963	0.0057	0.0533	0.0014	0.524	169.6	2.7	182.0	3.6	168.8	4.3	0.932
23	515	0.826	37.6364	0.8319	0.1827	0.0052	0.0497	0.0013	0.435	169.0	1.6	170.4	3.2	169.0	3.7	0.992
9	315	0.894	37.4392	0.8390	0.1855	0.0058	0.0504	0.0016	0.432	169.9	1.7	172.8	3.7	169.7	3.8	0.983
14	252	0.803	37.3832	0.9012	0.1803	0.0066	0.0492	0.0016	0.389	170.2	2.3	168.3	4.7	170.2	4.1	1.011
104	191	0.709	37.3692	1.0817	0.1763	0.0060	0.0488	0.0015	0.294	170.2	3.5	164.9	4.2	170.4	4.9	1.033
21	302	0.541	37.2578	0.9548	0.1889	0.0063	0.0508	0.0016	0.409	170.7	2.7	175.7	4.3	170.5	4.3	0.972
97	162	0.478	36.9959	1.0362	0.1762	0.0068	0.0495	0.0021	0.366	171.9	3.3	164.8	5.1	171.9	4.8	1.043
76	469	1.083	36.4166	1.1592	0.1865	0.0055	0.0501	0.0014	0.456	174.6	4.3	173.6	3.4	174.5	5.5	1.006
64	335	0.614	36.3240	0.8980	0.1806	0.0063	0.0482	0.0015	0.458	175.1	2.5	168.6	4.5	175.4	4.3	1.039
49	262	1.339	35.1617	0.8597	0.2386	0.0087	0.0616	0.0022	0.392	180.8	2.5	217.3	6.5	178.1	4.3	0.832
91	428	1.077	34.7947	0.8410	0.1930	0.0053	0.0497	0.0014	0.432	182.7	2.4	179.2	3.0	182.7	4.4	1.019
20	912	1.024	33.7268	0.8011	0.2290	0.0060	0.0561	0.0013	0.449	188.4	2.4	209.4	3.2	186.9	4.4	0.900
92	142	1.634	32.6904	0.9385	0.2350	0.0176	0.0566	0.0037	0.219	194.2	3.9	214.3	14.0	192.6	5.6	0.906
72	1190	1.250	25.2398	0.5837	0.2800	0.0069	0.0511	0.0011	0.440	250.5	2.9	250.7	3.1	250.5	5.7	0.999
83	601	3.351	24.9377	0.7313	0.2894	0.0084	0.0523	0.0013	0.413	253.5	5.3	258.1	4.8	253.1	7.3	0.982
87	251	1.016	24.9128	0.5936	0.2790	0.0076	0.0510	0.0014	0.521	253.7	3.2	249.9	4.1	253.8	6.0	1.015
119	721	0.655	24.5580	0.6137	0.2888	0.0076	0.0514	0.0012	0.281	257.3	3.8	257.6	3.9	257.3	6.4	0.999
93	1019	0.567	22.7118	0.5411	0.3181	0.0082	0.0530	0.0012	0.426	277.8	3.5	280.4	4.0	277.4	6.5	0.990
110	243	0.551	20.5381	0.5083	0.3450	0.0121	0.0518	0.0015	0.211	306.5	4.4	301.0	7.6	306.7	7.5	1.018
22	968	0.397	17.0590	0.3860	0.4447	0.0102	0.0546	0.0012	0.422	367.2	3.8	373.6	3.4	366.9	8.2	0.983
115	1266	0.119	13.3511	0.3536	0.5887	0.0146	0.0570	0.0012	0.508	465.6	7.5	470.0	5.6	465.2	12.1	0.991
58	3420	0.289	5.8789	0.1523	2.3030	0.0651	0.0983	0.0020	0.376	1012.7	15.0	1213.2	14.0	980.0	24.8	0.835
106	1213	1.001	3.9872	0.1010	3.6660	0.0887	0.1074	0.0022	0.464	1442.6	20.0	1564.0	11.0	1755.3	37.2	0.922

Sample JntA2-005 (35° 9' 5.684"" S - 70° 25' 21.151"" W)

spot #	U [ppm]	Th/U	$^{238}U/^{206}Pb$	±2σ [%]	$^{207}Pb/^{235}U$	±2σ [%]	$^{207}Pb/^{206}Pb$	±2σ [%]	rho	$^{206}Pb/^{238}U$ age [Ma]	±2σ [Ma]	$^{207}Pb/^{235}U$ age [Ma]	±2σ [Ma]	Preferred age [Ma]	±2σ [Ma]	concordance
76	973	0.752	48.7567	1.1807	0.2590	0.0071	0.0906	0.0030	0.241	130.9	1.8	233.9	4.0	123.9	3.1	0.560
83	307	0.863	39.9042	1.0833	0.1757	0.0056	0.0497	0.0016	0.416	159.6	2.9	164.4	3.7	159.5	4.3	0.971
27	822	1.375	39.7456	0.9961	0.1812	0.0055	0.0520	0.0013	0.540	160.2	2.4	169.1	3.5	159.6	4.0	0.947
34	532	1.006	39.5570	0.9804	0.1803	0.0057	0.0514	0.0014	0.478	160.9	2.3	168.3	3.8	160.5	4.0	0.956
28	951	0.964	39.5413	0.9798	0.1726	0.0048	0.0493	0.0012	0.455	161.0	2.3	161.7	2.8	161.0	4.0	0.996
35	547	0.909	39.2927	1.0091	0.1831	0.0049	0.0514	0.0013	0.563	162.0	2.6	170.7	2.8	161.6	4.1	0.949
87	600	0.998	39.3701	0.9562	0.1742	0.0055	0.0493	0.0014	0.276	161.7	2.2	163.1	3.7	161.7	3.9	0.992
105	463	0.828	39.2619	0.8960	0.1782	0.0045	0.0510	0.0012	0.461	162.1	1.8	166.5	2.4	161.8	3.7	0.974
110	491	0.941	39.2465	1.0889	0.1759	0.0060	0.0506	0.0014	0.474	162.2	3.1	164.5	4.3	161.9	4.5	0.986
86	548	0.683	39.2619	1.1221	0.1736	0.0052	0.0493	0.0012	0.365	162.1	3.3	162.5	3.4	162.1	4.6	0.998
79	374	1.043	38.5357	1.0009	0.2270	0.0166	0.0631	0.0044	0.392	165.2	2.7	207.7	13.0	162.3	4.3	0.795
65	639	0.851	39.2157	0.8947	0.1719	0.0049	0.0490	0.0013	0.385	162.3	1.7	161.1	3.0	162.4	3.7	1.008
31	757	1.013	39.1850	0.9863	0.1761	0.0055	0.0491	0.0012	0.414	162.4	2.5	164.7	3.6	162.5	4.1	0.986
47	559	1.011	39.1083	0.9565	0.1800	0.0054	0.0504	0.0014	0.410	162.8	2.2	168.1	3.5	162.5	4.0	0.968
112	324	0.567	39.0778	1.0508	0.1782	0.0060	0.0508	0.0016	0.394	162.9	2.9	166.5	4.2	162.6	4.3	0.978
117	634	0.938	39.1389	0.9488	0.1717	0.0046	0.0490	0.0012	0.412	162.6	2.2	160.9	2.6	162.7	3.9	1.011
72	297	0.779	39.0930	0.9560	0.1806	0.0077	0.0499	0.0017	0.305	162.8	2.3	168.6	5.8	162.7	4.0	0.966
13	519	0.922	39.0625	0.8628	0.1770	0.0048	0.0504	0.0014	0.385	163.0	1.5	165.5	2.8	162.7	3.6	0.985
8	425	0.698	39.0473	1.0599	0.1754	0.0057	0.0506	0.0014	0.339	163.0	3.0	164.1	3.9	162.7	4.4	0.993
67	383	0.633	39.0778	1.0014	0.1769	0.0050	0.0498	0.0015	0.454	162.9	2.6	165.4	3.1	162.8	4.1	0.985
50	322	0.676	39.0320	0.9124	0.1761	0.0053	0.0499	0.0013	0.447	163.1	2.0	164.7	3.4	163.0	3.8	0.990
107	424	1.116	39.0168	0.9624	0.1739	0.0052	0.0497	0.0015	0.276	163.1	2.4	162.8	4.2	163.1	4.0	1.002
70	403	0.631	39.0320	0.9204	0.1766	0.0062	0.0493	0.0016	0.331	163.1	2.0	165.1	4.4	163.1	3.8	0.988
71	230	0.821	38.6548	1.1283	0.2029	0.0073	0.0561	0.0019	0.364	164.6	3.5	187.6	5.1	163.2	4.7	0.878
58	662	0.887	38.9560	0.9181	0.1757	0.0048	0.0499	0.0012	0.339	163.4	2.0	164.4	2.7	163.3	3.8	0.994
17	302	0.764	38.9257	1.0969	0.1779	0.0072	0.0503	0.0016	0.448	163.5	3.2	166.3	5.4	163.3	4.6	0.984
104	702	0.825	38.8954	0.9326	0.1770	0.0063	0.0504	0.0013	0.419	163.6	2.2	165.5	4.5	163.4	3.9	0.989
82	616	0.697	38.9257	0.9506	0.1772	0.0046	0.0496	0.0013	0.434	163.5	2.3	165.6	2.6	163.5	4.0	0.987
99	563	0.792	38.8803	1.1384	0.1804	0.0062	0.0503	0.0013	0.488	163.7	3.4	168.4	4.3	163.5	4.8	0.972

19	389	0.773	38.9105	1.0050	0.1755	0.0052	0.0494	0.0012	0.501	163.6	2.6	164.2	3.3	163.6	4.2	0.996
32	524	0.882	38.8954	0.8242	0.1779	0.0053	0.0495	0.0013	0.421	163.6	1.1	166.3	3.4	163.6	3.4	0.984
80	507	0.884	38.8500	1.0124	0.1809	0.0058	0.0503	0.0013	0.432	163.8	2.7	168.8	3.9	163.6	4.2	0.970
88	426	0.713	38.8651	1.0326	0.1798	0.0057	0.0491	0.0015	0.519	163.8	2.8	167.9	3.8	163.8	4.3	0.975
3	436	0.724	38.7898	0.8976	0.1752	0.0050	0.0500	0.0016	0.280	164.1	1.9	163.9	3.0	163.9	3.8	1.001
102	406	0.550	38.8048	0.8693	0.1752	0.0069	0.0496	0.0016	0.475	164.0	1.6	163.9	5.2	164.0	3.7	1.001
39	851	1.100	38.7597	0.9627	0.1824	0.0056	0.0503	0.0013	0.452	164.2	2.4	170.1	3.7	164.0	4.0	0.965
1	439	0.868	38.7597	0.9627	0.1755	0.0050	0.0501	0.0014	0.447	164.2	2.4	164.2	3.1	164.1	4.1	1.000
106	333	0.688	38.8199	1.2857	0.1749	0.0076	0.0487	0.0015	0.401	164.0	4.3	163.7	5.9	164.1	5.4	1.002
94	321	0.565	38.7747	1.1670	0.1764	0.0062	0.0496	0.0014	0.444	164.1	3.6	165.0	4.4	164.1	4.9	0.995
96	861	1.042	38.7597	1.1221	0.1781	0.0057	0.0499	0.0011	0.431	164.2	3.4	166.4	3.5	164.1	4.7	0.987
77	549	0.820	38.7898	1.0199	0.1772	0.0056	0.0492	0.0015	0.274	164.1	2.8	165.6	3.7	164.1	4.3	0.991
29	367	0.717	38.7447	0.9117	0.1767	0.0047	0.0501	0.0014	0.316	164.3	2.0	165.2	2.6	164.1	3.8	0.994
97	244	0.691	38.6847	0.9968	0.1827	0.0061	0.0512	0.0016	0.434	164.5	2.7	170.4	4.2	164.1	4.2	0.966
53	699	0.807	38.7747	1.0001	0.1738	0.0051	0.0492	0.0013	0.411	164.1	2.6	162.7	3.2	164.2	4.2	1.009
69	438	0.754	38.7297	1.0993	0.1797	0.0048	0.0499	0.0012	0.537	164.3	3.3	167.8	2.8	164.2	4.6	0.979
63	424	0.906	38.7747	0.8824	0.1745	0.0048	0.0489	0.0015	0.285	164.1	1.7	163.3	2.9	164.2	3.7	1.005
109	356	0.853	38.5208	0.9050	0.1915	0.0061	0.0532	0.0017	0.423	165.2	2.0	177.9	4.0	164.4	3.8	0.929
114	504	0.908	38.7147	0.9702	0.1753	0.0064	0.0490	0.0013	0.423	164.4	2.4	164.0	4.7	164.5	4.1	1.002
10	575	0.799	38.5803	0.9394	0.1817	0.0053	0.0512	0.0016	0.308	165.0	2.3	169.5	3.3	164.6	4.0	0.973
59	485	0.804	38.6847	0.9782	0.1755	0.0047	0.0487	0.0012	0.470	164.5	2.5	164.2	2.8	164.7	4.1	1.002
25	392	0.802	38.6698	0.9597	0.1755	0.0056	0.0488	0.0015	0.475	164.6	2.4	164.2	3.8	164.7	4.1	1.002
33	240	0.814	38.6250	0.9762	0.1769	0.0067	0.0497	0.0016	0.303	164.8	2.5	165.4	4.9	164.7	4.1	0.996
21	408	0.717	38.6250	0.9241	0.1775	0.0052	0.0496	0.0012	0.438	164.8	2.1	165.9	3.3	164.7	3.9	0.993
92	234	0.630	38.5505	1.0504	0.1831	0.0051	0.0511	0.0016	0.270	165.1	3.0	170.7	3.1	164.7	4.5	0.967
5	334	0.702	38.5803	0.9480	0.1761	0.0053	0.0501	0.0013	0.512	165.0	2.3	164.7	3.3	164.8	4.0	1.002
38	262	0.719	38.6100	0.9237	0.1756	0.0065	0.0491	0.0017	0.371	164.8	2.1	164.3	4.7	164.9	3.9	1.003
48	345	0.676	38.3877	0.8716	0.1933	0.0070	0.0536	0.0019	0.313	165.8	1.7	179.4	4.9	164.9	3.7	0.924
115	273	0.723	38.5951	1.1256	0.1735	0.0073	0.0488	0.0017	0.453	164.9	3.4	162.5	5.5	165.0	4.8	1.015
41	366	0.948	38.4468	0.9791	0.1863	0.0061	0.0515	0.0014	0.441	165.5	2.6	173.5	4.1	165.1	4.2	0.954
62	225	0.943	38.5803	1.2029	0.1735	0.0083	0.0479	0.0018	0.435	165.0	3.9	162.5	6.5	165.3	5.1	1.015
78	687	1.194	38.4172	1.5090	0.1838	0.0074	0.0510	0.0013	0.406	165.7	5.5	171.3	5.5	165.3	6.4	0.967
44	263	0.613	38.5060	0.9124	0.1769	0.0090	0.0489	0.0022	0.322	165.3	2.1	165.4	7.2	165.4	3.9	0.999
14	254	0.685	38.4912	1.0380	0.1766	0.0060	0.0491	0.0016	0.348	165.3	3.0	165.1	4.1	165.4	4.4	1.001
95	243	0.561	38.4025	1.3954	0.1845	0.0073	0.0509	0.0017	0.449	165.7	5.0	171.9	5.4	165.4	6.0	0.964
9	322	0.799	38.5060	0.8151	0.1738	0.0054	0.0488	0.0014	0.345	165.3	1.1	162.7	3.5	165.4	3.5	1.016
75	741	1.279	38.4320	0.9517	0.1824	0.0057	0.0501	0.0012	0.476	165.6	2.4	170.1	3.8	165.4	4.1	0.973
6	456	0.833	38.4320	1.0457	0.1782	0.0046	0.0498	0.0012	0.376	165.6	3.0	166.5	2.5	165.5	4.5	0.994
93	405	0.788	38.4172	1.0756	0.1815	0.0081	0.0500	0.0016	0.543	165.7	3.2	169.4	6.2	165.5	4.6	0.978
2	499	0.776	38.4172	0.8942	0.1745	0.0051	0.0495	0.0014	0.365	165.7	1.9	163.3	3.2	165.6	3.8	1.014
55	514	0.805	38.4320	1.0162	0.1736	0.0049	0.0485	0.0013	0.478	165.6	2.8	162.5	2.9	165.8	4.4	1.019
100	491	0.773	38.3289	0.9749	0.1800	0.0050	0.0503	0.0013	0.324	166.0	2.6	168.1	3.0	165.8	4.2	0.988
116	543	0.688	38.3142	0.8838	0.1809	0.0050	0.0503	0.0012	0.453	166.1	1.9	168.8	2.9	165.9	3.8	0.984
18	613	0.512	38.2848	0.8252	0.1827	0.0053	0.0504	0.0014	0.357	166.2	1.3	170.4	3.2	166.0	3.6	0.976
24	385	0.800	38.2848	0.9917	0.1803	0.0057	0.0502	0.0015	0.424	166.2	2.7	168.3	3.8	166.0	4.3	0.988
103	429	0.788	38.2848	0.9383	0.1761	0.0053	0.0498	0.0013	0.500	166.2	2.4	164.7	3.3	166.1	4.0	1.009
66	370	0.696	38.0952	0.9157	0.1938	0.0071	0.0534	0.0015	0.317	167.0	2.2	179.9	5.0	166.2	4.0	0.929
89	433	0.754	38.2556	1.0587	0.1820	0.0048	0.0500	0.0014	0.416	166.3	3.1	169.8	2.7	166.2	4.6	0.980
22	306	0.604	38.2556	0.9127	0.1803	0.0055	0.0499	0.0015	0.369	166.3	2.1	168.3	3.5	166.2	3.9	0.988
23	412	0.789	38.2409	1.0683	0.1807	0.0052	0.0498	0.0013	0.425	166.4	3.2	168.7	3.3	166.3	4.6	0.987
61	611	1.002	38.1679	1.0352	0.1862	0.0099	0.0513	0.0022	0.576	166.7	3.0	173.4	7.9	166.3	4.5	0.962
37	333	0.711	38.1971	1.0664	0.1829	0.0063	0.0506	0.0015	0.417	166.6	3.2	170.6	4.4	166.3	4.6	0.977
60	519	0.799	38.2702	0.9639	0.1791	0.0048	0.0489	0.0013	0.465	166.3	2.5	167.3	2.8	166.4	4.2	0.994
64	480	0.837	38.2117	0.9035	0.1801	0.0052	0.0501	0.0013	0.469	166.5	2.1	168.1	3.3	166.4	3.9	0.990
81	203	0.554	38.2702	0.9639	0.1791	0.0076	0.0489	0.0019	0.256	166.3	2.5	167.3	5.8	166.4	4.2	0.994
98	332	0.660	38.1679	1.1279	0.1787	0.0073	0.0505	0.0016	0.464	166.7	3.6	166.9	5.5	166.5	4.9	0.999
12	434	0.759	38.0373	0.9472	0.1915	0.0057	0.0531	0.0014	0.486	167.3	2.4	177.9	3.6	166.5	4.1	0.940
118	733	1.012	38.1679	1.1387	0.1784	0.0070	0.0493	0.0014	0.295	166.7	3.6	166.7	5.2	166.7	4.9	1.000
54	577	0.951	38.1534	0.9962	0.1779	0.0055	0.0493	0.0013	0.451	166.8	2.7	166.3	3.6	166.8	4.3	1.003
30	350	0.694	38.0952	0.8848	0.1840	0.0065	0.0502	0.0016	0.503	167.0	1.9	171.5	4.5	166.9	3.9	0.974
120	435	0.718	38.0952	0.9941	0.1801	0.0058	0.0499	0.0014	0.502	167.0	2.8	168.1	3.9	166.9	4.3	0.993
46	632	0.959	38.1098	1.0833	0.1792	0.0047	0.0495	0.0012	0.399	167.0	3.3	167.4	2.6	167.0	4.7	0.998
40	353	0.873	38.0952	0.8999	0.1810	0.0059	0.0497	0.0014	0.442	167.0	2.1	168.9	4.0	167.0	3.9	0.989

74	344	0.825	37.9363	0.9524	0.1956	0.0058	0.0526	0.0015	0.352	167.7	2.5	181.4	3.7	167.1	4.2	0.925
26	359	1.050	38.0228	0.9822	0.1829	0.0054	0.0508	0.0016	0.389	167.3	2.7	170.6	3.4	167.1	4.3	0.981
91	359	0.611	38.0518	1.0604	0.1835	0.0068	0.0501	0.0016	0.427	167.2	3.2	171.1	4.9	167.1	4.6	0.978
36	382	0.840	37.9363	1.0964	0.1921	0.0071	0.0524	0.0017	0.449	167.7	3.4	178.4	5.1	167.1	4.8	0.940
20	449	0.871	38.0662	0.9229	0.1806	0.0071	0.0495	0.0016	0.392	167.2	2.3	168.6	5.2	167.1	4.0	0.992
16	155	0.706	38.0084	0.8750	0.1815	0.0056	0.0505	0.0016	0.446	167.4	1.9	169.4	3.6	167.2	3.8	0.989
51	346	0.588	38.0518	0.9925	0.1787	0.0061	0.0494	0.0016	0.472	167.2	2.8	166.9	4.3	167.2	4.3	1.002
4	445	0.717	38.0518	0.8692	0.1757	0.0049	0.0492	0.0014	0.456	167.2	1.8	164.4	2.9	167.3	3.8	1.017
45	391	0.765	38.0518	0.9143	0.1780	0.0066	0.0486	0.0015	0.406	167.2	2.2	166.3	4.8	167.4	4.0	1.005
108	286	0.672	37.6932	1.1169	0.2033	0.0072	0.0559	0.0016	0.619	168.8	3.7	187.9	5.1	167.4	4.9	0.898
11	399	1.163	37.7501	0.9049	0.1971	0.0100	0.0543	0.0024	0.486	168.5	2.2	182.7	7.8	167.5	4.0	0.923
52	615	0.906	37.9795	1.0376	0.1773	0.0053	0.0493	0.0011	0.488	167.5	3.0	165.7	3.4	167.6	4.5	1.011
68	312	0.885	37.9363	0.8876	0.1807	0.0063	0.0493	0.0016	0.288	167.7	2.0	168.7	4.4	167.8	3.9	0.994
119	294	0.616	37.7216	1.0768	0.1954	0.0058	0.0537	0.0014	0.419	168.7	3.4	181.2	3.7	167.8	4.8	0.931
57	344	0.810	37.9075	1.0746	0.1787	0.0051	0.0485	0.0014	0.413	167.9	3.3	166.9	3.1	168.0	4.7	1.005
15	376	0.747	37.7786	0.9058	0.1880	0.0055	0.0511	0.0015	0.478	168.4	2.2	174.9	3.4	168.1	4.0	0.963
84	259	0.587	37.8215	0.9660	0.1857	0.0083	0.0502	0.0019	0.360	168.2	2.7	173.0	6.3	168.1	4.3	0.973
7	314	0.765	37.8501	0.9324	0.1745	0.0071	0.0484	0.0014	0.314	168.1	2.4	163.3	5.3	168.3	4.1	1.029
111	483	0.706	37.7786	0.8615	0.1798	0.0052	0.0497	0.0013	0.511	168.4	1.8	167.9	3.3	168.4	3.8	1.003
49	396	0.733	37.7216	0.9200	0.1809	0.0059	0.0496	0.0014	0.312	168.7	2.3	168.8	4.0	168.6	4.1	0.999
90	403	0.795	37.7216	1.2046	0.1790	0.0064	0.0488	0.0013	0.454	168.7	4.1	167.2	4.5	168.8	5.4	1.009
43	261	0.553	37.7074	0.9277	0.1781	0.0072	0.0485	0.0018	0.349	168.7	2.4	166.4	5.5	168.9	4.1	1.014
56	402	0.848	37.6364	0.9421	0.1791	0.0049	0.0494	0.0013	0.376	169.0	2.5	167.3	2.9	169.1	4.2	1.011
101	391	1.013	37.5375	1.1626	0.1861	0.0060	0.0510	0.0016	0.388	169.5	3.9	173.3	4.0	169.2	5.2	0.978
113	411	0.757	37.5094	1.0094	0.1815	0.0069	0.0495	0.0015	0.478	169.6	3.0	169.4	5.1	169.6	4.5	1.002
42	232	0.577	37.5235	0.9913	0.1774	0.0053	0.0481	0.0015	0.371	169.5	2.9	165.8	3.4	169.8	4.5	1.022
85	267	0.603	37.3972	0.9016	0.1800	0.0065	0.0486	0.0017	0.304	170.1	2.3	168.1	4.7	170.3	4.1	1.012
73	195	0.609	36.0360	0.7802	0.1970	0.0075	0.0510	0.0019	0.281	176.5	1.5	182.6	5.4	176.1	3.8	0.966

Sample JntA2-070 (35° 9' 35.539"" S - 70° 26' 27.637"" W)

spot #	U [ppm]	Th/U	$^{238}U/^{206}Pb$	±2σ [%]	$^{207}Pb/^{235}U$	±2σ [%]	$^{207}Pb/^{206}Pb$	±2σ [%]	rho	$^{206}Pb/^{238}U$ age [Ma]	±2σ [Ma]	$^{207}Pb/^{235}U$ age [Ma]	±2σ [Ma]	Preferred age [Ma]	±2σ [Ma]	concordance
120	1790	0.924	45.4133	1.4371	0.1830	0.0083	0.0604	0.0030	0.281	140.4	3.4	170.6	6.5	138.4	4.4	0.823
57	1011	1.612	40.6669	1.1957	0.1780	0.0049	0.0516	0.0012	0.507	156.6	3.4	166.3	2.9	156.1	4.6	0.941
99	951	1.008	40.5186	0.9483	0.1718	0.0046	0.0500	0.0012	0.249	157.2	1.9	161.0	2.6	157.0	3.7	0.976
59	767	1.339	40.4204	1.0293	0.1718	0.0044	0.0500	0.0013	0.364	157.5	2.4	161.0	2.3	157.4	4.0	0.979
56	554	0.845	40.0160	1.0558	0.1699	0.0052	0.0493	0.0012	0.462	159.1	2.7	159.3	3.5	159.1	4.2	0.999
70	859	1.442	39.7931	1.0682	0.1758	0.0044	0.0504	0.0012	0.522	160.0	2.8	164.4	2.3	159.8	4.3	0.973
62	577	0.747	39.7931	0.9790	0.1710	0.0055	0.0486	0.0014	0.435	160.0	2.3	160.3	3.7	160.1	3.9	0.998
105	911	1.254	39.6983	1.2713	0.1736	0.0053	0.0496	0.0013	0.526	160.4	4.0	162.5	3.5	160.3	5.1	0.987
37	445	0.935	38.7898	0.9052	0.2297	0.0088	0.0647	0.0024	0.395	164.1	1.9	210.0	6.1	160.9	3.8	0.782
118	656	0.877	39.4011	1.1849	0.1741	0.0051	0.0498	0.0013	0.450	161.6	3.6	163.0	3.2	161.5	4.8	0.991
77	471	0.831	39.3856	1.0322	0.1756	0.0070	0.0493	0.0013	0.320	161.6	2.7	164.3	5.2	161.6	4.2	0.984
86	607	0.806	39.2003	0.9776	0.1849	0.0045	0.0524	0.0012	0.432	162.4	2.4	172.3	2.3	161.8	4.0	0.943
53	711	1.028	39.3082	0.9812	0.1735	0.0052	0.0493	0.0013	0.391	161.9	2.4	162.5	3.4	161.9	4.0	0.997
119	278	0.671	39.2311	0.9605	0.1756	0.0060	0.0499	0.0015	0.312	162.3	2.2	164.3	4.3	162.1	3.9	0.988
48	569	0.794	39.2311	1.0069	0.1741	0.0053	0.0498	0.0014	0.424	162.3	2.6	163.0	3.5	162.2	4.1	0.996
61	601	1.012	39.2157	0.9512	0.1769	0.0045	0.0501	0.0012	0.453	162.3	2.2	165.4	2.4	162.2	3.9	0.981
17	688	0.753	39.2157	0.9099	0.1765	0.0047	0.0500	0.0012	0.325	162.3	1.9	165.0	2.7	162.2	3.7	0.984
98	582	0.881	39.1696	0.9674	0.1773	0.0053	0.0504	0.0013	0.351	162.5	2.4	165.7	3.3	162.3	4.0	0.981
107	582	0.923	39.2465	1.1214	0.1718	0.0054	0.0486	0.0012	0.372	162.2	3.3	161.0	3.6	162.3	4.6	1.008
64	947	1.419	39.2003	0.9421	0.1747	0.0045	0.0494	0.0011	0.435	162.4	2.1	163.5	2.4	162.4	3.9	0.993
116	434	0.674	39.1543	0.8930	0.1767	0.0066	0.0499	0.0017	0.319	162.6	1.8	165.2	4.8	162.5	3.7	0.984
44	588	0.836	39.1543	1.0236	0.1760	0.0058	0.0498	0.0013	0.463	162.6	2.7	164.6	3.9	162.5	4.2	0.988
28	644	1.095	38.8803	1.0844	0.1913	0.0061	0.0538	0.0014	0.580	163.7	3.1	177.7	4.1	162.8	4.5	0.921
32	450	0.750	39.0473	0.9545	0.1766	0.0048	0.0500	0.0012	0.496	163.0	2.3	165.1	2.7	162.9	4.0	0.987
115	529	0.931	39.0016	0.9800	0.1776	0.0051	0.0503	0.0012	0.378	163.2	2.5	166.0	3.1	163.0	4.1	0.983
41	463	0.572	39.0473	0.8499	0.1754	0.0047	0.0491	0.0014	0.337	163.0	1.4	164.1	2.6	163.1	3.5	0.993
12	512	0.724	38.9712	0.8807	0.1786	0.0060	0.0504	0.0016	0.432	163.3	1.7	166.9	4.2	163.1	3.7	0.979
111	639	0.920	38.8350	1.0931	0.1895	0.0066	0.0530	0.0014	0.477	163.9	3.2	176.2	4.6	163.1	4.6	0.930
43	400	0.770	38.9257	0.9015	0.1754	0.0060	0.0492	0.0016	0.464	163.5	1.9	164.1	4.3	163.5	3.8	0.996
79	368	0.693	38.8954	1.1954	0.1753	0.0055	0.0496	0.0013	0.500	163.6	3.7	164.0	3.6	163.6	5.0	0.998

96	183	0.739	39.0320	0.8896	0.1652	0.0068	0.0467	0.0019	0.382	163.1	1.8	155.2	5.2	163.6	3.7	1.050
3	564	0.748	38.8803	0.9079	0.1751	0.0044	0.0497	0.0012	0.395	163.7	2.0	163.8	2.3	163.6	3.8	0.999
112	388	0.659	38.8350	1.3228	0.1753	0.0069	0.0501	0.0013	0.478	163.9	4.4	164.0	5.2	163.7	5.5	0.999
63	527	0.774	38.8350	0.9144	0.1789	0.0057	0.0499	0.0013	0.360	163.9	2.0	167.1	3.9	163.8	3.8	0.981
31	287	0.604	38.7898	1.0102	0.1812	0.0067	0.0502	0.0017	0.393	164.1	2.7	169.1	4.8	163.9	4.2	0.970
39	545	0.928	38.8048	1.0012	0.1775	0.0049	0.0495	0.0012	0.502	164.0	2.6	165.9	3.0	164.0	4.2	0.989
18	341	0.584	38.6548	0.8236	0.1885	0.0049	0.0523	0.0013	0.427	164.6	1.2	175.3	2.7	164.0	3.5	0.939
71	351	0.870	38.4615	0.9441	0.2015	0.0064	0.0557	0.0019	0.334	165.5	2.3	186.4	4.2	164.1	4.0	0.888
47	566	0.877	38.7597	0.9717	0.1773	0.0048	0.0495	0.0014	0.299	164.2	2.4	165.7	2.7	164.2	4.1	0.991
67	434	0.705	38.7898	1.0497	0.1739	0.0054	0.0487	0.0013	0.426	164.1	3.0	162.8	3.5	164.2	4.4	1.008
74	417	0.796	38.7597	1.0091	0.1754	0.0052	0.0492	0.0013	0.403	164.2	2.7	164.1	3.4	164.2	4.2	1.001
19	541	0.745	38.6548	0.9012	0.1809	0.0049	0.0501	0.0011	0.349	164.6	2.0	168.8	2.8	164.5	3.8	0.975
21	317	0.757	38.6997	0.8803	0.1768	0.0064	0.0490	0.0018	0.464	164.5	1.8	165.3	4.6	164.5	3.7	0.995
33	538	0.786	38.6548	1.0052	0.1811	0.0058	0.0498	0.0013	0.478	164.6	2.7	169.0	3.9	164.6	4.3	0.974
89	354	0.836	38.5505	0.9470	0.1846	0.0048	0.0514	0.0014	0.453	165.1	2.3	172.0	2.6	164.7	4.0	0.960
36	330	0.769	38.6100	1.0837	0.1802	0.0061	0.0500	0.0014	0.401	164.8	3.2	168.2	4.2	164.7	4.6	0.980
30	368	0.840	38.5803	0.8841	0.1804	0.0059	0.0503	0.0017	0.235	165.0	1.8	168.4	4.7	164.8	3.8	0.980
95	785	1.173	38.4763	1.0990	0.1862	0.0061	0.0524	0.0014	0.397	165.4	3.3	173.4	4.1	164.8	4.7	0.954
34	365	0.917	38.3289	0.8842	0.2003	0.0074	0.0549	0.0019	0.531	166.0	1.9	185.4	5.2	164.9	3.8	0.896
100	555	0.777	38.5357	1.0201	0.1786	0.0047	0.0505	0.0013	0.378	165.2	2.8	166.9	2.6	164.9	4.3	0.990
20	452	0.766	38.2263	0.9118	0.2057	0.0054	0.0567	0.0014	0.429	166.5	2.1	189.9	2.9	164.9	3.9	0.876
14	919	1.211	38.5208	1.0003	0.1818	0.0057	0.0507	0.0012	0.474	165.2	2.7	169.6	3.8	164.9	4.3	0.974
81	261	0.830	38.5951	0.9936	0.1752	0.0068	0.0491	0.0016	0.452	164.9	2.6	163.9	5.0	165.0	4.2	1.006
15	372	0.675	38.5505	0.9557	0.1775	0.0068	0.0499	0.0015	0.421	165.1	2.4	165.9	5.0	165.0	4.1	0.995
110	518	0.681	38.5654	1.0923	0.1750	0.0062	0.0495	0.0014	0.448	165.0	3.3	163.7	4.4	165.0	4.6	1.008
73	469	0.722	38.5060	0.9287	0.1832	0.0059	0.0506	0.0015	0.510	165.3	2.2	170.8	3.9	165.0	4.0	0.968
101	846	0.998	38.5060	1.0690	0.1805	0.0057	0.0504	0.0012	0.449	165.3	3.1	168.5	3.8	165.1	4.6	0.981
8	620	0.850	38.5951	0.8774	0.1731	0.0057	0.0485	0.0014	0.444	164.9	1.7	162.1	3.9	165.1	3.7	1.017
55	253	0.674	38.5505	0.9138	0.1766	0.0074	0.0494	0.0019	0.337	165.1	2.1	165.1	5.6	165.1	3.9	1.000
106	420	0.671	38.5060	1.1767	0.1798	0.0058	0.0502	0.0015	0.481	165.3	3.8	167.9	4.0	165.1	5.0	0.984
29	286	1.057	38.4025	0.9960	0.1907	0.0075	0.0519	0.0015	0.446	165.7	2.7	177.2	5.6	165.2	4.3	0.935
69	421	0.955	38.5208	0.8898	0.1760	0.0057	0.0491	0.0013	0.474	165.2	1.9	164.6	3.9	165.3	3.8	1.004
35	393	0.618	38.4615	0.9705	0.1821	0.0053	0.0501	0.0015	0.333	165.5	2.5	169.9	3.3	165.3	4.1	0.974
40	482	0.782	38.3583	1.0835	0.1902	0.0065	0.0520	0.0016	0.417	165.9	3.3	176.8	4.5	165.4	4.6	0.938
104	561	0.977	38.4615	0.9982	0.1819	0.0056	0.0498	0.0014	0.317	165.5	2.7	169.7	3.7	165.4	4.3	0.975
82	373	1.000	37.9651	0.9711	0.2159	0.0083	0.0598	0.0019	0.224	167.6	2.6	198.5	5.9	165.4	4.2	0.844
66	498	0.725	38.4468	1.0665	0.1814	0.0058	0.0498	0.0013	0.381	165.5	3.1	169.3	3.9	165.4	4.6	0.978
45	380	0.961	38.4172	0.9342	0.1800	0.0055	0.0500	0.0014	0.403	165.7	2.3	168.1	3.6	165.5	4.0	0.986
88	453	0.747	38.4468	0.9610	0.1754	0.0052	0.0489	0.0014	0.398	165.5	2.4	164.1	3.3	165.6	4.1	1.009
87	529	0.645	38.3730	0.9765	0.1786	0.0061	0.0500	0.0012	0.487	165.8	2.6	166.9	4.3	165.7	4.2	0.994
114	311	1.006	38.4025	0.9867	0.1772	0.0051	0.0493	0.0015	0.570	165.7	2.6	165.6	3.2	165.7	4.2	1.000
102	364	0.897	38.3877	1.2391	0.1766	0.0070	0.0494	0.0013	0.329	165.8	4.1	165.1	5.2	165.8	5.3	1.004
117	790	0.927	38.3877	1.1489	0.1792	0.0052	0.0494	0.0011	0.478	165.8	3.7	167.4	3.2	165.8	4.9	0.990
51	736	1.302	38.4025	0.9684	0.1749	0.0045	0.0486	0.0013	0.391	165.7	2.5	163.7	2.4	165.9	4.2	1.013
25	324	0.760	38.2848	1.0106	0.1839	0.0055	0.0509	0.0015	0.334	166.2	2.8	171.4	3.5	165.9	4.4	0.970
58	521	0.753	38.3583	0.8851	0.1775	0.0043	0.0490	0.0012	0.363	165.9	1.9	165.9	2.1	166.0	3.8	1.000
76	432	0.766	38.2995	0.9649	0.1795	0.0067	0.0501	0.0014	0.390	166.2	2.5	167.6	4.8	166.0	4.2	0.991
93	422	0.715	38.3142	1.1564	0.1775	0.0067	0.0493	0.0012	0.438	166.1	3.7	165.9	4.9	166.1	5.0	1.001
9	492	0.714	38.2995	0.8908	0.1767	0.0060	0.0494	0.0013	0.384	166.2	2.0	165.2	4.1	166.2	3.8	1.006
91	514	1.064	38.2409	1.0480	0.1813	0.0062	0.0503	0.0013	0.464	166.4	3.1	169.2	4.3	166.2	4.5	0.984
42	161	0.502	36.5497	1.0177	0.3250	0.0604	0.0850	0.0141	0.284	174.0	3.3	285.7	46.0	166.2	5.6	0.609
113	454	0.856	38.1971	1.0073	0.1832	0.0052	0.0510	0.0014	0.569	166.6	2.8	170.8	3.2	166.3	4.4	0.975
83	506	0.957	38.3142	0.9928	0.1746	0.0055	0.0486	0.0013	0.413	166.1	2.7	163.4	3.6	166.3	4.3	1.016
11	273	0.686	37.7786	0.9301	0.2095	0.0078	0.0581	0.0022	0.287	168.4	2.4	193.1	5.5	166.6	4.1	0.872
24	451	0.723	38.1825	0.9521	0.1822	0.0063	0.0497	0.0016	0.382	166.7	2.4	170.0	4.4	166.6	4.1	0.981
84	705	1.355	38.1825	1.0163	0.1783	0.0046	0.0493	0.0012	0.346	166.7	2.9	166.6	2.5	166.7	4.4	1.000
2	319	0.912	38.0807	0.8700	0.1821	0.0050	0.0510	0.0014	0.423	167.1	1.8	169.9	2.9	166.8	3.8	0.984
72	134	0.718	38.1098	0.8779	0.1792	0.0097	0.0494	0.0027	0.265	167.0	1.9	167.4	7.8	167.0	3.9	0.998
94	273	0.713	38.0518	1.0504	0.1821	0.0065	0.0502	0.0016	0.393	167.2	3.2	169.9	4.6	167.1	4.6	0.984
5	657	0.817	38.0952	0.8153	0.1763	0.0050	0.0492	0.0013	0.301	167.0	1.3	164.9	3.0	167.1	3.6	1.013
109	398	0.839	38.0662	1.2683	0.1791	0.0060	0.0496	0.0013	0.497	167.2	4.4	167.3	4.2	167.1	5.5	0.999
10	516	0.727	38.0373	0.8247	0.1786	0.0056	0.0496	0.0015	0.293	167.3	1.4	166.9	3.7	167.2	3.6	1.003
65	271	0.638	38.0084	0.8680	0.1831	0.0056	0.0501	0.0012	0.484	167.4	1.8	170.7	3.6	167.3	3.8	0.981

6	514	0.735	37.9795	0.8603	0.1794	0.0046	0.0499	0.0012	0.342	167.5	1.8	167.5	2.5	167.4	3.8	1.000	
54	535	0.725	37.9507	1.1394	0.1828	0.0068	0.0496	0.0013	0.425	167.7	3.7	170.5	4.9	167.6	5.0	0.984	
85	423	0.630	37.9363	1.0457	0.1800	0.0058	0.0497	0.0013	0.568	167.7	3.1	168.1	4.0	167.7	4.6	0.998	
7	608	1.118	37.8931	0.9509	0.1814	0.0045	0.0505	0.0012	0.474	167.9	2.5	169.3	2.3	167.7	4.2	0.992	
27	460	0.653	37.8645	0.8639	0.1870	0.0066	0.0511	0.0017	0.325	168.0	1.8	174.1	4.7	167.7	3.8	0.965	
16	470	0.595	37.7644	0.9729	0.1953	0.0059	0.0527	0.0014	0.224	168.5	2.7	181.1	3.7	167.8	4.3	0.930	
26	371	0.825	37.8931	1.0148	0.1829	0.0056	0.0494	0.0015	0.366	167.9	2.9	170.6	3.6	167.9	4.5	0.985	
52	542	1.031	37.6932	0.8731	0.1960	0.0049	0.0533	0.0012	0.537	168.8	1.9	181.7	2.5	168.0	3.9	0.929	
97	382	0.852	37.7786	1.0491	0.1777	0.0055	0.0494	0.0014	0.345	168.4	3.2	166.1	4.0	168.4	4.6	1.014	
90	412	0.738	37.6932	0.9615	0.1850	0.0047	0.0500	0.0015	0.314	168.8	2.7	172.4	2.5	168.7	4.3	0.979	
50	1000	1.075	37.7216	0.9365	0.1806	0.0047	0.0494	0.0011	0.494	168.7	2.4	168.6	2.6	168.7	4.2	1.001	
22	373	0.755	37.6932	0.9527	0.1814	0.0059	0.0495	0.0014	0.355	168.8	2.6	169.3	4.3	168.8	4.2	0.997	
92	331	0.656	37.6081	1.0132	0.1846	0.0072	0.0504	0.0016	0.236	169.2	3.0	172.0	5.4	169.0	4.5	0.983	
75	325	0.877	37.6364	1.1567	0.1832	0.0068	0.0498	0.0019	0.369	169.0	3.9	170.8	4.9	169.0	5.2	0.990	
46	707	0.829	37.5375	0.9140	0.1833	0.0049	0.0502	0.0013	0.443	169.5	2.3	170.9	2.9	169.3	4.1	0.992	
68	314	1.081	37.5516	0.8910	0.1830	0.0056	0.0495	0.0014	0.395	169.4	2.1	170.6	3.7	169.4	4.0	0.993	
38	344	0.762	37.5235	0.9056	0.1817	0.0057	0.0497	0.0012	0.414	169.5	2.3	169.5	3.8	169.5	4.1	1.000	
49	944	1.279	37.5235	0.9822	0.1817	0.0053	0.0496	0.0012	0.438	169.5	2.8	169.5	3.3	169.5	4.4	1.000	
80	232	0.718	37.4672	0.9118	0.1804	0.0077	0.0489	0.0015	0.366	169.8	2.3	168.4	5.8	169.9	4.1	1.008	
23	394	0.872	37.1886	0.9353	0.2028	0.0084	0.0541	0.0021	0.282	171.1	2.6	187.5	6.2	170.1	4.3	0.912	
78	277	0.669	37.2995	1.1723	0.1850	0.0079	0.0504	0.0014	0.493	170.6	4.1	172.4	6.0	170.4	5.3	0.990	
60	266	0.691	37.3134	0.9655	0.1861	0.0055	0.0495	0.0015	0.400	170.5	2.8	173.3	3.5	170.5	4.4	0.984	
103	343	0.692	37.2717	0.8679	0.1849	0.0057	0.0502	0.0013	0.408	170.7	2.0	172.3	3.7	170.5	3.9	0.991	
13	322	0.691	37.1886	0.9188	0.1892	0.0052	0.0506	0.0013	0.432	171.1	2.5	175.9	3.0	170.8	4.2	0.972	
4	441	0.707	36.9549	0.9440	0.1940	0.0077	0.0529	0.0018	0.405	172.1	2.7	180.0	5.7	171.4	4.4	0.956	
1	337	0.820	36.9413	0.7876	0.1794	0.0055	0.0491	0.0016	0.445	172.2	1.3	167.5	3.6	172.3	3.7	1.028	
108	237	0.858	35.7271	0.9666	0.2797	0.0103	0.0723	0.0025	0.413	178.0	3.2	250.4	6.9	172.9	4.7	0.711	

Sample JntA2-019 (35° 9' 46.132"" S - 70° 29' 7.902"" W)

spot #	U [ppm]	Th/U	$^{238}U/^{206}Pb$	±2σ [%]	$^{207}Pb/^{235}U$	±2σ [%]	$^{207}Pb/^{206}Pb$	±2σ [%]	rho	$^{206}Pb/^{238}U$ age [Ma]	±2σ [Ma]	$^{207}Pb/^{235}U$ age [Ma]	±2σ [Ma]	Preferred age [Ma]	±2σ [Ma]	concordance
6	1259	0.708	47.0367	1.2326	0.1905	0.0055	0.0649	0.0015	0.540	135.6	2.3	177.1	3.4	132.8	3.5	0.766
35	634	0.780	39.9042	1.0413	0.1713	0.0044	0.0499	0.0012	0.577	159.6	2.7	160.5	2.4	159.4	4.1	0.994
16	369	0.748	39.4322	0.9163	0.1741	0.0077	0.0495	0.0021	0.245	161.4	1.9	163.0	5.9	161.4	3.7	0.991
9	924	1.297	39.3236	1.0102	0.1761	0.0048	0.0501	0.0011	0.462	161.9	2.6	164.7	2.8	161.7	4.1	0.983
24	422	0.931	39.1850	0.9863	0.1746	0.0053	0.0490	0.0015	0.298	162.4	2.5	163.4	3.4	162.5	4.1	0.994
10	911	1.191	39.1236	1.1053	0.1726	0.0044	0.0494	0.0011	0.579	162.7	3.2	161.7	2.4	162.7	4.6	1.006
21	618	1.092	38.8954	1.0539	0.1783	0.0053	0.0503	0.0012	0.533	163.6	2.9	166.6	3.4	163.4	4.4	0.982
7	546	0.953	38.8803	0.9239	0.1780	0.0049	0.0503	0.0014	0.296	163.7	2.1	166.3	2.9	163.5	3.9	0.984
20	717	0.955	38.9105	0.9955	0.1738	0.0054	0.0488	0.0013	0.509	163.6	2.6	162.7	3.6	163.7	4.2	1.005
36	726	1.023	38.8199	0.8984	0.1806	0.0048	0.0501	0.0013	0.330	164.0	1.9	168.6	2.7	163.8	3.8	0.973
29	396	0.936	38.8350	0.9307	0.1750	0.0059	0.0487	0.0013	0.303	163.9	2.1	163.7	4.1	164.0	3.9	1.001
27	576	0.819	38.7147	0.9438	0.1780	0.0043	0.0499	0.0012	0.479	164.4	2.3	166.3	2.0	164.3	4.0	0.988
18	304	0.532	38.6698	1.0757	0.1795	0.0065	0.0506	0.0017	0.294	164.6	3.1	167.6	4.7	164.3	4.5	0.982
37	604	0.733	38.6399	1.0240	0.1805	0.0050	0.0503	0.0011	0.431	164.7	2.8	168.5	2.9	164.5	4.3	0.978
14	423	0.643	38.6250	0.9160	0.1816	0.0059	0.0501	0.0013	0.401	164.8	2.1	169.4	3.9	164.6	3.9	0.972
40	748	1.078	38.5951	1.1475	0.1832	0.0056	0.0507	0.0013	0.489	164.9	3.6	170.8	3.6	164.6	4.9	0.965
11	571	0.780	38.6100	0.9404	0.1786	0.0059	0.0503	0.0014	0.390	164.8	2.2	166.9	4.0	164.6	4.0	0.988
19	590	1.005	38.6100	0.9490	0.1783	0.0054	0.0494	0.0012	0.443	164.8	2.3	166.6	3.5	164.8	4.0	0.989
30	575	1.047	38.5357	1.3301	0.1818	0.0084	0.0507	0.0016	0.439	165.2	4.6	169.6	6.5	164.9	5.7	0.974
23	258	0.671	38.5208	0.9460	0.1831	0.0092	0.0507	0.0022	0.323	165.2	2.3	170.7	7.2	164.9	4.0	0.968
26	448	0.720	38.4468	0.8951	0.1840	0.0057	0.0507	0.0014	0.264	165.5	2.0	171.5	3.7	165.3	3.8	0.965
15	416	0.726	38.3289	1.0219	0.1802	0.0055	0.0496	0.0012	0.308	166.0	2.9	168.2	3.6	166.0	4.4	0.987
31	543	0.770	38.2995	0.9923	0.1787	0.0054	0.0496	0.0012	0.536	166.2	2.7	166.9	3.6	166.1	4.3	0.995
28	427	0.962	38.2117	0.9619	0.1803	0.0061	0.0496	0.0013	0.416	166.5	2.5	168.3	4.2	166.5	4.2	0.989
38	584	0.880	38.0662	0.9481	0.1862	0.0058	0.0508	0.0012	0.306	167.2	2.5	173.4	3.8	166.9	4.1	0.964
32	656	0.904	37.9219	0.8947	0.1851	0.0053	0.0505	0.0013	0.350	167.8	2.1	172.4	3.2	167.6	3.9	0.973
4	455	0.676	37.9795	0.9283	0.1799	0.0064	0.0493	0.0014	0.526	167.5	2.3	168.0	4.5	167.6	4.1	0.997
33	324	0.869	37.9651	0.8960	0.1804	0.0055	0.0492	0.0014	0.384	167.6	2.1	168.4	3.6	167.6	3.9	0.995
34	312	0.672	37.8358	1.3135	0.1852	0.0088	0.0513	0.0020	0.281	168.2	4.7	172.5	6.8	167.8	5.8	0.975
3	704	1.121	37.8215	1.2322	0.1886	0.0054	0.0511	0.0013	0.490	168.2	4.3	175.4	3.4	167.9	5.4	0.959
1	438	0.657	37.8358	0.9846	0.1799	0.0073	0.0494	0.0016	0.317	168.2	2.8	168.0	5.5	168.2	4.4	1.001

39	484	1.103	37.5516	0.9924	0.2010	0.0061	0.0545	0.0015	0.535	169.4	2.9	186.0	3.9	168.3	4.4	0.911
5	494	0.713	37.7074	1.0561	0.1874	0.0060	0.0510	0.0015	0.527	168.7	3.3	174.4	4.0	168.4	4.7	0.967
17	152	0.453	37.6790	1.4712	0.1885	0.0070	0.0514	0.0017	0.554	168.9	5.6	175.3	5.0	168.4	6.5	0.963
22	361	0.788	37.6932	0.9527	0.1783	0.0064	0.0492	0.0015	0.422	168.8	2.6	166.6	4.6	168.8	4.2	1.013
13	248	0.738	37.6364	1.3841	0.1816	0.0081	0.0499	0.0015	0.462	169.0	5.1	169.4	6.2	168.9	6.2	0.998
8	338	0.659	37.4252	0.8947	0.1880	0.0066	0.0507	0.0017	0.403	170.0	2.2	174.9	4.6	169.7	4.0	0.972
2	410	0.622	36.9959	0.9124	0.1864	0.0061	0.0496	0.0014	0.422	171.9	2.5	173.6	4.1	171.9	4.2	0.991
25	441	0.837	36.9413	0.9965	0.1851	0.0061	0.0491	0.0013	0.365	172.2	3.1	172.4	4.1	172.3	4.6	0.999
12	353	0.790	36.7377	0.8809	0.1839	0.0069	0.0495	0.0016	0.514	173.1	2.3	171.4	5.0	173.1	4.1	1.010

Sample JntA1-088 (35° 9' 35.079"" S - 70° 26' 3.479"" W)

spot #	U [ppm]	Th/U	$^{238}U/^{206}Pb$	±2σ [%]	$^{207}Pb/^{235}U$	±2σ [%]	$^{207}Pb/^{206}Pb$	±2σ [%]	rho	$^{206}Pb/^{238}U$ age [Ma]	±2σ [Ma]	$^{207}Pb/^{235}U$ age [Ma]	±2σ [Ma]	Preferred age [Ma]	±2σ [Ma]	concordance
11	509	0.934	38.0518	0.9742	0.1874	0.0053	0.0516	0.0013	0.511	167.2	2.7	174.4	3.3	166.8	4.2	0.959
2	2528	1.907	37.2856	1.0581	0.1966	0.0061	0.0529	0.0012	0.466	170.6	3.4	182.2	3.9	169.9	4.8	0.936
8	960	1.620	37.0920	0.9155	0.1889	0.0052	0.0506	0.0013	0.482	171.5	2.4	175.7	3.1	171.3	4.2	0.976
9	340	0.600	37.0782	0.9399	0.1875	0.0072	0.0503	0.0017	0.410	171.6	2.6	174.5	5.2	171.4	4.3	0.983
6	634	0.812	37.0233	0.9379	0.1900	0.0060	0.0508	0.0013	0.392	171.8	2.6	176.6	3.9	171.5	4.3	0.973
4	756	0.905	37.0370	0.9911	0.1871	0.0064	0.0501	0.0014	0.468	171.7	3.0	174.2	4.4	171.6	4.6	0.986
10	837	1.542	37.0096	0.8602	0.1876	0.0050	0.0502	0.0011	0.481	171.9	2.0	174.6	2.8	171.7	4.0	0.984
7	334	0.415	36.5497	0.9055	0.2109	0.0071	0.0552	0.0016	0.346	174.0	2.5	194.3	4.8	172.8	4.3	0.896
3	887	1.502	36.6973	1.0052	0.1885	0.0062	0.0501	0.0014	0.448	173.3	3.2	175.3	4.2	173.2	4.7	0.988
1	659	1.290	36.6703	0.8862	0.1885	0.0073	0.0504	0.0014	0.409	173.4	2.3	175.3	5.4	173.3	4.2	0.989
5	191	0.895	36.1402	0.8918	0.2117	0.0074	0.0549	0.0015	0.417	175.9	2.5	195.0	5.1	174.8	4.3	0.902